AD-A185 671 AN OBSERVATIONAL CASE STUDY OF MESOSCALE CONVECTION OVER LAKE MICHIGAN ON 10 JANUARY 1984(U) AIR FORCE INST OF TECH WRIGHT-PATTERSON AFB OH S R GILBERT 1987 1/2

UNCLASSIFIED AFIT/CI/NR-87-74T F/G 4/2 NL

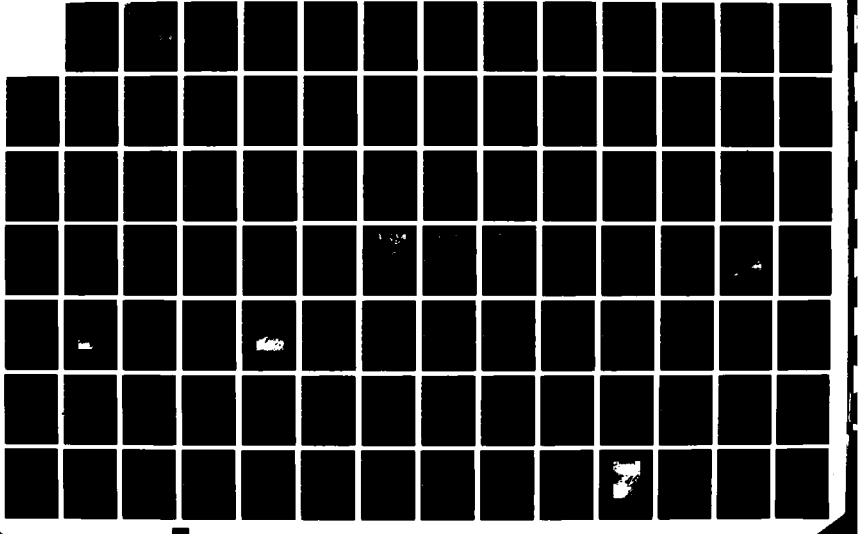

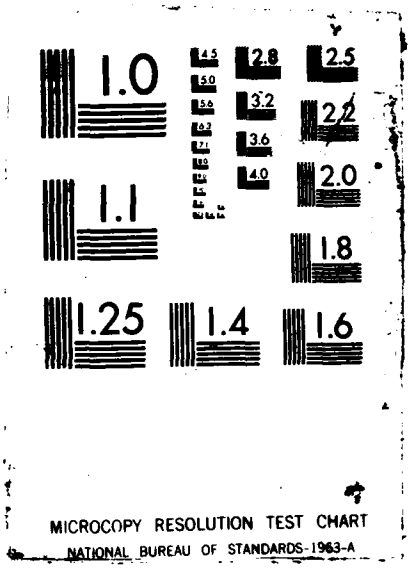
1.0
1.1
1.25
1.4
1.6
1.8
2.0
2.2
2.5
2.8
3.2
3.6
4.0
4.5
5.0
5.6
6.3
7.1
8.0
MICROCOPY RESOLUTION TEST CHART
NATIONAL BUREAU OF STANDARDS-1963-A

UNCLASSIFIED
SECURITY CLASSIFICATION OF THIS PAGE (When Data Entered)

# REPORT DOCUMENTATION PAGE

READ INSTRUCTIONS BEFORE COMPLETING FORM

| | |
|---|---|
| REPORT NUMBER: AFIT/CI/NR 87-74T | 2. GOVT ACCESSION NO.: A185671 |
| 3. RECIPIENT'S CATALOG NUMBER: | |
| 4. TITLE (and Subtitle): An Observational Case Study of Mesoscale Convection over Lake Michigan on 10 January 1984 | 5. TYPE OF REPORT & PERIOD COVERED: THESIS/~~DISSERTATION~~ |
| | 6. PERFORMING ORG. REPORT NUMBER: |
| 7. AUTHOR(s): Steven R. Gilbert | 8. CONTRACT OR GRANT NUMBER(s): |
| 9. PERFORMING ORGANIZATION NAME AND ADDRESS: AFIT STUDENT AT: Purdue University | 10. PROGRAM ELEMENT, PROJECT, TASK AREA & WORK UNIT NUMBERS: |
| 11. CONTROLLING OFFICE NAME AND ADDRESS: AFIT/NR WPAFB OH 45433-6583 | 12. REPORT DATE: 1987 |
| | 13. NUMBER OF PAGES: 105 |
| 14. MONITORING AGENCY NAME & ADDRESS(if different from Controlling Office): | 15. SECURITY CLASS. (of this report): UNCLASSIFIED |
| | 15a. DECLASSIFICATION/DOWNGRADING SCHEDULE: |

16. DISTRIBUTION STATEMENT (of this Report)

APPROVED FOR PUBLIC RELEASE; DISTRIBUTION UNLIMITED



17. DISTRIBUTION STATEMENT (of the abstract entered in Block 20, if different from Report)

18. SUPPLEMENTARY NOTES

APPROVED FOR PUBLIC RELEASE: IAW AFR 190-1

LYNN E. WOLAVER 23 Sept 87
Dean for Research and
Professional Development
AFIT/NR

19. KEY WORDS (Continue on reverse side if necessary and identify by block number)

20. ABSTRACT (Continue on reverse side if necessary and identify by block number)

ATTACHED

DD FORM 1 JAN 73 1473 EDITION OF 1 NOV 65 IS OBSOLETE

SECURITY CLASSIFICATION OF THIS PAGE (When Data Entered)

A

## ABSTRACT

Surface, upper air, and aerological data from the Lake-Effect Snow Studies (LESS) field program conducted during 1 December – 28 January 1984 have been examined to study the modification of continental polar air masses heated from below by the large, comparatively warm Great Lakes. This study has focused on one particular cold air outbreak (CAO) that occurred as a northerly flow event over Lake Michigan on 10 January 1984.

Several objective analysis schemes were used to analyze the conventional surface and upper-air data. Spatial cross-sections and streamline analyses show the combined effects of air mass modification by the Great Lakes. The total depth of the boundary layer at the southern end of Lake Michigan was uncharacteristically high, over 2.4 km, due to the air first being modified by Lake Superior, and then by the full fetch of Lake Michigan.

Aircraft data sets of ambient air temperature, virtual potential temperature, specific humidity, liquid water content, and the u, v, and w wind components sampled at a rate of 20 s$^{-1}$ by the NCAR King Air have been analyzed to determine the structure and interaction of the convectively mixed layer with the capping inversion layer. An important new finding of this study is the identification of a penetrative convection layer that resides between the top of the fully-mixed layer and the bottom of the inversion layer. Evidence from the aircraft data analysis shows the characteristics of this layer and the associated fluxes and entrainment. Penetrative convection into the traditional capping inversion is identified as convective turbulent eddies that continually mix with the stable air and thus lose their identity.

Spectral representations of the convective well-mixed layer contain length scales at approximately 3 and 10 km. These correspond to the onset of convection or basic convective mode (BCM) and a higher convective mode (HCM) which is manifest in GOES satellite imagery as two-dimensional cloud bands. A third spectral energy peak is present at ~30 km corresponding to the length scale of Mesoscale Cellular Convection (MCC) and Mesoscale Entrainment Instability (MEI). Also, observational evidence from the raw data and covariance calculations is presented to support the incorporation of a transition layer between the inversion and well-mixed layers in the conceptual model of a Type I CTBL.

Gilbert, Steven R.

An Observational Case Study of Mesoscale Convection over Lake Michigan on 10 January 1984

Captain, USAF

1987

105 pages

Master of Science

Purdue University

## LIST OF REFERENCES


Agee, E.M. and T.S. Chen, 1973: A model for investigaing eddy viscosity effects on mesoscale cellular convection. *J. Atmos. Sci.*, **30**, 180–199.

Agee, E.M., T.S. Chen and K.E. Dowell, 1973: A review of mesoscale cellular convection. *Bull. Amer. Meteor. Soc.*, **54**, 1004–1012.

Agee, E.M. and R.P. Howley, 1977: Latent and sensible heat flux calculations at the air–sea interface during AMTEX 74. *J. Appl. Meteor.*, **16**, 443–447.

Agee, E.M. and F.E. Lomax, 1978: Structure of the mixed layer and inversion layer associated with patterns of mesoscale cellular convection during AMTEX 75. *J. Atmos. Sci.*, **35**, 2281–2301.

Agee, E.M., 1987: Mesoscale cellular convection over the oceans. *Dyn. Atmos. Oceans*, **10**, 317–341.

Atlas, D., B. Walter, S. Chou and P.J. Sheu, 1986: The structure of the unstable marine boundary layer viewed by lidar and aircraft observations. *J. Atmos. Sci.*, **43**, 1301–1318.

Barnes, S.L., 1964: A technique for maximizing detail in numerical weather map analysis. *J. Appl. Meteor.*, **3**, 396–409.

Barnes, S.L., 1973: Mesoscale objective map analysis using weighted time–series observations. NOAA Tech. Memo. ERL–NSSL–62, 60 pp.

Benard, H., 1901: Les tourbillons cellulaires dans une nappe liquids transportant de la chaleur par convection en regime permanent. *Ann. Chim. Phys.*, **23**, 62–144.

Bunker, A.F., 1960: Heat and water vapor fluxes in air flowing southward over the western North Atlantic Ocean. *J. Meteor.*, **17**, 52–63.

Caughey, S.J., B.A. Crease and W.T. Roach, 1982: A field study of nocturnal stratocumulus II turbulence structure and entrainment. *Quart. J. Roy. Met. Soc.*, **108**, 125–144.

Caughey, S.J. and M. Kitchen, 1984: Simultaneous measurements of the turbulent and microphysical structure of nocturnal stratosumulus cloud. *Quart. J. Roy. Met. Soc.*, **110**, 13–34.

Chandrasekhar, S., 1957: Thermal convection. *Daedalus*, **86**, No. 4, 325–339.

Christopherson, D.G., 1940: Note on the vibrations of membranes. *Quart. J. Math.*, **11**, 63–63.

Fiedler, B.H., 1984: The mesoscale stability of entrainment into cloud–topped mixed layers. *J. Atmos. Sci.*, **41**, 92–101.

Helfand, H.M. and E. Kalnay, 1983: A model to determine open or closed cellular convection. *J. Atmos. Sci.*, **40**, 631–650.

Hubert, L.F., 1966: Mesoscale cellular convection. *Rept. 37*, Meteorological Satellite Laboratory, Washington, D.C., 68 pp.

Kaimal, J., J. Wyngaard, O. Cote, V. Izumi, S. Coughey and C. Readings, 1976: Turbulence structure in the convective boundary layer. *J. Atmos. Sci.*, **33**, 2152–2169.

Kelley, N.D., and M.N. Zrubek, 1973: Instrumentation aboard the Electra. *Atmospheric Technology*, **1**, 18–20.

Koch, S.E., M. des Jardin and P.J. Kochin, 1983: An interactive Barnes objective map analysis scheme for use with satellite and conventional data. *J. Climate. Appl. Meteor*, **22**, 1487–1503.

Krishnamurti, R., 1975: On cellular cloud patterns. Part 3: Applicability of the mathematical and laboratory models. *J. Atmos. Sci.*, **32**, 1373–1383.

Krueger, A.F. and S. Fritz, 1961: Cellular cloud patterns revealed by TIROS I. *Tellus*, **13**, 1–7.

LeMone, M.A., 1973: The structure and dynamics of horizontal roll vortices in the planetary boundary layer. *J. Atmos. Sci.*, **33**, 1308–1320.

Lemone, M.A. 1976: Modulation of turbulence energy by longitudinal rolls in an unstable planetary boundary layer. *J. Atmos. Sci.*, **33**, 1308–1320.

Lenschow, D.H., 1965: Airborne measurements of atmospheric boundary layer structure. Studies of the Effects of Variations in Boundary Conditions on the Atmospheric Boundary Layer, Sec. 4, Final Rept., Contract DA-36-039-AMC-00878(E), Dept. of Meteor., University of Wisconsin, 147–208.

Lenschow, D.H., 1973a: Two examples of planetary boundary layer modification over the Great Lakes. *J. Atmos. Sci.*, **30**, 568–581.

Lenschow, D.H., 1973b: Air sensing probes on the Buffalo. *Atmospheric Technology*, **1**, 40–43.

Lenschow, D.H. and P.L. Stevens, 1980: The role of thermals in the convective boundary layer. *Bound.-Layer Meteor.* **19**, 509–532.

Lidrbauch, J.J., 1986: An observational study of polar low phenomena in the vicinity of Lake Michigan. M.S. thesis, Purdue University, 147 pp.

Lilly, D.K., 1968: Models of cloud-topped mixed layers under a strong inversion. *Quart. J. Roy. Met. Soc.*, **94**, 292–309.

O'Brien, J.J., 1970: Alternative solutions to the classical vertical velocity problem. *J. Appl. Meteor.*, **9**, 197–203.

Orlanski, I. 1975: A rational subdivision of scales for atmospheric processes. *Bull. Amer. Meteor. Soc.*, **56**, 527–530.

Palm, E., 1960: On the tendency toward hexagonal cells in steady convection. *J. Fluid Mech.*, **8**, 183–192.

Pellew, A. and R.V. Southwell, 1940: On maintained convection motion in a fluid heated from below. *Proc. Roy. Soc.*, A, **176**, 312–343.

Randall, D.A., 1980: Conditional instability of the first kind upside-down. *J. Atmos. Sci.*, **37**, 125–130.

Rayleigh, O.M., 1916: On convection currents in a horizontal layer of fluid, when the higher temperature is on the underside. *Phil. Mag.*, Ser. 6, **32**, 529–546.

Roberts, P.H., 1967: Convection in horizontal layers with internal heat generation. Theory. *J. Fluid Mech.*, **30**, 33–50.

Rokosz, S. D., 1985: Modification of polar air mases over Lake Michigan. M.S. thesis, Purdue University, 216 pp.

Ross, B. and E.M. Agee, 1985: Aircraft investigation of wintertime convective and non–convective boundary layers over the East China Sea. *J. Meteor. Soc. Japan*, **63**, 405–416.

Rothermel, J. and E.M. Agee, 1980: Aircraft investigation of mesoscale cellular convection during AMTEX 75. *J. Atmos. Sci.*, **37**, 1027–1040.

Rothermel, J. and E.M. Agee, 1986: A numerical study of atmospheric convective scaling. *J. Atmos. Sci.*, **43**, 1185–1197.

Sheu, P. J. and E. M. Agee, 1977: Kinematic analysis and air–sea heat flux associated with mesoscale cellular convection during AMTEX 75. *J. Atmos. Sci.*, **34**, 793–801.

Sheu, P.J., E.M. Agee, and J.J. Tribbia, 1980: A numerical study of physical processes affecting convective cellular geometry. *J. Meteor. Soc. Japan*, **58**, 489–499.

Smith, D. R., and F. W. Leslie, 1982: Evaluation of a Barnes–type objective analysis scheme for surface meteorological data. NASA Tech. Memo., 82509, 25 pp.

Smith, D. R., M. E. Pumphry and J. T. Snow, 1986: A comparison of errors in objectively analyzed fields for uniform and nonuniform station distributions. *J. Atmos. Oceanic Technol.*, **3**, 123–132.

Van Delden, A., 1985: On the preferred mode of cumulus convection. *Beitr. Phys. Atmosph.*, **58**, 202–219.

Walters, B. A., Jr., 1986: The mesoscale organization, dynamics, and evolution of the marine planetary boundary layer during cold air outbreaks. Ph.D. dissertation, University of Washington, 200 pp.

PURDUE UNIVERSITY

Graduate School

This is to certify that the thesis prepared

By Steven R. Gilbert

Entitled

"An observational case study of mesoscale convection over Lake Michigan on 10 January 1984"

Complies with University regulations and meets the standards of the Graduate School for originality and quality

For the degree of Master of Science

Signed by the final examining committee:

Ernest M. Agee, chair

Philip J. Smith

Judith A. Curry

Approved by the head of school or department:

29 May 1987 [signature]

This thesis ☑ is not to be regarded as confidential

Ernest M. Agee
Major professor

Grad. School
Form No. 9
Revised 9-85

# AN OBSERVATIONAL CASE STUDY OF MESOSCALE CONVECTION OVER LAKE MICHIGAN ON 10 JANUARY 1984

A Thesis

Submitted to the Faculty

of

Purdue University

by

Steven R. Gilbert

In Partial Fulfillment of the

Requirements for the Degree

of

Master of Science

August 1987

## ACKNOWLEDGEMENTS

My sincere gratitude is extended to my major professor, Dr. Ernest Agee. Without his helpful comments and guidance this work could not have been completed.

I would also like to thank the other members of my committee, Dr. Phillip Smith and Dr. Judith Curry, for their many helpful suggestions.

Finally, and most importantly, I would like to thank my family for putting up with the long hours away from home with few complaints and lots of support.

This research has been sponsored in part by the National Science Foundation Experimental Meteorology Program, through the auspices of Grant ATM-8505477 awarded to Ernest M. Agee and Purdue University.

TABLE OF CONTENTS

Page

# LIST OF TABLES

LIST OF FIGURES

## ABSTRACT

Gilbert, Steven R. M.S., Purdue University, August 1987. An Observational Case Study of Mesoscale Convection over Lake Michigan on 10 January 1984. Major Professor: Ernest M. Agee.

Surface, upper air, and aerological data from the Lake-Effect Snow Studies (LESS) field program conducted during 1 December – 28 January 1984 have been examined to study the modification of continental polar air masses heated from below by the large, comparatively warm Great Lakes. This study has focused on one particular cold air outbreak (CAO) that occurred as a northerly flow event over Lake Michigan on 10 January 1984.

Several objective analysis schemes were used to analyze the conventional surface and upper-air data. Spatial cross-sections and streamline analyses show the combined effects of air mass modification by the Great Lakes. The total depth of the boundary layer at the southern end of Lake Michigan was uncharacteristically high, over 2.4 km, due to the air first being modified by Lake Superior, and then by the full fetch of Lake Michigan.

Aircraft data sets of ambient air temperature, virtual potential temperature, specific humidity, liquid water content, and the u, v, and w wind components sampled at a rate of 20 $s^{-1}$ by the NCAR King Air have been analyzed to determine the structure and interaction of the convectively mixed layer with the capping inversion layer. An important new finding of this study is the identification of a penetrative convection layer that resides between the top of the fully-mixed layer and the bottom of the inversion layer. Evidence from the aircraft data analysis shows the characteristics of this layer and the associated fluxes and entrainment. Penetrative convection into the traditional capping inversion is identified as convective turbulent eddies that continually mix with the stable air and thus lose their identity.

Spectral representations of the convective well-mixed layer contain length scales at approximately 3 and 10 km. These correspond to the onset of convection or basic convective mode (BCM) and a higher convective mode (HCM) which is manifest in GOES

satellite imagery as two–dimensional cloud bands. A third spectral energy peak is present at ~30 km corresponding to the length scale of Mesoscale Cellular Convection (MCC) and Mesoscale Entrainment Instability (MEI). Also, observational evidence from the raw data and covariance calculations is presented to support the incorporation of a transition layer between the inversion and well–mixed layers in the conceptual model of a Type I CTBL.

# 1. INTRODUCTION AND STATEMENT OF OBJECTIVES

In 1834 William Prout introduced the term convection (from the Latin *convectio*, to carry), which defines the three-dimensional mass motion of a fluid that results in the transfer of fluid properties such as heat and momentum. Since then, the field of meteorology has used this term exclusively to denote the vertical transport of fluid properties which takes place within the atmosphere. This overturning in a fluid layer results in both up and down motion, where each couplet of ascent and descent constitutes a convection cell. Such motion can be freely driven due to thermal effects (buoyancy) or externally forced (e.g. by convergence, topography or fronts). The extent of the vertical motion further defines convection to be either shallow or deep. Deep convection such as thunderstorms can extend throughout the entire depth of the troposphere, while shallow convection is confined to the lowest 1 – 2 km of the atmosphere, the planetary boundary layer (which is approximately one order of magnitude less than the scale height of the troposphere). A convective planetary boundary layer in which some fraction of cloud is formed (typically beneath the capping inversion) is referred to as a cloud-topped boundary layer (CTBL). Several types of CTBLs are discussed in a later section.

## 1.1 Early Studies in Shallow Convection

At the turn of the twentieth century, Henri Benard (1901) demonstrated and quantified the phenomenon of shallow convection in the laboratory. These classical experiments showed that a thin layer of fluid, initially at rest, will readily resolve itself into a regular array of cells when heated uniformly from below. These cells were hexagonal in shape with an apsect ratio (defined as the dimensionless ratio of cell diameter to depth of the convective layer) on the order of 2 or 3. As a follow-up to these experiments, Lord Rayleigh (1916) presented a mathematical model describing the thermal convection which Benard created in the

laboratory. Rayleigh worked with a set of four linearized Boussinesq equations (shown below) consisting of the momentum, continuity, state and energy equations in three dimensions to mathematically solve for this type of buoyant motion:

$$\frac{\partial u_i}{\partial t} = \frac{-1}{\rho_m}\frac{\partial p}{\partial x_i} + \nu \nabla^2 u_i - \frac{g\rho}{\rho_m}\delta_{i3} \qquad (1.1)$$

$$\frac{\partial u_i}{\partial x_i} = 0 \qquad (1.2)$$

$$\rho = -\rho_m \alpha T \qquad (1.3)$$

$$\frac{\partial T}{\partial t} + u_3 \frac{\partial \bar{T}}{\partial x_3} = \kappa \nabla^2 T \,. \qquad (1.4)$$

Here $\rho_m$ is the mean state density of the fluid layer, $\bar{T}$ is the undisturbed mean state temperature, $\alpha$ is the coefficient of thermal expansion, $\kappa$ is the thermal diffusivity, and $\nu$ is the molecular kinematic viscosity.

In the process of finding a solution for this type of buoyant motion, Lord Rayleigh derived an important non-dimensional stability parameter which predicts the onset of convection. In his honor, Chandrasekhar (1957) adopted the name Rayleigh number (Ra) for this dimensionless ratio given by

$$Ra = \frac{g \alpha \beta d^4}{\kappa \nu} \,, \qquad (1.5)$$

where g is gravitational acceleration, $\alpha$ is the coefficient of thermal expansion, $\beta$ is the temperature lapse rate of the fluid, and d is the fluid depth. The numerator represents the buoyancy forces, and the denominator contains the viscous effects of thermal diffusivity $\kappa$ and molecular kinematic viscosity $\nu$. Examination of the Rayleigh number shows that the onset of convection will depend not only upon the molecular properties of the fluid, but also upon external fluid conditions such as the depth, change of temperature with height, and conditions at the boundaries. Rayleigh's experiments with free-free boundary conditions yielded a minimum critical value for the onset of convection ($Ra_c$ = 657.51) and a critical wavenumber of 2.22. An inherent weakness of Rayleigh's model was that the linear solution did not select the geometry. He assumed a square planform and, therefore, was not able to

truly simulate the hexagonal structure of Benard's cells. Later, Pellew and Southwell (1940) modified the linearized set of equations to include Christopherson's (1940) shape function for a hexagonal array. They were able to model the internal structures of the assumed hexagonal cells, which displayed extrema in vertical velocities at the cell center and at each of the vertices. The magnitude of the vertical motion in the cell center was twice that of each vertex and of the opposite direction. However, ground-based observations and low altitude aircraft flights were unable to detect convective organization of this type and the investigation of atmospheric manifestations of Benard-Rayleigh (B-R) convection went virtually dormant. It was not until some twenty years after Pellew and Southwell that the idea of B-R convection was again brought to the attention of meteorologists. The satellite imagery provided by TIROS I gave a view of mesoscale cloud cells that were arrayed over vast expanses of the oceans, but were individually too large to be recognized by conventional methods.

## 1.2 Atmospheric Observations of Shallow Convection

Krueger and Fritz (1961) were first to report a cellular cloud pattern in the atmosphere reminiscent of B-R convection. They observed arrays of cellular convection which occurred in marine planetary boundary layers heated from below and capped by subsidence inversions. In a subsequent paper, Hubert (1966) defined the approximately polygonal cloud patterns of cellular convection as being "open" or "closed" cells. As Fig. 1 shows, open cells are characterized by downward motion in the center of the cell and compensating upward motion in the periphery. This results in a cloud-free cell center surrounded by cloud walls. Closed cells have cloudy centers due to the presence of upward motion and clear cell walls due to downward motion. Hubert pointed to the frequency of occurrence and extensive areal coverage of mesoscale cellular convection over the oceans and a possible link to its formation as the result of air-sea interactions.

Two of Hubert's findings, however, were inconsistent with the laboratory results. Firstly, studies by Palm (1960) showed the vertical gradient of molecular kinematic viscosity determined the direction of cell circulation. Specifically, when the viscosity decreases with increasing temperature as with most liquids, then the cirulation direction is upward at the cell center and produces closed cells. Conversely, when viscosity increases with increasing

temperature (the general behavior of most gases), the circulation is directed downward at the cell center and creates open cells. This argument is based on recognition of where in the fluid the minimum critical value of Ra is first achieved. Thus, even though one would expect only open cells in the gaseous atmosphere, Hubert found that open and closed cells both occurred. Agee and Chen (1973) extended Palm's model result to the atmosphere, and showed that the circulation direction reverses if the vertical gradient of the eddy diffusion coefficient changes sign. Krishnamurti (1975) later showed that the direction of large scale vertical motion can determine the circulation direction of mesoscale cells. Helfand and Kalnay (1983), in a follow up to Roberts' (1967) earlier work, showed that local heating/cooling mechanisms in the convective layer can affect the circulation direction.

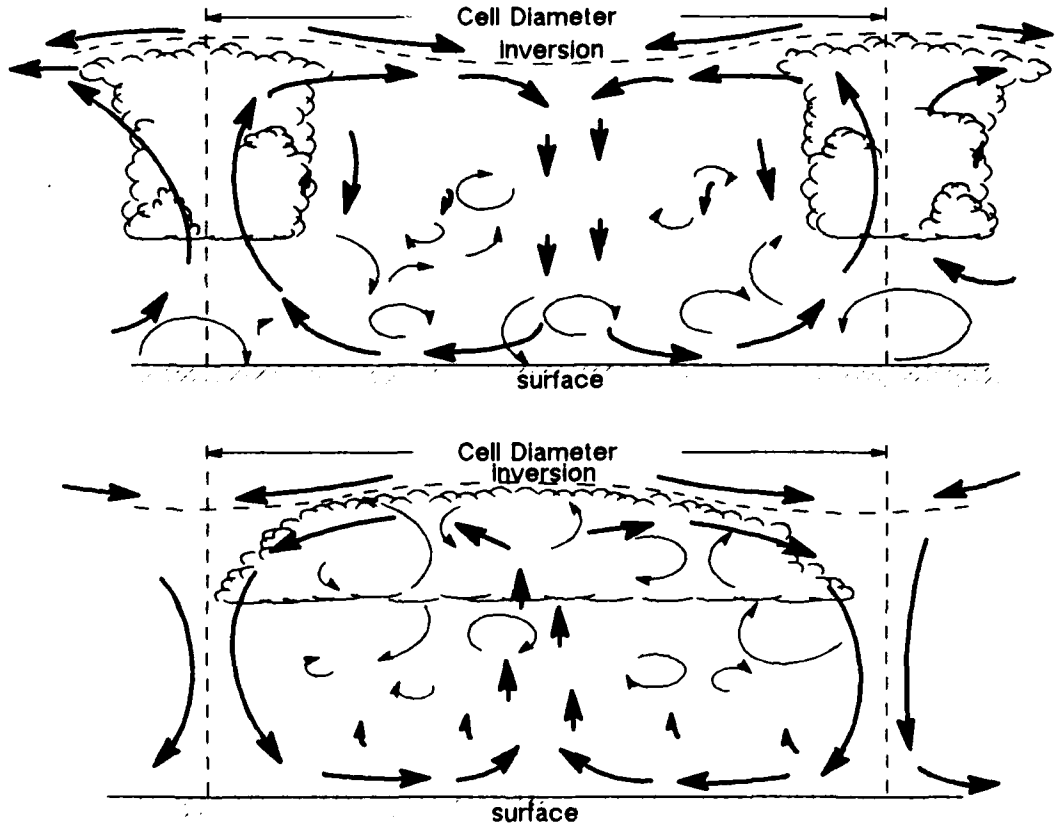


Figure 1. Cross-section of circulation direction for open and closed cells. Mesoscale cellular circulation is indicated by the heavy arrows, turbulent motion by light arrows (after Hubert, 1966; Agee and Lomax, 1978).

Secondly, Hubert noted the aspect ratio of atmospheric cells (20–40) is approximately an order of magnitude larger than that of laboratory cells (2–3). Similarly, a number of atmospheric effects have been examined to explain the flatter cell structure. Sheu *et al.* (1980) considered the effects of anisotropic turbulent diffusion, latent heat release and large–scale vertical motion. Van Delden (1985) also showed the effect of latent heat release in cell expansion. Fiedler (1984) has proposed an instability mechanism at the top of the CTBL due to entrainment effects, which introduces a much larger length scale. Finally, Rothermel and Agee (1986) have demonstrated that sufficiently strong thermal forcing (with no external physics) can produce large aspect ratio cells.

Agee *et al.* (1973) extended Hubert's initial study through an extensive world–wide analysis of satellite imagery, which was updated by Agee (1987). The results indicated that Mesoscale Cellular Convection (MCC)[1] occurs around the globe in climatologically preferred regions as shown in Fig. 2. Generally, open cells occur off the east coast of continents over warm ocean currents during the winter months, whereas closed cells are found primarily in the summer, to the west of continents over cooler ocean currents. Typically, MCC is a phenomenon observed over large regions of the oceans and is regarded as an important mechanism in the transport of heat, moisture, and momentum from the sea surface through the planetary boundary layer. These distinct formations of open and closed cells associated with air mass modification and air–sea interaction were labeled respectively as Class I and Class II MCC (but now correspond to the Type I and Type II CTBLs).

## 1.3 The Type I Cloud–Topped Boundary Layer

The World Meteorological Organization/World Climate Research Program workshop conducted at Colorado State University in April 1985 defined six types of CTBLs (see Agee, 1987). The importance of various thermodynamic and dynamic forcing mechanisms in each of these CTBLs is presented in Table 1. Since this case study concentrates on the Type I CTBL a more detailed discussion is included.

---

[1] Subsequent work by Agee, *et al.* (e.g., see Agee and Howley,1977 ) led to the use of the acronym MCC and a formal definition of Mesoscale Cellular Convection.

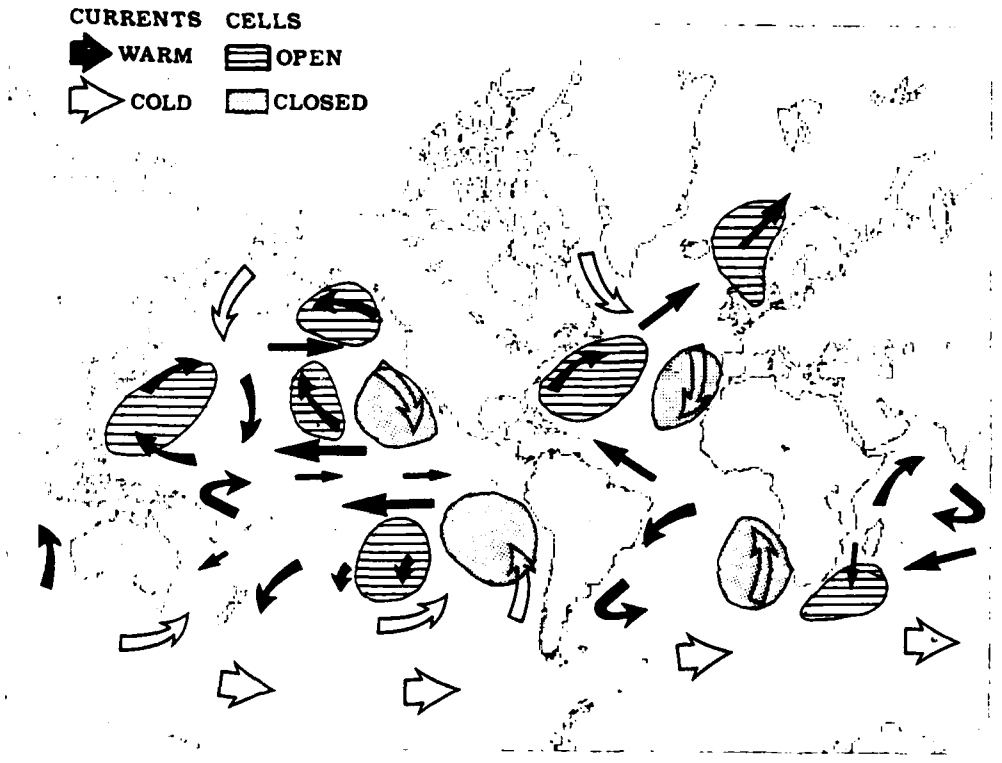


Figure 2. A depiction of favored regions of open and closed mesoscale cellular convection with respect to warm and cool ocean currents (after Agee *et al.*, 1973; Agee, 1987).

Table 1. The six types of cloud-topped boundary layers with the roles played by the major dynamic and thermodynamic forcing mechanisms in their formation and structure (after Agee, 1987).

| CTBL TYPE | Thermal Forcing | Radiative Forcing | Latent Heat Release | Cloud Evaporation | Inversion Layer/ Free Atmosphere | Small-scale Turbulence | Wind Shear | Large-scale Vertical Velocity | Dynamic Instability |
|---|---|---|---|---|---|---|---|---|---|
| I MCC | Dominated by surface heating and low level forcing | Important | Important with secondary effects | Important secondary mechanism Entrainment | Important due to collective entrainment effects | Important | Weak | Strong down Thins the layer | Important Thermal mode MEI |
| II MCC | Little effect Near neutral balanced | Dominant with diurnal sensitivity | Weak importance Diurnal | Entrainment of overlying dry air CIFKU | Important to entrainment and CIFKU effects | | Weak effect | Weak down Thins the layer | Thermal mode MEI |
| III Continental | Dominant surface heating Weak | Some importance Dominant | Very important Weak effect | Secondary importance Weak | Important Important | Important | Very important Weak | Important Weak | Important thermal symmetric MEI |
| IV Polar Stratus | Cooling bottom sfc thermal sink | Dominant Seasonal cycle | Not important | None in winter Weak in summer | Temperature and moisture profiles important | Weak effect | Weak effect | Weak effect | |
| V Large Scale | Not important | Diurnal importance | Important | Weak | Important | | Very important | Important | Forcing from large-scale instabilities |
| VI Trade Winds | Moisture Bouyancy | | Important | Weak effect | Important | | Important | Weak down | Thermal mode |

Briefly, the Type I CTBL is a convective marine boundary layer which evolves as polar or arctic air masses move off to the east of continents. Here the air mass encounters a warm ocean current, such as the Gulf Stream or the Kuroshio, and receives substantial amounts of heat and moisture from the sea surface. This creates a shallow superadiabatic surface layer which continues to build a deeper convective layer in time, further off shore. As the fetch increases, the air becomes modified by the transport of heat and moisture so that the cloud free area gives way to the formation of cloud streets with a wavelength on the order of 4–8 km. The initial cumulus cloud formation typically occurs 12–18 hours after frontal passage. Further downstream, as time progresses, the two-dimensional cloud bands can give way to cellular arrays of clouds. These arrays will likely consist of open MCC with diameters of 20–60 km in a boundary layer with depths on the order of 1.5–2.0 km. This pattern may persist for several days and typically extends from the point of formation, eastward, to the frontal cloud band. Figure 3 presents a cross-section through a typical Type I CTBL and also shows the two scales of undulation present at the top of the convectively-mixed layer. The large scale changes in the height of the inversion base are due to the difference between open and closed MCC layers. The closed MCC is deeper, in part due to the effect of additional latent heat release in the more cloudy region. Radiation and entrainment effects are also suspected. The smaller scale undulations are associated with the motions occurring in

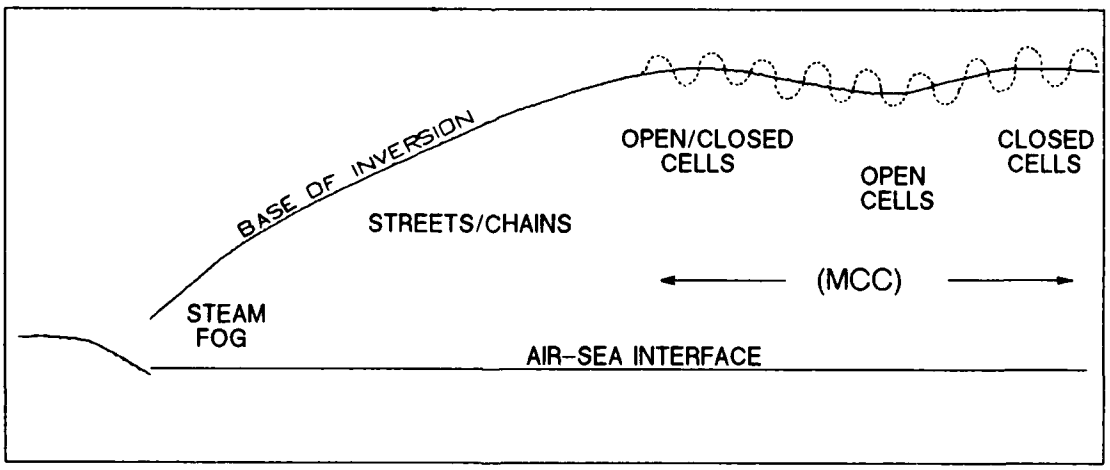


Figure 3. Schematic of a vertical cross-section through a typical Type I CTBL (from shoreline to sea) and associated convective phenomena. Variation of convective depth between open and closed cell regions is noted, as well as the dashed line for individual cell circulations (after Agee, 1987).

individual cells. The branches of rising motion cause a convective penetration or increase in the inversion base height, while the branches of descending motion are associated with a lower inversion base.

As stated previously, strong thermal forcing due to heating at the surface is the main factor contributing to the formation and structure of the Type I cloud–topped boundary layer. Other important thermodynamic and dynamic mechanisms noted by Agee (1987) include:

a) radiative forcing due to differential heating and cooling at the cloud top. Strong infrared cooling can occur through the top 30 m of the cloud while shortwave solar heating may extend through the top 100 m. This can result in the radiative destabilization of the cloud top (but this is perceived to be more important in the Type II CTBL).

b) Latent heat release from cloud formation yields additional convective buoyancy, further augmenting the turbulence and entrainment;

c) large–scale vertical motion, the strength of which may determine the type of cells and affect their vertical extent;

d) properties of the capping inversion, since this is the source region of air entrained into the convective layer;

e) dynamic instability through the interaction of length scales for the various physical processes that can occur (*e.g.*, mesoscale entrainment instability);

f) cloud evaporation associated with the entrainment of very dry parcels at the top of the CTBL possibly resulting in the formation of upside down convection (see Randall, 1980);

g) small–scale turbulence due to thermals and mechanical eddies (which largely result from the processes discussed above) and the combined effect of this turbulence field on the entrainment[2].

---

[2] Entrainment is defined as the movement or "pulling down" of stable inversion layer air into the convective layer, which generally results in the destruction of turbulent kinetic energy.

## 1.4 Airborne Investigations of Type I CTBLs

As interest in the area of shallow mesoscale convection increased, it became apparent that the ground–based surface and upper–air observational network was insufficent for detailed studies. In this respect, the use of airborne instruments, particularly aircraft, has proven invaluable as a measurement platform for investigating the cold air outbreak phenomenon and the subsequent air mass modification which occurs in the Type I CTBL. Bunker (1960) reported the first measurements from a cold air outbreak in the form of direct heat and moisture flux over the North Atlantic. Lenschow (1965) followed shortly therafter, but concentrated efforts over Lake Michigan while detailing the vertical flux of sensible heat and the resultant air modification. The flux measurements in these early cases used the eddy correlation techniques and were thus limited to wavelengths less than 1 – 2 km.

Lenschow (1973a) conducted further studies and found that the boundary layer which develops over the Great Lakes during cold air outbreaks shows striking similarities to those observed off the east coast of continents. Both have a well developed convective layer which exists between a strong inversion layer and a warm water surface. The amount of heat and moisture transfer from the surface to the air mass is comparable, as is the duration of the phenomena. A major difference between the Great Lakes and the oceans is the limited extent of water, resulting in a much smaller fetch and a difference in cloud geometry. The clouds over Lake Michigan are organized into streets and two–dimensional bands, whereas those over open ocean surfaces are allowed to organize into both 2–D bands and large polygonal convective cells. These well–mixed boundary layers, capped by a stratus cloud layer, with a sharp interface at the top, were modeled by Lilly (1968). In Lilly's model, radiational cloud top cooling was the driving mechanism of the turbulent mixed layer. While Lenschow found this to be an important mechanism, it was thermal forcing in the form of large upward heat fluxes at the surface which played the dominant role. The large vertical fluxes of latent and sensible heat over the lake lead to strong downstream heating, as shown in Fig. 4.

A significant study on the growth of the convective boundary layer was reported by Kaimal *et al.* (1976). This study investigated the development of the boundary layer over Minnesota using an instrumented 32 m tower and a tethered 1300 $m^3$ kite balloon. Though this

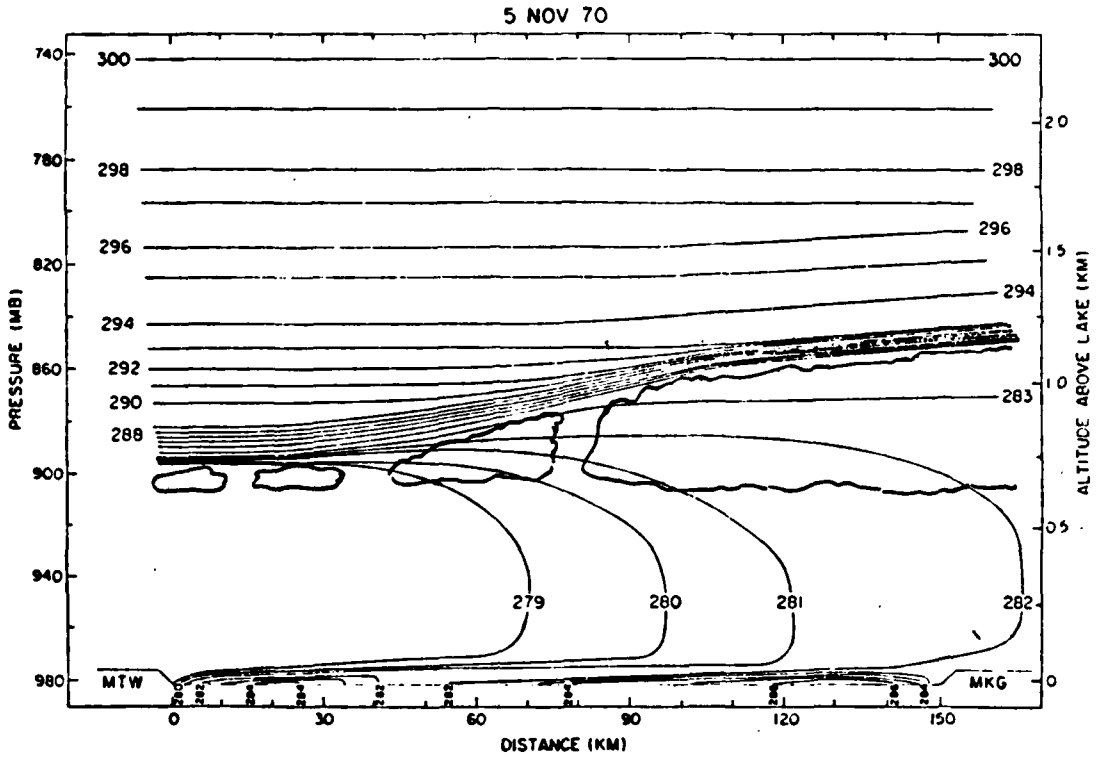


Figure 4. Vertical cross-section of potential temperature across Lake Michigan based on aircraft measurements (from Lenschow, 1973a) during a cold air outbreak.

study was conducted over land, was concentrated principally on the aspects of turbulence; and contained no clouds beneath the capping inversion, several aspects of the study are pertinent to this research.

The first of these was a simple conceptual model of the convective boundary layer. This model consisted of a three-layer structure in which different parameters were considered relevant to turbulence. These layers were 1) the surface layer, 2) the free convection layer, and 3) the mixed layer. Almost all wind shear and potential temperature gradient is confined in the very shallow surface layer, which extends up to 0.1 $z_i$, where $z_i$ is defined as the height of the lowest inversion base. Thus, wind shear plays a dominant role in this layer. In the free convection layer the height is the most significant length scale, while in the mixed layer the thickness of the boundary layer is the important length scale. The

thickeness of the boundary layer was further found to emerge as the controlling length scale through the entire convective boundary layer.

Second, they found that as the depth of the boundary layer grew throughout the day, there was a strong tendency in the mixed layer for the wavelength in all components to be the same and roughly equal to 1.5 times the boundary layer thickness. This was also evident in the wind velocity and temperature spectra. All four spectra displayed prominent peaks at a wavelength ~1.5 $z_i$, which corresponds to the length scale of large thermals that dominate the circulation in the boundary layer. They concluded that these were the longitudinal roll vortices which LeMone (1973) found in convective boundary layers with mean mixed layer wind speed in excess of 7 m/s. The spectra of the velocity components were also generalized to give the onset of the intertial subrange in the mixed layer at a wavelength ~ 0.1 $z_i$.

Lastly, this study demonstrated that there was evidence of substantial heat and momentum entrainment into the boundary layer through the capping inversion. The temperature and heat flux statistics in the upper half of the boundary layer were strongly affected by the inverted plumes of entrained warm air descending into the region. Large stress values were also encountered but could be explained in terms of momentum entrainment across the velocity jump within the inversion. The roll vortices must then provide an effective mechanism for transporting heat and momentum between the earth's surface and the inversion base in a convective boundary layer.

Several studies along the same lines as those mentioned above have reported on findings from aircraft data collected during the AMTEX (Air Mass Transformation Experiment) field program which took place over the East China Sea during February in 1974 and 1975. Rothermel and Agee (1980) analyzed a 1 $s^{-1}$ Electra aircraft data set to develop a model of the circulation within a closed cell. Data taken from 100 m and 970 m above sea level were analyzed through regions of closed cell MCC and represented in spectral form. The model presented shows a double cycle in the temperature profile at the 100 m level where the cell walls and center were warm with cool regions in between. At the 970 m level the temperature profile exhibited a single cycle where the cell was cool in the center and warm in the periphery. Explanations presented for this double cycle at 100 m included both warming and cooling mechanisms. The warming mechanisms included sensible heat tranfer from the

warmer sea surface, dry adiabatic subsidence and the entrainment of warmer air from the inversion layer. Evaporative cooling was regarded as a possible factor near the sea surface. A second finding was an energy shift with height in the vertical velocity spectrum. Generally the shift was to larger wavelengths, but not uniformly at all frequencies.

Further studies on the AMTEX data were conducted by Ross and Agee (1985). This consisted of seventeen cases of 20 Hz data collected by aircraft flights in the marine boundary layer. The cases were categorized into one of three convective states for the boundary layer based upon the air–sea temperature difference $\Delta T$. The categories were : 1) strongly convective ($\Delta T \geq 5°C$), 2) weakly convective ($2°C \leq \Delta T < 5°C$), and 3) non–convective ($\Delta T < 2°C$). They found evidence for the existence of a basic convective mode (BCM) with aspect ratio comparable to that of B–R convection in the spectral representations of the strongly convective cases. They postulated that an upscale transfer of energy leads to the evolution of MCC from the BCM. The transfer from high wavenumbers to lower wavenumbers was reported to be driven by the strong thermal forcing present whenever the Class I MCC (due to heating from below) was observed. Intermediate modes were also thought to play an important role in the upscale energy transfer.

Another important finding of Ross and Agee concerned the energy spectra of strongly convective cases. Non–MCC cases showed the presence of greater energy in the spectra at high wavenumbers compared to MCC cases. This suggests that in similarly strong convective cases, there is an upscale energy cascade from the smaller modes to the larger modes. Specifically, in the strongly convective MCC cases this cascade of energy appears to happen, while in the strongly convective non–MCC cases it apparently does not happen. Thus, more energy exists at the higher wavenumbers.

More recently Atlas et al. (1986) combined lidar and 40 Hz aircraft observations to examine the details of the marine boundary layer off the Atlantic coast of the US during the MASEX (Mesoscale Air–Sea Exchange) project conducted in January 1983. In examining the lidar data they found entrainment across the inversion in the form of small scale perturbations (~200–300 m) superimposed upon the larger scale (1–2 km) undulations of the inversion. The raw aircraft temperature data displayed sharp oscillations in this region, as well, with typical horizontal scales of 1 to 2 km. These undulations along the top of the inversion

obviously represent the transition zone between the clear warm air above and the well-mixed cooler air below.

Combining features from all these studies, one can devise the sounding of potential temperature for a typical Type I cloud-topped boundary layer as shown in Fig. 5. The development of the Type I CTBL which occurred after a cold air outbreak (CAO) over Lake Michigan on 10 January 1984 is the focus of this research.

## 1.5 Research Objectives

In general, the objective of this research is to study a well-mixed convective boundary layer under maritime influences (i.e. the Type I CTBL). More specifically, the goal is to conduct an observational case study of the cold air outbreak (CAO) which occurred over Lake Michigan on 10 January 1984. Toward this end, there were five major objectives:

1. Determine the synoptic setting which led to the CAO over Lake Michigan.
2. Perform regional analyses to determine the extent and strength of the outbreak.

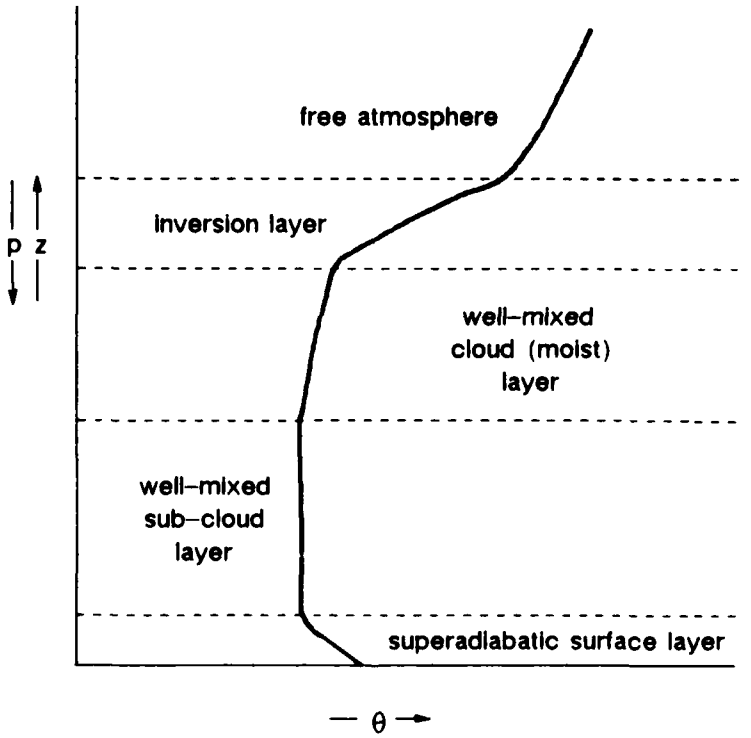


Figure 5. Vertical profile of potential temperature for a Type I CTBL.

3. Examine the variation of the depth of the CTBL due to the modifying influences of Lake Superior and Lake Michigan.

4. Using the special aircraft data sets and spectral representation of the aircraft data, examine the dynamic and thermodynamic structure of the CTBL to determine the mode of the organized mesoscale convection, the magnitude of the heat, momentum and moisture fluxes, and the relationship of the capping inversion layer to the underlying well-mixed convective layer.

5. Incorporate any findings into an improved conceptual model of a Type I CTBL.

# 2. DATA SETS AND ANALYSIS METHODS

## 2.1 Conventional Data Set

Observational data in the form of surface and upper air reports were provided by two sources. Upper air soundings at 0000 and 1200 GMT for the United States and Canada were provided by the National Center for Atmospheric Research (NCAR), for the period 7 – 11 January 1984. NCAR also provided surface observations at three hour intervals, beginning at 0000 GMT, for the same area and time frame. The surface observations were supplemented by data collected by the Purdue Mesoscale Convection Research Group. This consisted of hourly observations from 1300 – 2000 GMT for 10 January 1984. Finally, one and two km resolution visible and two km resolution infrared GOES satellite images during 9 – 11 January 1984 were used in this research.

## 2.2 Lake Effect Snow Studies (Project LESS) Data Set

Project LESS was a cooperative field experiment conducted from 1 December 1983 to 24 January 1984 with the purpose of collecting data from regions directly over, to the south, and to the east of Lake Michigan. Of primary interest were data gathered during cold air outbreaks of polar and arctic air masses and their subsequent modification as they crossed the comparatively much warmer surface of Lake Michigan (Rokosz, 1985).

The groups involved in Project LESS were positioned around the lake for the optimum measurement of the lake effect phenomenon. The University of Chicago Cloud Physics Group was located on the east side of the lake at Muskegon, Michigan (MKG) while the Purdue University Mesoscale Convection Research Group manned two other locations. The first of these was on the south end of Lake Michigan at the Indiana Dunes National Lakeshore Headquarters in Porter, Indiana (NWI) and the second at the Purdue University campus in

West Lafayette, Indiana (LAF). NCAR provided the field program with highly specialized equipment used in the collection of supplemental upper air and surface observations.

### 2.2.1 Portable Automated Mesonet (PAM II) Network

One type of specialized observational equipment supplied by NCAR were 24 PAM II remote surface weather stations. These units measure the surface pressure, air temperature, humidity, wind direction, wind speed, and precipitation amount, and communicate the data back to NCAR in real-time (via the GOES satellite). The PAM II sites were located (see Fig. 6) to increase the station density on the leeward side of the lake during cold air outbreak (CAO) events. However, Rokosz (1985) reported that data from 9 of the 24 sites contained enough uncertainty in their measurements (due to calibration errors) to exclude them from the analyses. Of the fifteen remaining, the pressure measurements were accurate to within $\pm$ 1mb, and the dewpoint temperatures were completely unreliable. Even though the pressure variation does not appear important, it can cause a significant error in a mesoscale analysis. As a result, only the temperature and wind data were used to complement the regular observations.

### 2.2.2 Special Rawinsondes

The research groups from Chicago and Purdue manned rawinsonde stations at Muskegon and Porter, respectively. They provided upper air soundings at 1200 GMT on a daily basis. Additional soundings were taken at these stations as necessary during periods of CAOs. The U. S. Army *SNOW TWO* field experiment conducted at Camp Grayling, Michigan (CGR) was a source of additional rawinsonde information. These soundings were used in conjunction with the National Weather Service and Canadian Atmospheric Environment Service rawinsonde soundings to perform upper air analyses.

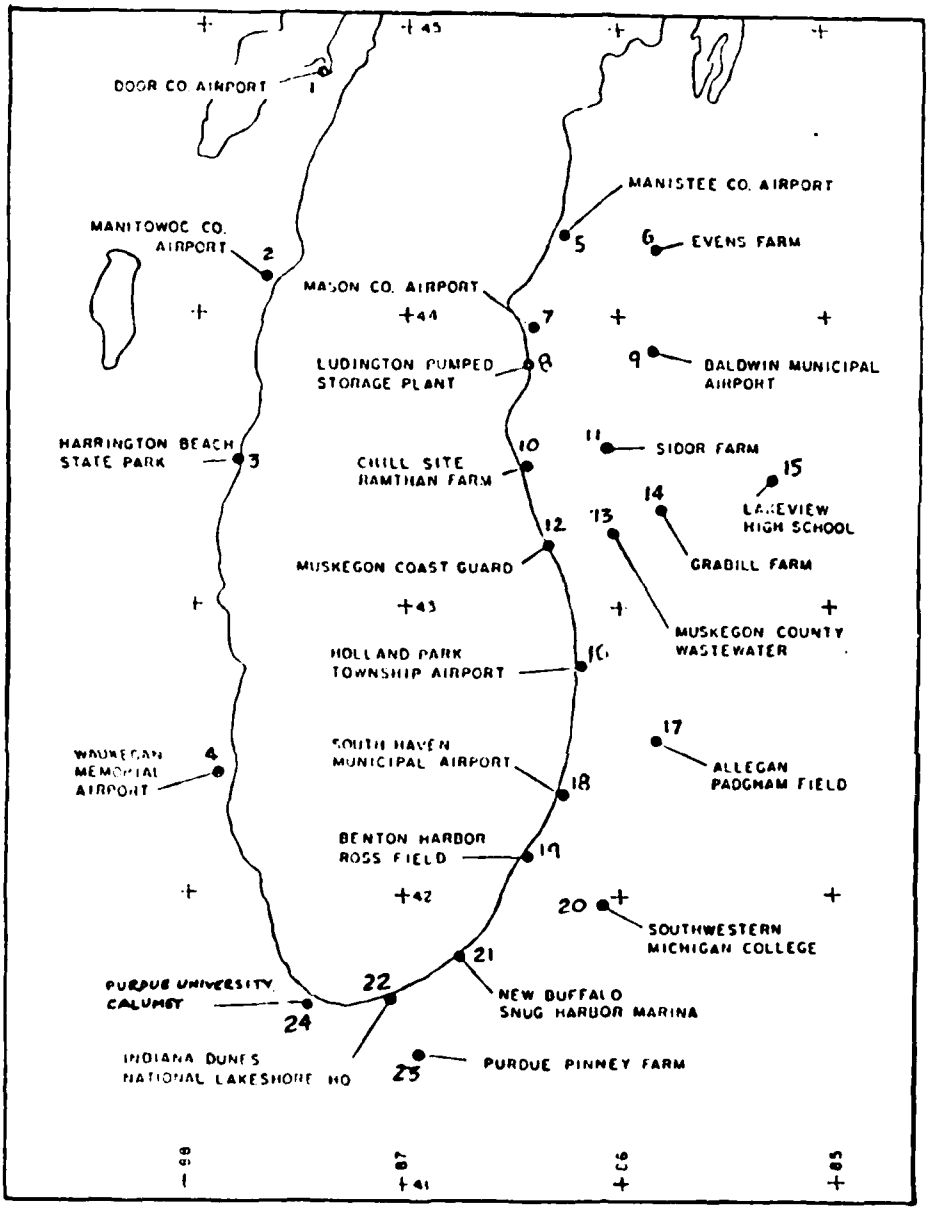


Figure 6. Location of the 24 PAM II stations deployed around Lake Michigan during Project LESS (from Rokosz, 1985).

### 2.2.3 Aircraft Flights

Highly detailed flight level data were provided by NCAR's King Air and Queen Air research aircraft under the operational control of the University of Chicago Cloud Physics Group. These aircraft are capable of measuring and recording over 150 variables which detail information for both the atmosphere and the aircraft's operation. Depending on the variable, instruments on board and those attached to the exterior of the aircraft can sampie at either one or twenty measurements per second. The King Air aircraft flew 15 research missions during Project LESS. Of these missions, flight #85 (see Fig. 7), from 1558 to 2042 GMT on 10 January 1984, showed the most promise of having penetrated a well defined convective boundary layer associated with a CAO over Lake Michigan.

## 2.3 Analysis Methods

A variety of methods were needed to obtain the different types of analysis used in the completion of this research. Computer-aided objective analysis schemes developed at Purdue University made up the majority of the standard surface and upper air analysis. These included thermodynamic and kinematic methods. A man-machine mix was also judiciously used for the upper air analyses. This was reserved for the few times the objective methods provided too much detail which generated or masked features not acceptable to a knowledgeable analyst. A brief discussion of each of the principal analysis routines follows.

### 2.3.1 PROAM

The Purdue Regional Objective Analysis of the Mesoscale (PROAM) and its upper air counterpart described later (PROAMU) were two analysis packages used in this study. Although these packages were used as tools (i.e. no enhancements, developments, or add-on features), several aspects of each method do merit a brief description. PROAM is an objective surface analysis package implemented at Purdue by Smith and Leslie (1982) using a two-pass Barnes-type analysis scheme (Barnes 1964, 1973). The idea behind the Barnes

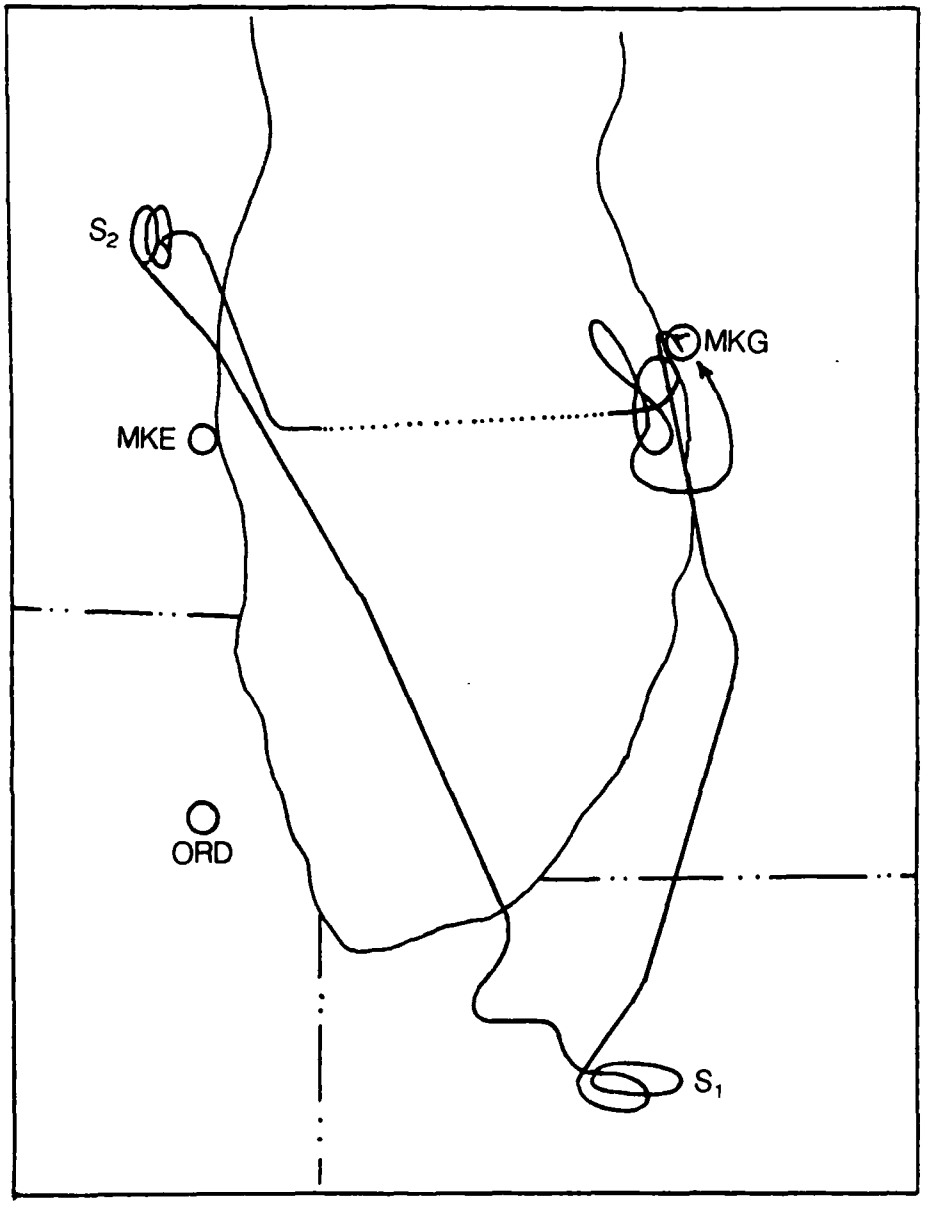


Figure 7. Path of NCAR King Air research aircraft flight #85 from 1558–2045 GMT on 10 January 1984. Vertical scundings were made as $S_1$ and $S_2$. The dashed line denotes the flight segmeni selected for spectral decomposition (discussed in a later chapter).

scheme is to fit irregularly spaced data to a uniformly spaced grid by means of a weighted average. This scheme uses all stations within a circular region around a grid point to determine the value at the grid point. The weight applied to each station decreases exponentially with distance from the grid point. Surface reports of ambient air temperature, dew point temperature, wind direction, wind speed, and pressure make up the state variables required for input. Uniform grid point values can then be used to calculate derived quantities such as vorticity and divergence by means of finite differencing.

The fundamental premise behind the Barnes scheme is that all atmospheric variables can be represented as the summation of an infinite number of independent harmonic waves. PROAM acts to enhance those of a selected wavelength and damp others. This is done by a filter parameter, $\alpha$, and a convergence parameter, $\gamma$, embodied in the response function.

The response function is a low pass filter which determines the percentage of the signal to retain. Ideally, the filter will be a step function with zero response for waves shorter than the minimum resolvable wavelength and 100% for those longer. Barnes (1964) and Koch *et al.* (1983) have shown that the minimum resolvable wavelength is 2 $\bar{d}$, where $\bar{d}$ represents the mean station spacing. For the first pass of PROAM the response function is given by

$$R_1(f) = \begin{cases} 1 & f \leq f_c \\ 0 & f > f_t \\ \exp\left[-\alpha \left(\frac{\pi}{\lambda}\right)^2\right] & f_c \leq f \leq f_t \end{cases} \qquad (2.1)$$

where $R_1(f)$ is the response function after the first pass, $f_c$ is the cutoff frequency and $f_t$ is the terminating frequency. This type of low pass filter will suppress high frequency short waves and retain large waves. Selecting larger values of $\alpha$ will produce a smoother analysis (i.e. decrease the magnitude of the difference between the highest and lowest grid point values).

A second pass is made through the data to keep the response for short waves small and to increase the longer resolvable waves. The response function for this pass is given by

$$R_2(f) = \begin{cases} 1 & f \leq f_c \\ 0 & f > f_t \\ R_1(f)\left[1 + R_1(f)^{\gamma-1} - R_1(f)^{\gamma}\right] & f_c \leq f \leq f_t \end{cases} \qquad (2.2)$$

where $\gamma$ is the convergence parameter. The purpose of the convergence parameter is to 1) recover the short wave amplitudes quickly and save computer time, and 2) adjust grid point

values to approach the value of the closest station. Koch *et al.* (1983) suggests a method of choosing $\gamma$ to prevent what has been coined as the "plateau effect". This occurs when the grid spacing, $\Delta x$, is chosen to be less than 1/3 $\bar{d}$. For this choice of $\Delta x$ an average of two grid points will lie between reporting stations. On the second pass $\gamma$ will cause each grid point value to approach the value of its closest station and create an artificial gradient. With a grid spacing near one-half $\bar{d}$, on the average only one grid point will lie between stations. The grid point can then take on a value approximating the average of the stations. Thus, it is important to determine the wavelength of the phenomenon under examination and then select appropriate values for the filter and convergence parameters. The values used for this case study are included below in Table 3.1. Generally, surface observations in the Midwest have a mean station spacing of between 75 and 100 km ($150 \leq 2\bar{d} \leq 200$ km). Under these circumstances Smith *et al.* (1986) have shown that values of $\alpha = 0.6$ and $\gamma = 0.2$ yield good results. A complete description of PROAM and early test results can be found in Smith and Leslie (1982). An error analysis of PROAM is presented in Smith *et al.* (1986).

Table 2. Parameter specifications for case study PROAM and PROAMU analyses.

| | meso $-\beta$ | meso $-\alpha$ | |
|---|---|---|---|
| | PROAM | PROAM | PROAMU |
| Latitude of central grid point (°N) | 43.5 | 44.0 | 44.0 |
| Longitude of central grid point (°W) | 86.5 | 89.5 | 89.5 |
| Grid spacing $-\Delta x$ (km) | 60 | 150 | 150 |
| Filter Parameter $-\alpha$ ($10^{-4}$ km$^2$) | 0.6 | 13 | 13 |
| Initial radius of influence (km) | 150 | 450 | 450 |
| Number of grid points in N-S direction | 25 | 20 | 20 |
| Number of grid points in E-W direction | 25 | 20 | 20 |
| Minimum number of stations affecting grid point | 3 | 3 | 2 |

### 2.3.2 PROAMU

PROAMU is a modification of PROAM for the analysis of upper air data. Since upper air stations are spaced on the average of 400 km, this method is only useful for resolving waves greater than 800 km or on the meso-$\alpha$ and larger scales. A PROAM-type objective analysis usually provides better detail for the small scale features when compared to the standard National Weather Service (NWS) facsimile products. In addition, the derived fields not available from NWS can be examined. Lidrbauch (1986) provides a comparison of NWS facsimile charts and PROAMU output along with a detailed discussion of PROAMU. A brief discussion of PROAMU is included here for completeness.

For input, PROAMU requires the ambient and dewpoint temperatures, wind direction and speed, and height of the mandantory pressure surface (either 850, 700, or 500 mb). Table 3.1 contains the PROAMU analysis parameters used in this study. The output is the same as for PROAM except heights of the isobaric surface are substituted for pressure and there is no altitude field. For the present study, the following quantities were calculated/analyzed routinely at all levels: 1) height, 2) streamlines, 3) ambient temperature, 4) specific humidity, 5) velocity vectors, 6) relative vertical vorticity, and 7) horizontal divergence.

### 2.3.3 PUKAM

PUKAM (Purdue University Kinematic Analysis of the Mesoscale) is a collection of programs which perform kinematic and thermodynamic analyses on rawindsonde data. The method employs a scheme used by Sheu and Agee (1977) to assess the vertical structure of the atmosphere. This includes vertical profiles of horizontal divergence, vertical vorticity, and vertical motion derived through a first-order Taylor series expansion on the u and v wind components for three stations. The triangulation permits the calculations of four wind shears

at the center of the triangle from the sounding data of the three stations. The series expansions for the wind components are expressed as

$$u_i = u_o + \left(\frac{\partial u}{\partial x}\right)_o (x_i - x_o) + \left(\frac{\partial u}{\partial y}\right)_o (y_i - y_o) \tag{2.3}$$

$$v_i = v_o + \left(\frac{\partial v}{\partial y}\right)_o (x_i - x_o) + \left(\frac{\partial v}{\partial x}\right)_o (y_i - y_o) \tag{2.4}$$

where i = 1,2,3 represents the station locations at the verticies and o represents the center of the triangle. The four wind shears can be found by substitution of the observed u and v values into the above equations. This method allows for the solution of the wind shears at the center of the triangle without knowing the actual wind components at the center. From the shears the values of horizontal divergence and relative vorticity can be expessed by

$$\nabla \cdot V = \left(\frac{\partial u}{\partial x}\right)_o + \left(\frac{\partial v}{\partial y}\right)_o \tag{2.5}$$

$$\zeta = \left(\frac{\partial v}{\partial x}\right)_o + \left(\frac{\partial u}{\partial y}\right)_o . \tag{2.6}$$

Vertical motion can also be calculated using the kinematic method through use of the continuity equation in isobaric coordinates given by

$$\nabla_h \cdot V + \left(\frac{\partial \omega}{\partial p}\right) = 0 . \tag{2.7}$$

Taking the mean divergence $(\overline{\nabla_h \cdot V})$ of a layer ($\Delta p$) and integrating over that layer (taken to be 25 mb thick), Eq. (2.7) becomes

$$\omega_t = \omega_b + (\overline{\nabla_h \cdot V})(\Delta p) \tag{2.8}$$

where $\omega_t$ and $\omega_b$ deliniate the mean vertical motions at the top and bottom levels of the triangular region. Calculations are carried out from the surface to 500 mb. At one time an O'Brien (1970) adjustment scheme was used to reduce cumulative error in the calculations. However, Sheu and Agee (1977) found that adjustments were only significant in the middle and upper troposhere. Comparison of these vertical profiles between triangular regions

upstream and downstream of Lake Michigan show the modification that has taken place within the air mass.

Other features of PUKAM include spatial and time cross-sections. The cross-section programs can display temperature data in the form of ambient, dewpoint, equivalent potential and virtual potential temperatures, as well as specific humidity and geopotential height fields. The plots can contain a maximum of ten stations or time periods. These plots must then be subjectively analyzed to produce the vertical cross-sections. Finally, the PUKAM programs have the ability to produce automated skew T – log p thermodynamic diagrams up to 500 mb which include wind barbs at all reported height and mandatory pressure levels.

### 2.3.4 Spectral Decomposition

The method of analysis for the microscale and the lower end of the mesoscale in this study is spectral decomposition. This employs transforming the data from real space into Fourier space by means of the previously mentioned fast Fourier transform. Selection of data for examination from the total amount gathered was based on the following requirements:

1) the aircraft must remain at a constant height or pressure level within the boundary layer,

2) the aircraft must maintain a constant heading, and

3) the flight leg must contain a number of data points equivalent to a power of two.

The reason for this later constraint comes about because of the fast Fourier transform, which is used to spectrally represent the detail present in the data rich aircraft information. In addition to the above criteria, the flight path must be long enough to provide statistically significant results. As the parameters examined by spectral means were 20 per second measurements, the final result was the choice of a flight segment 819.2 seconds ($2^{14}$ measurements) long. Although several areas appear likely candidates for inclusion, only the fllight leg from MKE to MKG fulfilled all requirements. This is represented by the dashed line on the Fig. 7.

Spectral representation is also regarded as an objective method of data analysis. In effect, it allows the detection of intermediate modes, even in the presence of larger

circulations and the "noise" of small scale turbulence, which are often not easily detected using conventional methods. In the same fashion that an atmospheric variable can be represented by the sum of an infinite number of independent waves, it's measurement can be expressed as the sum of the scale components plus an error term as shown below.

$$\Phi_{total} = \Phi_{synoptic} + \Phi_{mesoscale} + \Phi_{microscale} + \Phi_{error} \qquad (2.9)$$

Here $\Phi_{synoptic}$ is the contribution to the variable from the larger meso $\alpha$ and macro $\beta$ scales, $\Phi_{mesoscale}$ shows the effects of convection including meso $\beta$ and meso $\gamma$ scales, and $\Phi_{microscale}$ represents large eddies and random small scale turbulence. The error term contains both systematic error and random error. Since the micro and meso scale are the primary interest of this study, the other signals must be removed from the data. This was accomplished by using the IMSL algorithm RLONE to fit the data to a linear profile and thereby to determine the slope and y-intercept. The data are detrended by removing both of these features. Removal of the intercept eliminates any systematic error due to improper calibration, inaccurate measurements, etc., while any random error will still be present. Subtracting the slope removes the synoptic scale which leaves the desired meso and micro scales.

The spectral energy densities were calculated using the fast Fourier transform FORTRAN subroutine FFTRC, also, developed by IMSL. Given N obervations, this algorithm computes the first (N/2 + 1) complex Fourier coefficients. The remaining coefficients are their complex conjugates. The energy densities are found by multiplying each coefficient by its complex conjugate and then normalized by multiplying by 1/N to yield results for the range of wavelengths from L to 2 L/N. In this case, L is the length of the flight segment in meters. The spectral density is then multiplied by the frequency and, lastly, plotted versus the log of the frequency. In this way, equal areas under the curve represent equal energy.

# 3. COLD AIR OUTBREAK: MESOSCALE $\alpha$ SETTING

This chapter is intended to detail the meso-$\alpha$ (see scale terminology given by Orlanski, 1975) synoptic scale events which occurred during the cold air outbreak (CAO) over Lake Michigan on 10 January 1984. Firstly, a brief description of daily surface weather features and the accompanying 500 mb analysis at 1200 GMT for the period 9 – 11 January 1984 is provided below to describe the circumstances which led to the CAO. Secondly, results from the different analysis methods are described to show the extent of the modification of the air mass by Lake Superior and Lake Michigan.

## 3.1 Synoptic Discussion

The first week of January 1984 consisted of mild weather for the Great Lakes with little mesoscale convective activity over Lake Michigan during this time. However, by 1200 GMT 9 January (as shown in Fig. 8) a strong cold front associated with a low pressure center in northern Canada entered the US and southerly flow in advance of this front brought snow showers to the northern Great Lakes region. Behind the front, high pressure (~1044 mb) in western Canada moved rapidly southeastward into Montana and North Dakota.

At 500 mb the main features of interest were the strong northerly flow found in the large amplitude wave in western Canada and a developing short wave over Lake Winnipeg moving through the base of the broad trough. Strong cold air advection in this northerly flow continued to push the cold air aloft southward into the upper Midwest.

As Fig. 9 shows, by 1200 GMT 10 January the cold front, under the influence of the strong flow at 500 mb, moved through the Great Lakes and became situated along the western slopes of the Appalachians. The high pressure center (~1040 mb) was centered over northern Minnesota and created light to moderate north-northwesterly flow over Lake Michigan. Temperatures over the Upper Mississippi Valley and the western Great Lakes

ranged from −15°C to near −35°C. Lake-induced cloudiness developed as the much colder air crossed Lakes Superior and Michigan. The clouds extended into northwestern Indiana and western Michigan with lake-effect snow falling along the southern and southeastern shores of Lake Michigan.

The 500 mb upper-air pattern shows continued cold air advection into the base of the upper level trough. As a consequence, the amplitude of the long wave increased further, moving to the south as the short wave continued around the base of the trough.

On 11 January the entire region was dominated by high pressure with centers to the northeast (~1033 mb), northwest (~1034 mb) and south (~1031 mb) of the Great Lakes. This brought light surface winds, generally less than 5 m/s, from variable directions. Over Lake Michigan weak northwest flow off the west shore became opposed by east-northeasterly flow off the east shore. Prior to the dissipation of the cloudiness, the convection became concentrated into one near-shore mesoscale band on the Michigan side of the lake due to the opposing flows.

The increase in zonal flow at 500 mb over the Northern Plains, as manifest in Fig. 10, came about for two reasons. The first is that the short wave has nearly completed its rotation through the base of the upper level trough but has not yet started moving northeastward. Secondly, another short wave has moved into the Rockies and significant cold air advection associated with this wave has deepened the portion of the upper air trough over the western US which, consequently, decreased the northerly flow in the Midwest.

To summarize, the key point of the synoptic discussion is that the weather pattern evolved and resulted in polar air with northerly flow over Lake Michigan and environ on 10 January 1984. This pattern was fortuitous in that a lake-effect convective boundary layer was produced, with lake-effect snow in northwestern Indiana. This weather event created an ideal Type I CTBL for the Purdue Mesoscale Convection Research Group's participation in Project LESS.

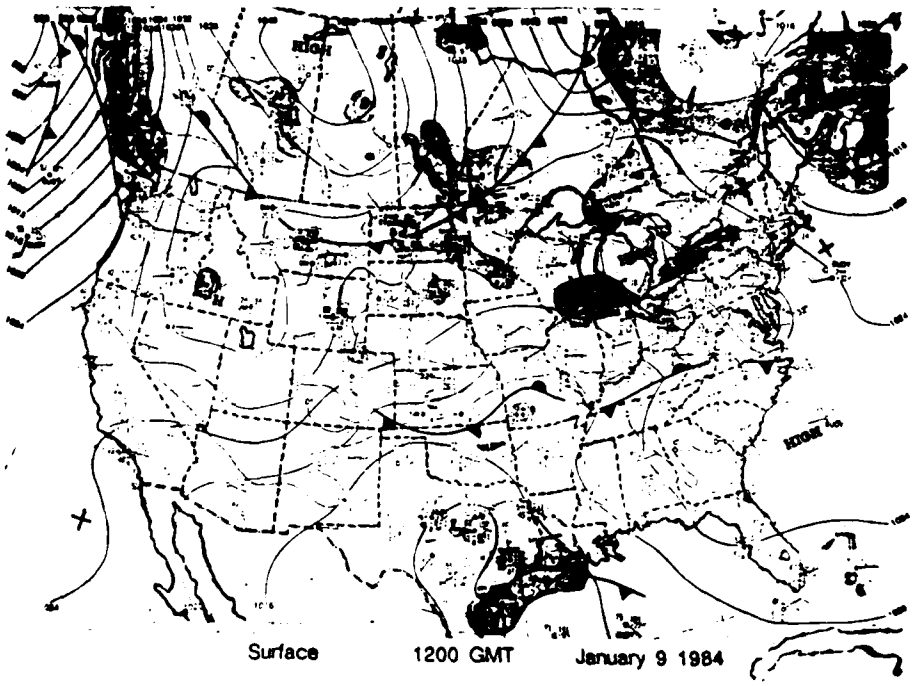


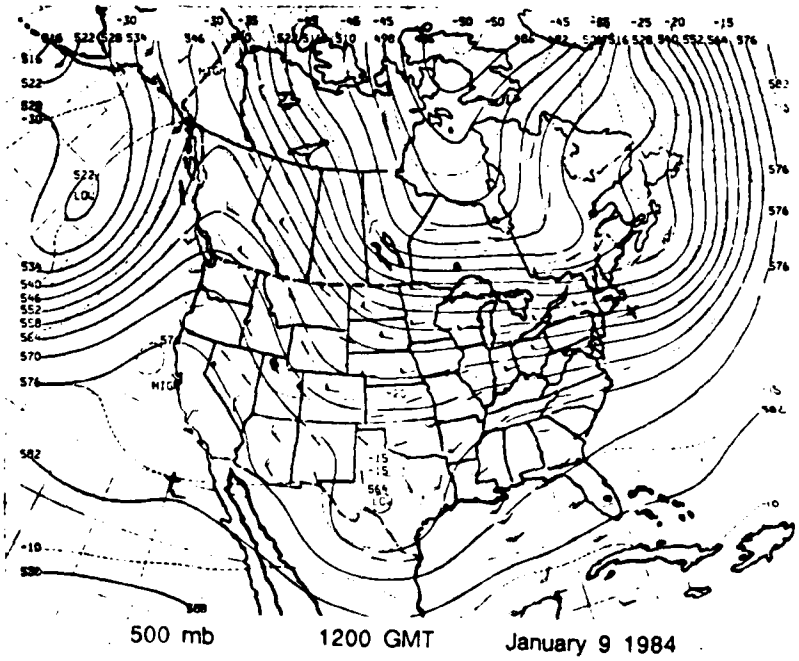


Figure 8. Surface and 500 mb analyses for 1200 GMT 9 January 1984.

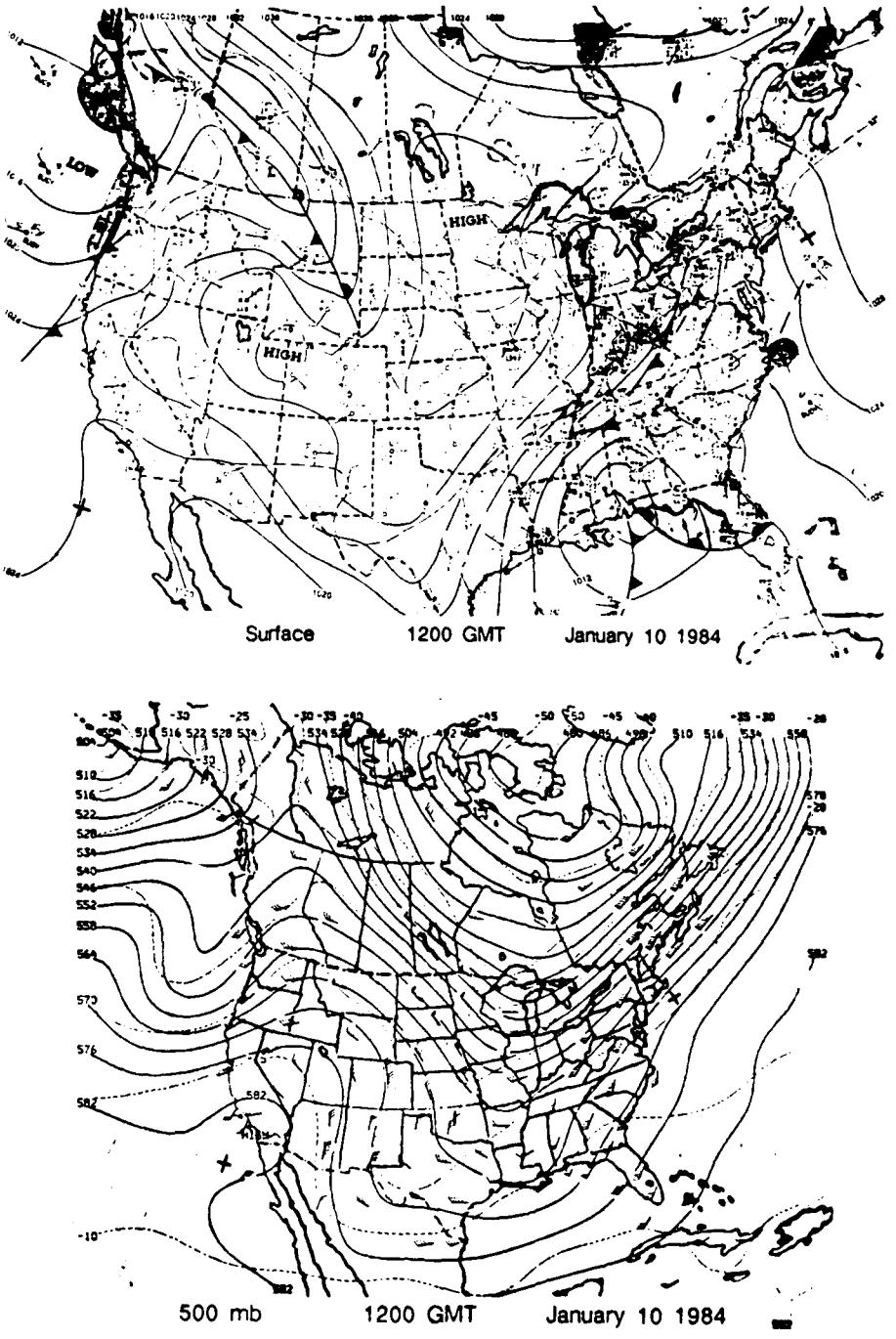


Figure 9. Surface and 500 mb analyses for 1200 GMT 10 January 1984.

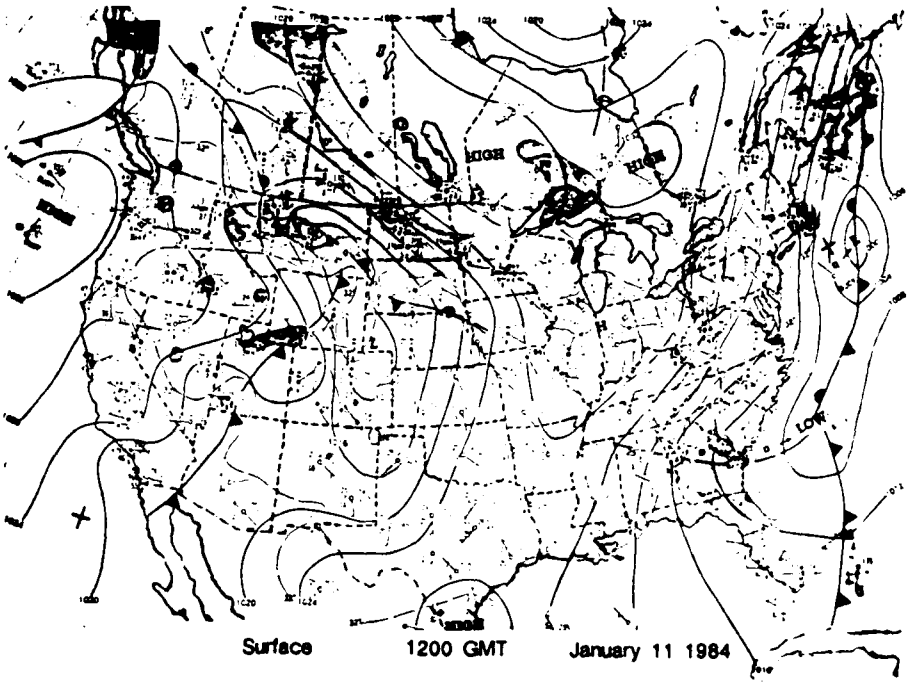


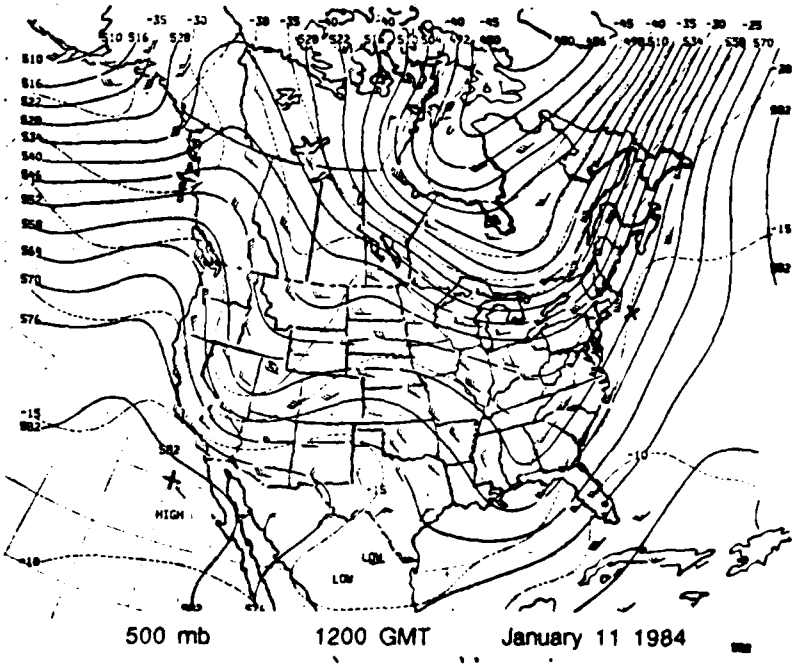


Figure 10. Surface and 500 mb analyses for 1200 GMT 11 January 1984.

## 3.2 Meso-$\alpha$ Analyses

As mentioned previously, the main area of interest is the Great Lakes region, specifically Lake Michigan. Therefore, the meso-$\alpha$ domain was selected to include the entire region. The surface and upper air stations included in this region which were used for the PROAM, PROAMU, and PUKAM analyses are shown within the dashed lines of Fig. 11. The following paragraphs show the presence of the leading edge of the cold air mass in the GOES satellite images and in the PROAM and PROAMU analyses as it moves through the area of the Great Lakes.

At 0000 GMT 10 January the GOES infrared satellite imagery (Fig. 12) has a frontal cloud band oriented slightly southwest to northeast across central South Dakota, southern Minnesota, and the northern tip of Wisconsin. Turning to the PROAM analyses, the pressure pattern has a weak trough (see Fig. 13) extending through most of the Great Lakes and Ohio Valley states, but little indication in the contours for the cold front in the Northern Plains. The surface temperature field, on the other hand, has a strong gradient for the cold front. This thermal support continues upward through the atmosphere to 850 mb; but, as one might expect for a shallow cold air mass, little support is indicated at 700 or 500 mb. Flow at the surface (see Fig. 14) is strong (generally > 10 m/s) and northerly from Minnesota westward, while it remains light and variable over the lakes. From 850 to 500 mb the flow is from the northwest, becoming westerly with increasing with height over the Great Lakes.

By 1200 GMT 10 January, GOES imagery (Fig. 15) shows the cold front angled southwest to northeast from northern Missouri, across the southern one-third of Lake Michigan and across northern Lake Huron. The surface isotherms (shown in Fig. 16) result in a complex pattern as the cold front moves into the region where a quasi-stationary front was present just 24 hours previous. The isotherms, however, do show a warm pocket over the southeast end of Lake Michigan. This indicates the heat flux from the lake surface into the air mass which is modifying the continental polar air mass over this small area while leaving most of the surrounding region undisturbed. Figure 16 also shows that the 850 mb trough previously in central Canada has moved through the Great Lakes and connected with the long wave trough over the Midwest. Strong cold air advection continues throughout the Great

Lakes and Ohio Valley states. Figure 17 shows the winds in the lower troposphere going from northerly at the surface to north-northwest at 850 mb to west-northwest at 500 mb.

During the next 12 hours, the satellite portrayal of 0000 GMT 11 January (Fig. 18) shows the convective boundary layer well established over Lake Michigan with a cloud free path on the west shore, clouds over the eastern 3/4 of the lake and nearly clear skies with snow covering the ground elsewhere. The surface is dominated by weak high pressure with the thermal pattern still showing some signs of air mass modification in the form of a warm pocket of air over the southern tip of Lake Michigan (see Fig. 19). Weak cold air advection is still indicated at the 850 mb level over Lake Michigan, but the winds are now more westerly at all levels. The isotherms over the Great Lakes are uniformly spaced and oriented west to east, indicating a ceasation to the air mass modification. The surface winds (Fig. 20) are variable in direction, but principally out of the west in Wisconsin and from the northeast in Michigan. Aloft, winds are northwesterly at all levels.

### 3.3 Meso-$\alpha$ Indications of Air Mass Modification

As stated previously, at 1200 GMT 10 January there were two types of air present over the Great Lakes; unmodified and modified continental polar air. The limits to the areal modification are demonstrated in Fig. 21. Note the backing of the winds (due to cold air advection) from the surface to 850 mb over most of the area. The heavy solid line and heavy dashed line follow the streamlines at the surface and 850 mb, respectively, which pass by the western tip of Lake Superior and, thereby, represent the furthest western extent of lake-induced air mass modification. Air which lies to the west of the heavy streamlines is unmodified continental polar air, while air which lies to the east has been modified to some extent by the flux of heat and moisture from the surface of Lake Superior. The amount of modification which the air receives is determined by the length of time spent over the water; therefore, the fetch and wind speed are important. This can be seen in the streamlines to the south of Lake Michigan where the winds at the surface and 850 mb are from the same direction. The long fetch over water ( ~400 km) has allowed the warming influence of Lake Michigan to wipe out approximately 20 degrees of backing.

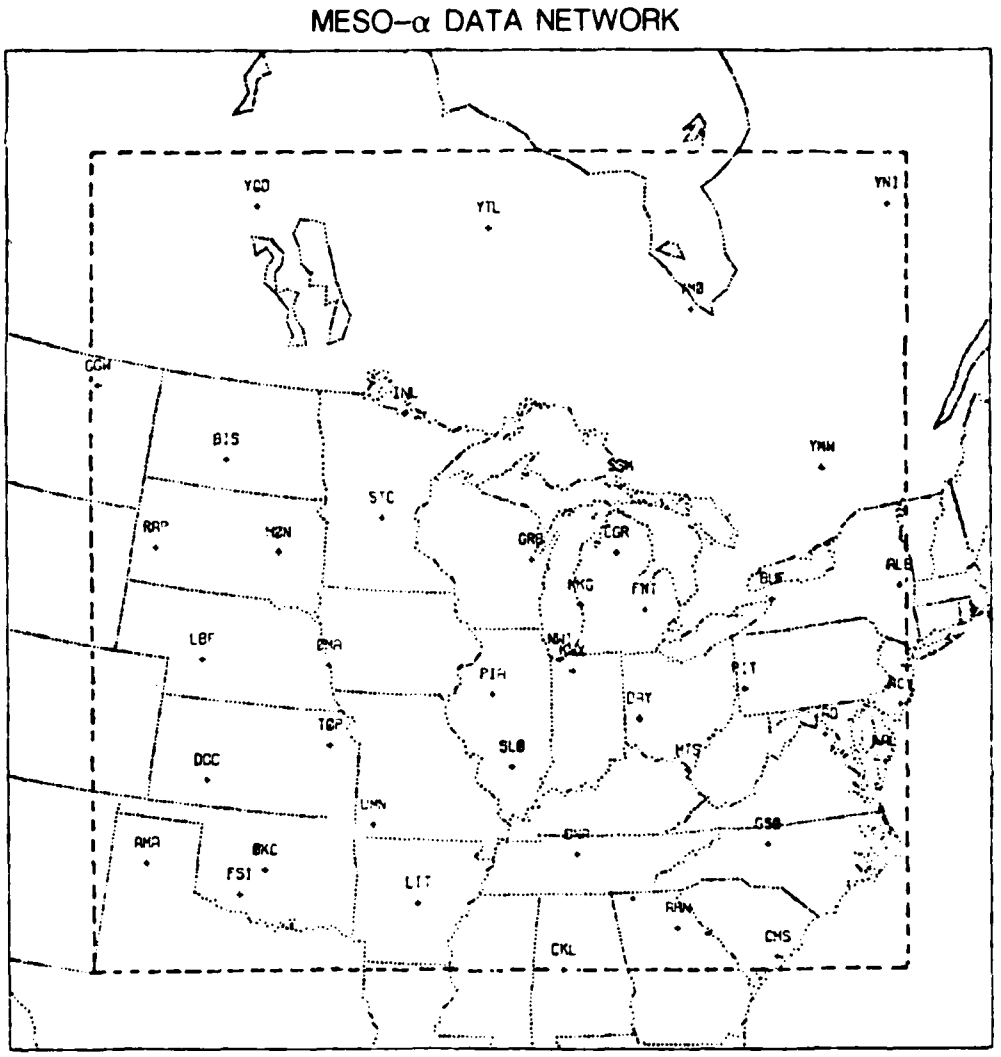


Figure 11. Data domain for the meso-α analyses. Stations used in PROAM, PROAMU, and PUKAM are shown within the dashed lines.

0000 GMT 10 January 1984

Figure 12. GOES satellite imagery for 0000 GMT 10 January 1984.

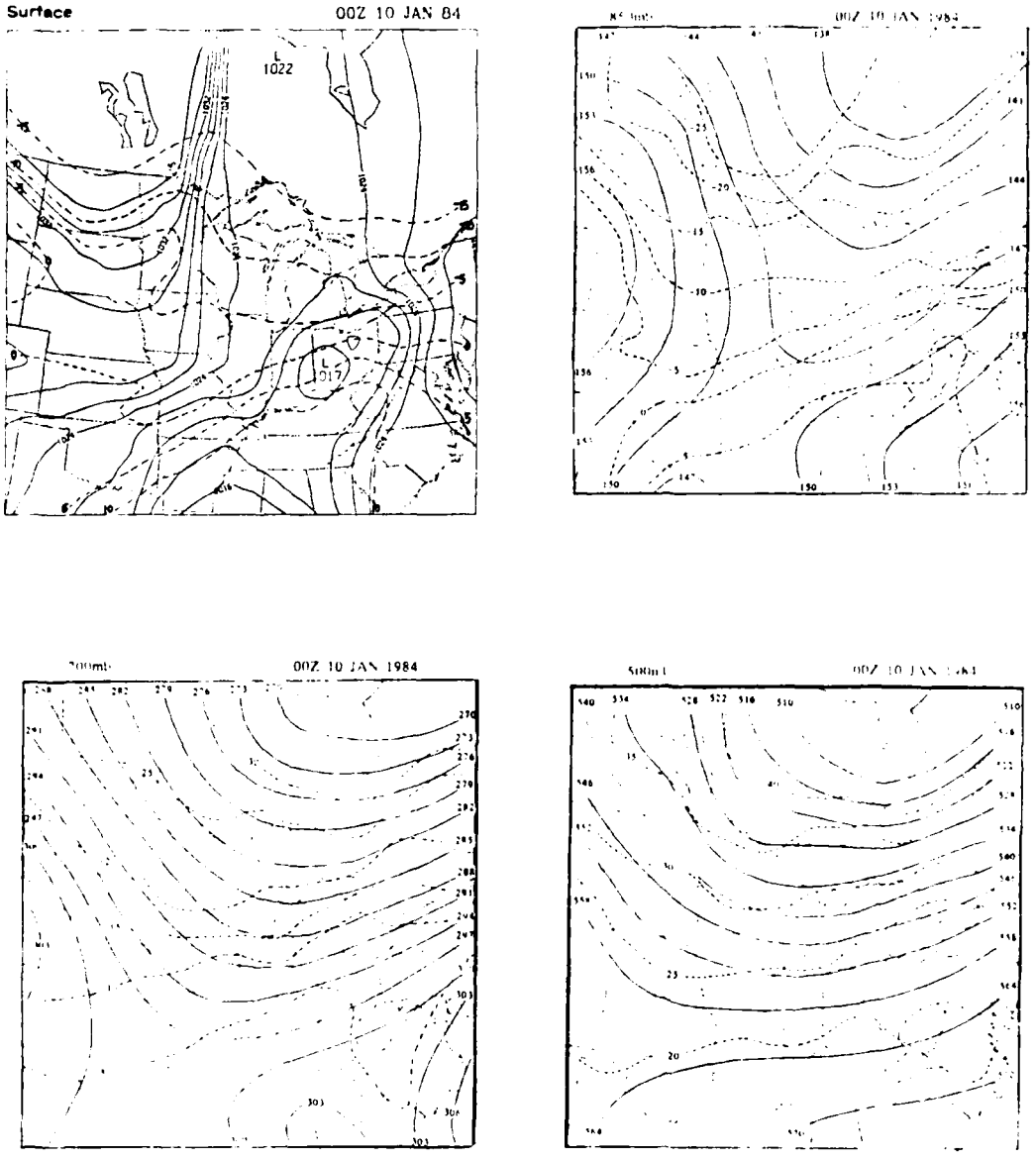


Figure 13. Surface, 850, 700, and 500 mb analyses from PROAM/PROAMU for 0000 GMT 10 January 1984. Surface analysis consists of pressure and temperature fields while upper-air analyses are of heights and temperatures.

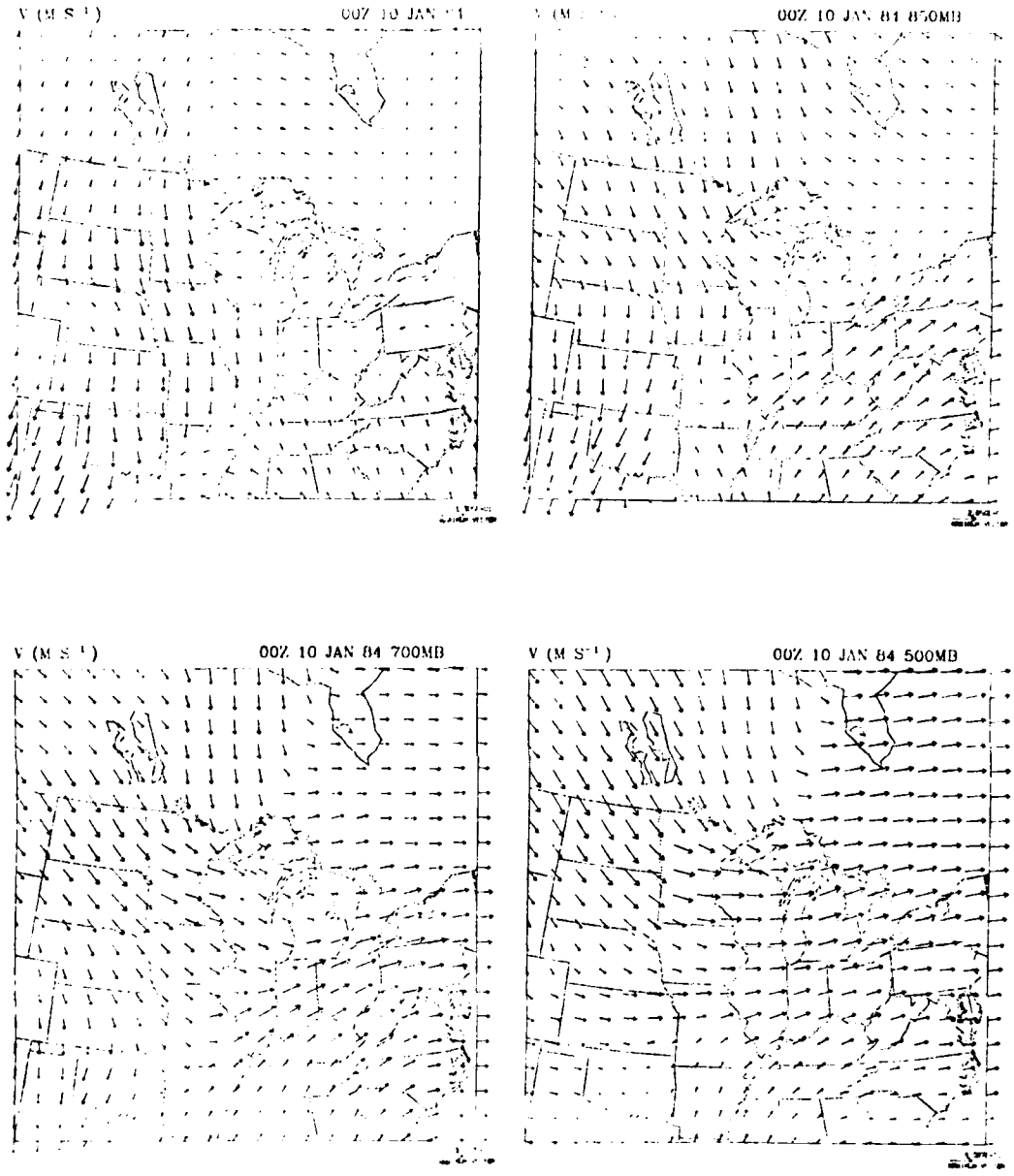


Figure 14. Surface, 850, 700 and 500 mb analyses of the velocity field for 0000 GMT 10 January 1984.


Figure 15. GOES satellite imagery for 1200 GMT 10 January 1984.

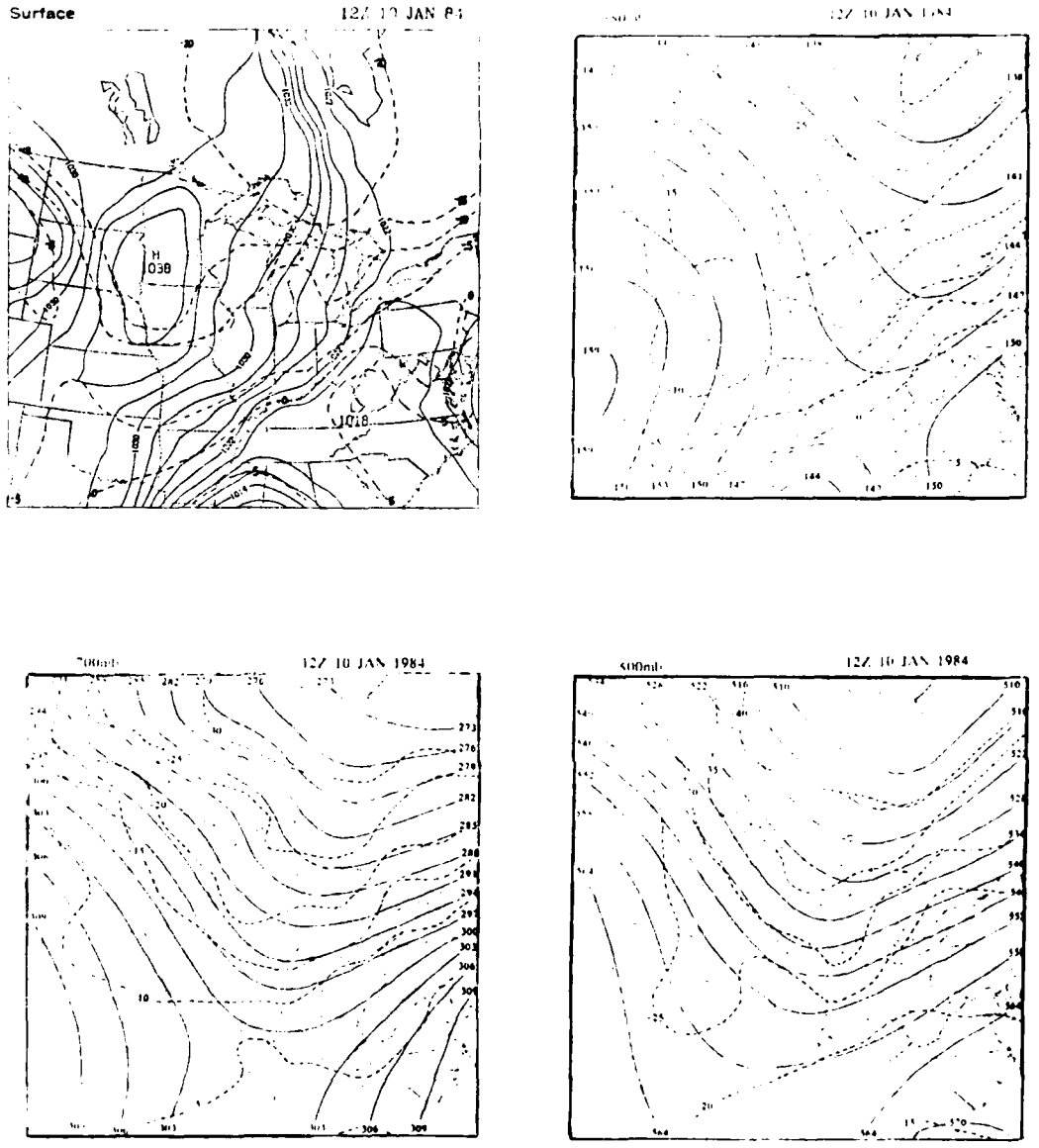


Figure 16. Surface, 850, 700, and 500 mb analyses from PROAM/PROAMU for 1200 GMT 10 January 1984. Surface analysis consists of pressure and temperature fields while upper-air analyses are of heights and temperatures.

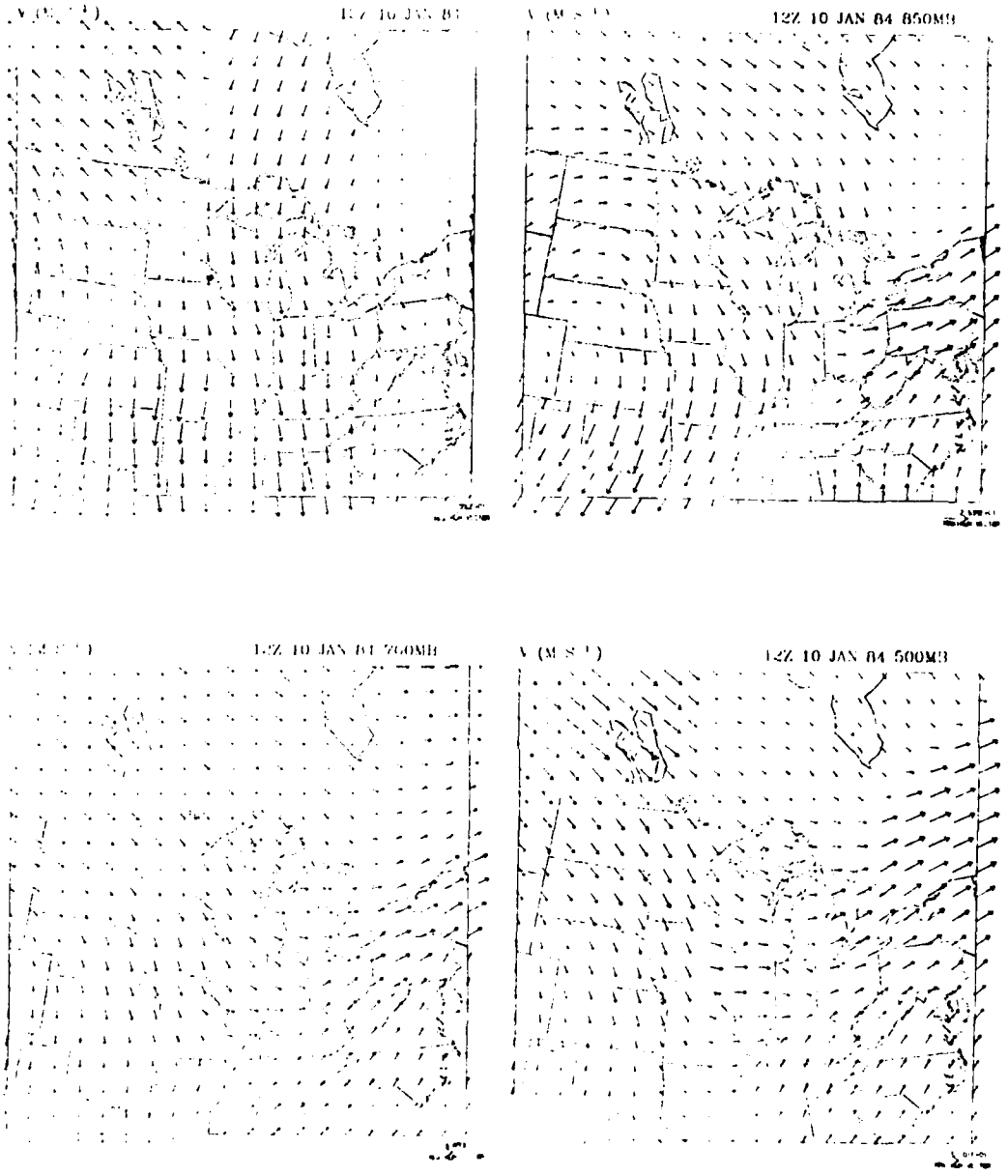


Figure 17. Surface, 850, 700 and 500 mb analyses of the velocity field for 1200 GMT 10 January 1984.

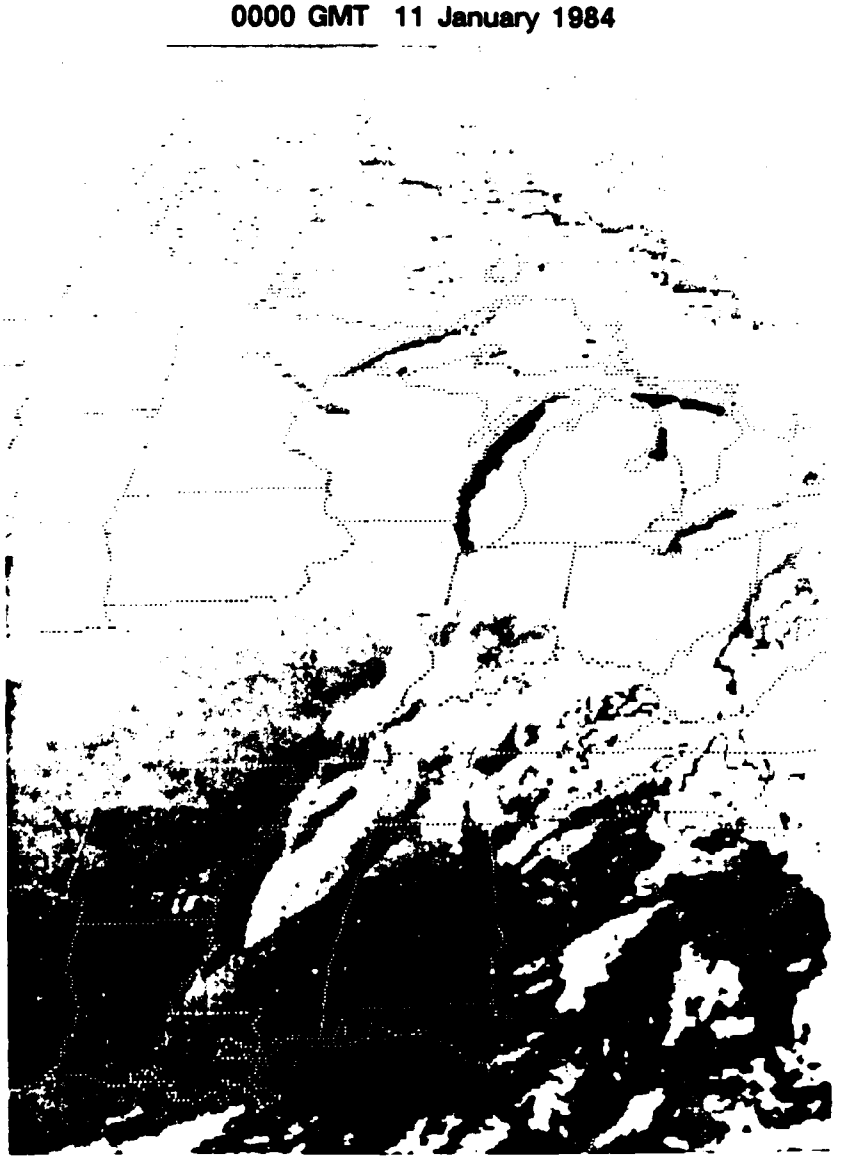


Figure 18. GOES satellite imagery for 0000 GMT 11 January 1984.

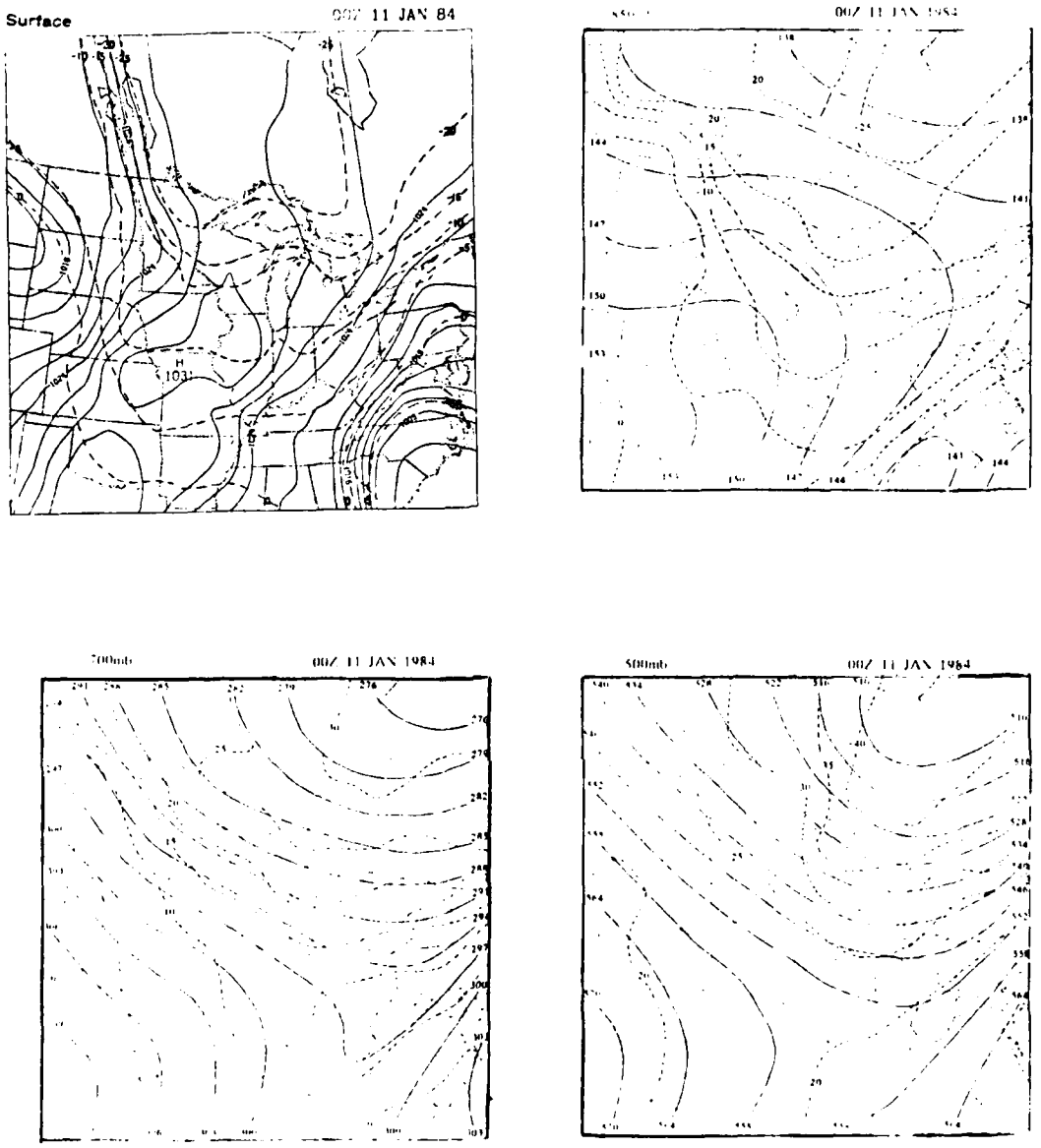


Figure 19. Surface, 850, 700, and 500 mb analyses from PROAM/PROAMU for 0000 GMT 11 January 1984. Surface analysis consists of pressure and temperature fields while upper-air analyses are of heights and temperatures.

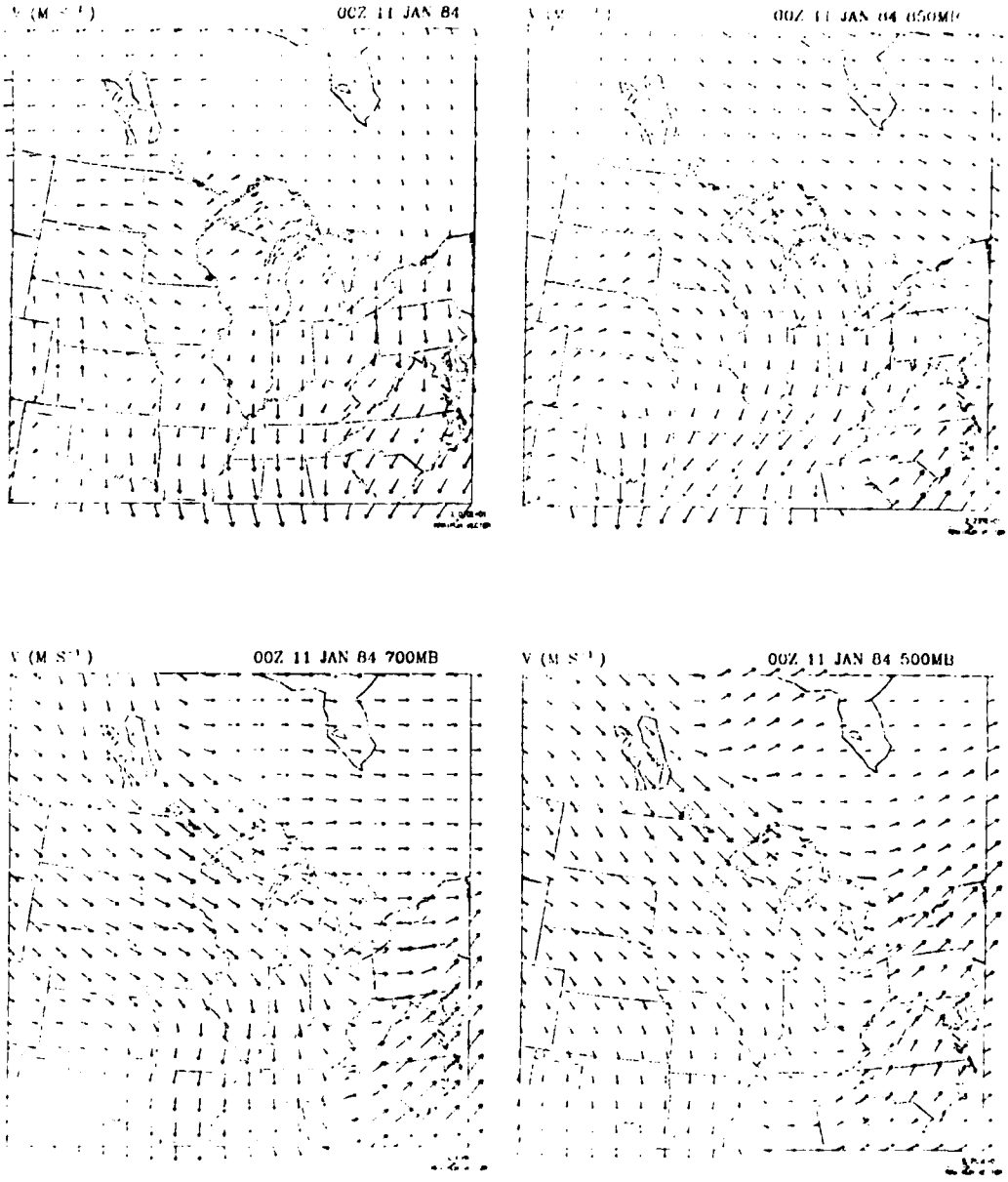


Figure 20. Surface, 850, 700 and 500 mb analyses of the velocity field for 0000 GMT 11 January 1984.

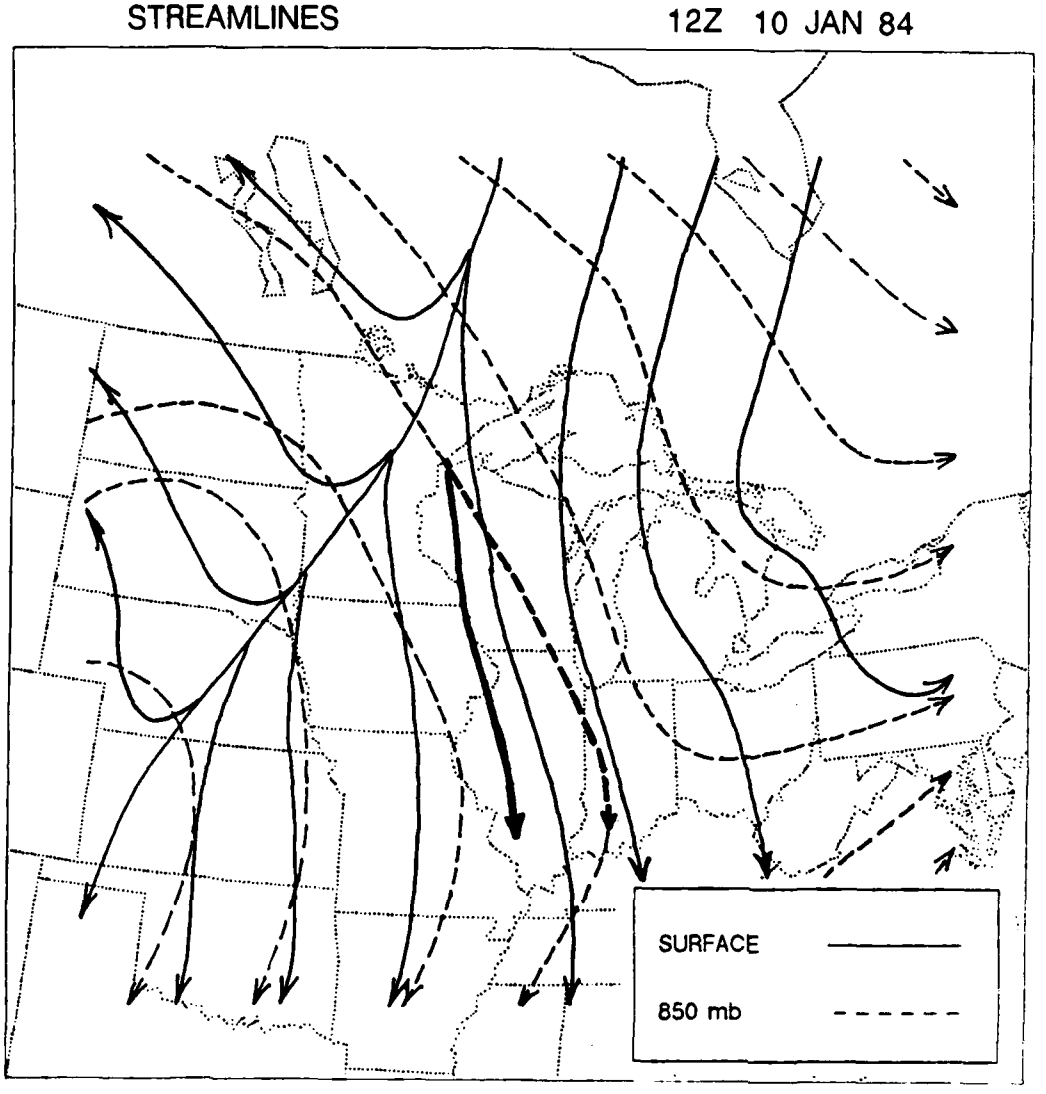


Figure 21. PROAM/PROAMU streamline analyses for the surface and 850 mb for 1200 GMT 10 January 1984. Heavy lines represent the westward limit of air mass modification by Lake Superior.

The differences between the modified and unmodified air can also be noticed by examining the divergence, vorticity, and vertical velocity plots created by PUKAM. The three stations, INL, STC, and SSM, were chosen to represent the unmodified polar air. Looking at these soundings (Fig. 22) one can see a strong, stable inversion extending from the surface to approximately 850 mb and surface temperartures colder than −25°C in both the INL and the STC soundings. These two soundings are also nearly dry throughout the troposphere. The sounding at SSM, particularly from the surface to 800 mb, does show some weak signs of modification by Lake Superior. Either solar heating occurred at the surface to increase the lapse rate in the layer from 1000–950 mb to create an almost superadiabatic layer, or the northwest flow over the lake has caused some modification. Since the later is most likely, the results of the kinematic analyses will not be as stable in the lower layers as might otherwise be expected. However, SSM was included because it represented the only choice available for the third station necessary to show the conditions upwind of the lakes.

Examination of the kinematic analyses for the unmodified continental polar air, as demonstrated in Fig. 23, reveals signs of significant stability as the entire depth of the lower troposhere (up to 500 mb) possesses weak downward vertical velocity. Weak divergence is also present throughout most of the area with a thin, weakly convergent layer between 875–800 mb. The vorticity, likewise, yields a stable boundary layer with negative vorticity up to ~790 mb and slightly positive vorticity above. The thin layer of convergence, and the weakness of the downward vertical motion, divergence, and negative vorticity may all be due to the inclusion of the slightly modified SSM sounding in the stable area analyses.

The convective boundary layer is best demonstrated by examining the stations on the downwind side of the lakes. GRB, KNX, and MKG were chosen as representative of the modified continental polar air. Although GRB is located on the upwind side of Lake Michigan, the sounding, as demonstrated in Fig. 24, demonstrates that Lake Superior has significantly warmed the air, which displays a near-neutral lapse rate. A shallow boundary layer is also present up to 870 mb or ~1300 m. The soundings of MKG and KNX show the effects of additional heat and moisture, which deepened the CTBL. The air within the convective boundary layer is nearly saturated, but dries out rapidly at the base of the inversion at ~800 mb (~2000 m). The modification is further demonstrated in Fig. 25, the

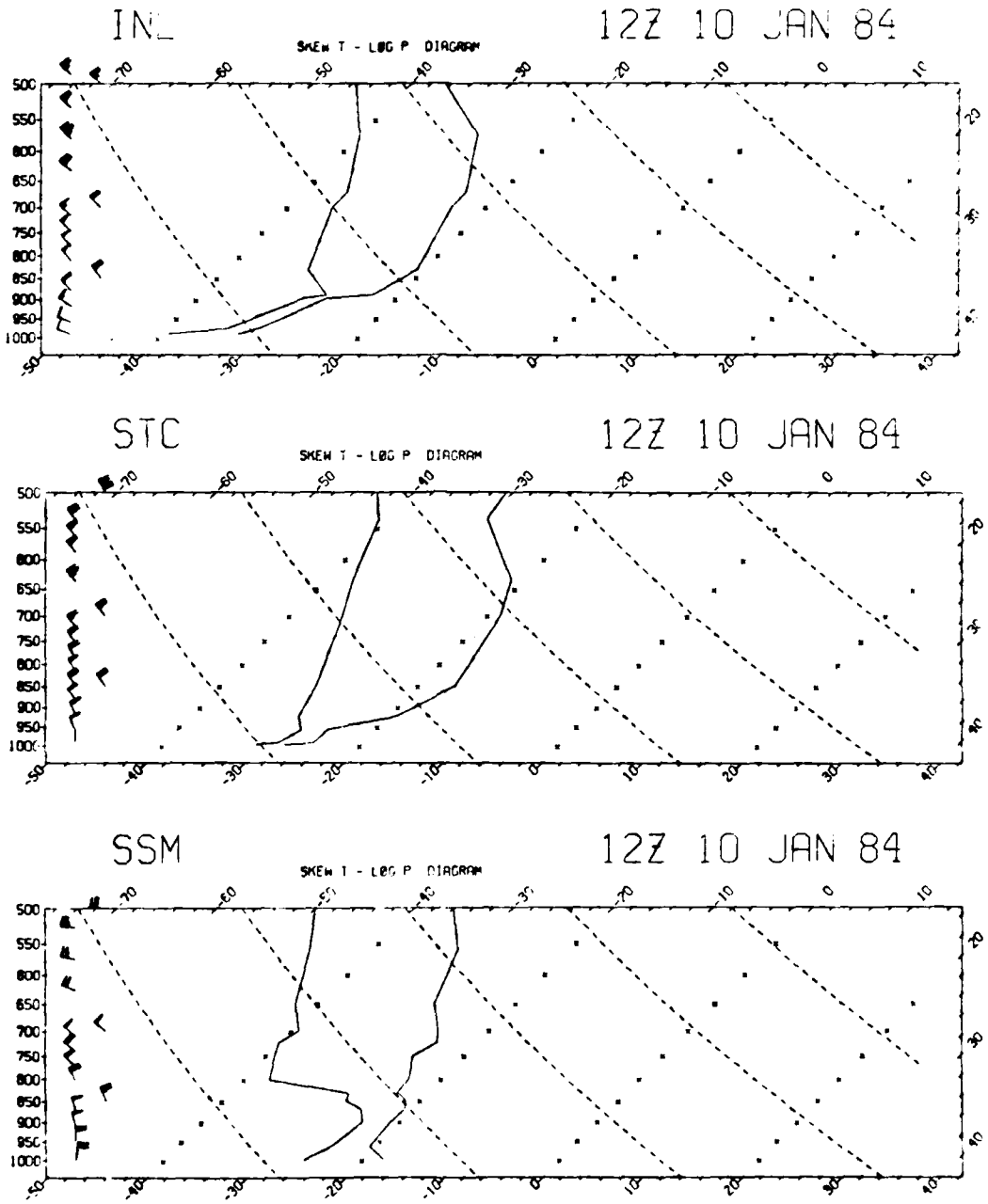


Figure 22. Temperature and dewpoint soundings for International Falls, Minnesota (INL), St. Cloud, Minnesota (STC), and Sault Ste. Marie, Michigan (SSM) at 1200 GMT 10 January 1984.

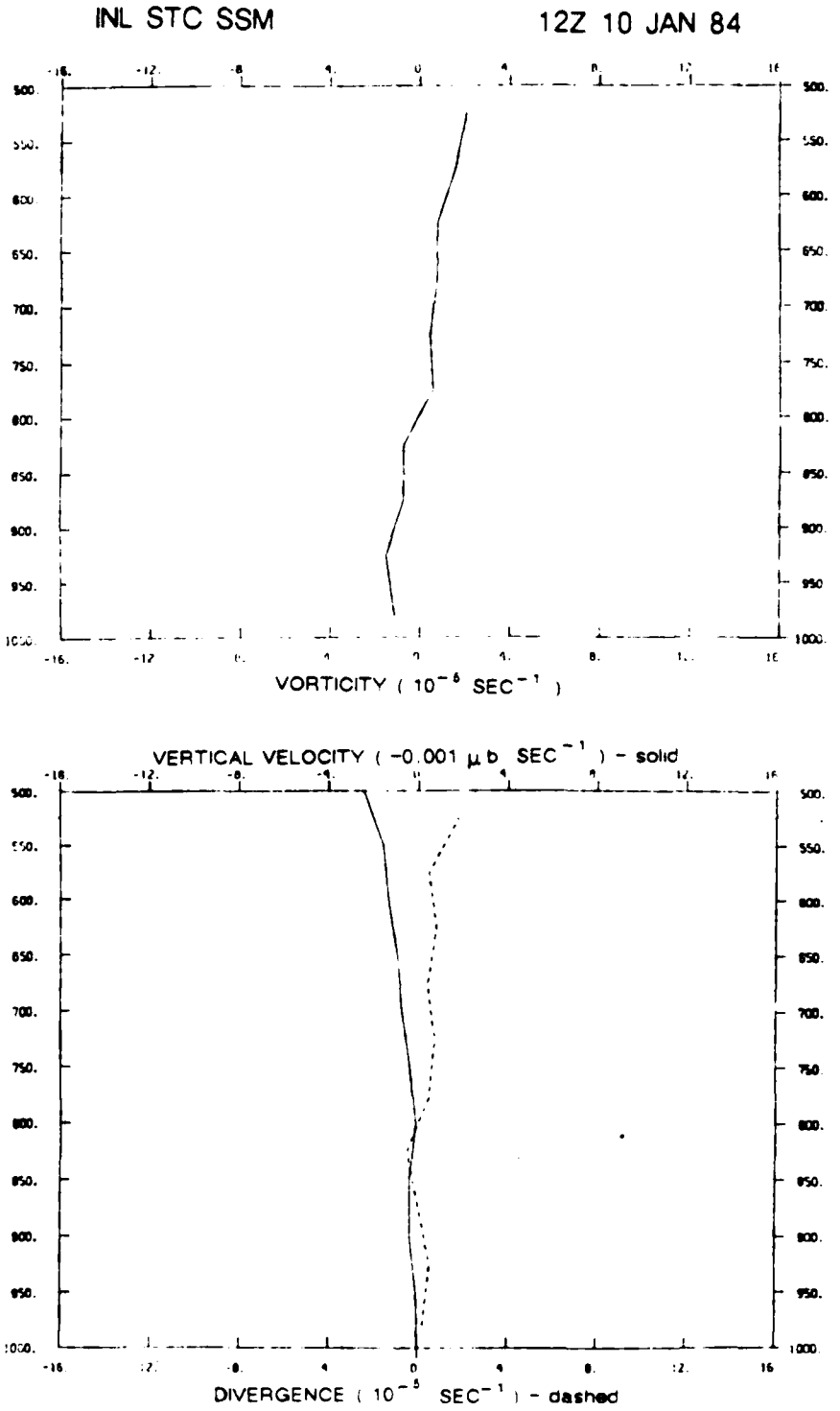


Figure 23. Top panel is the kinematic analysis of vorticity for INL, STC, and SSM at 1200 GMT 10 January 1984. Lower panel shows the divergence (dashed line) and vertical velocity (solid line) for the same region.

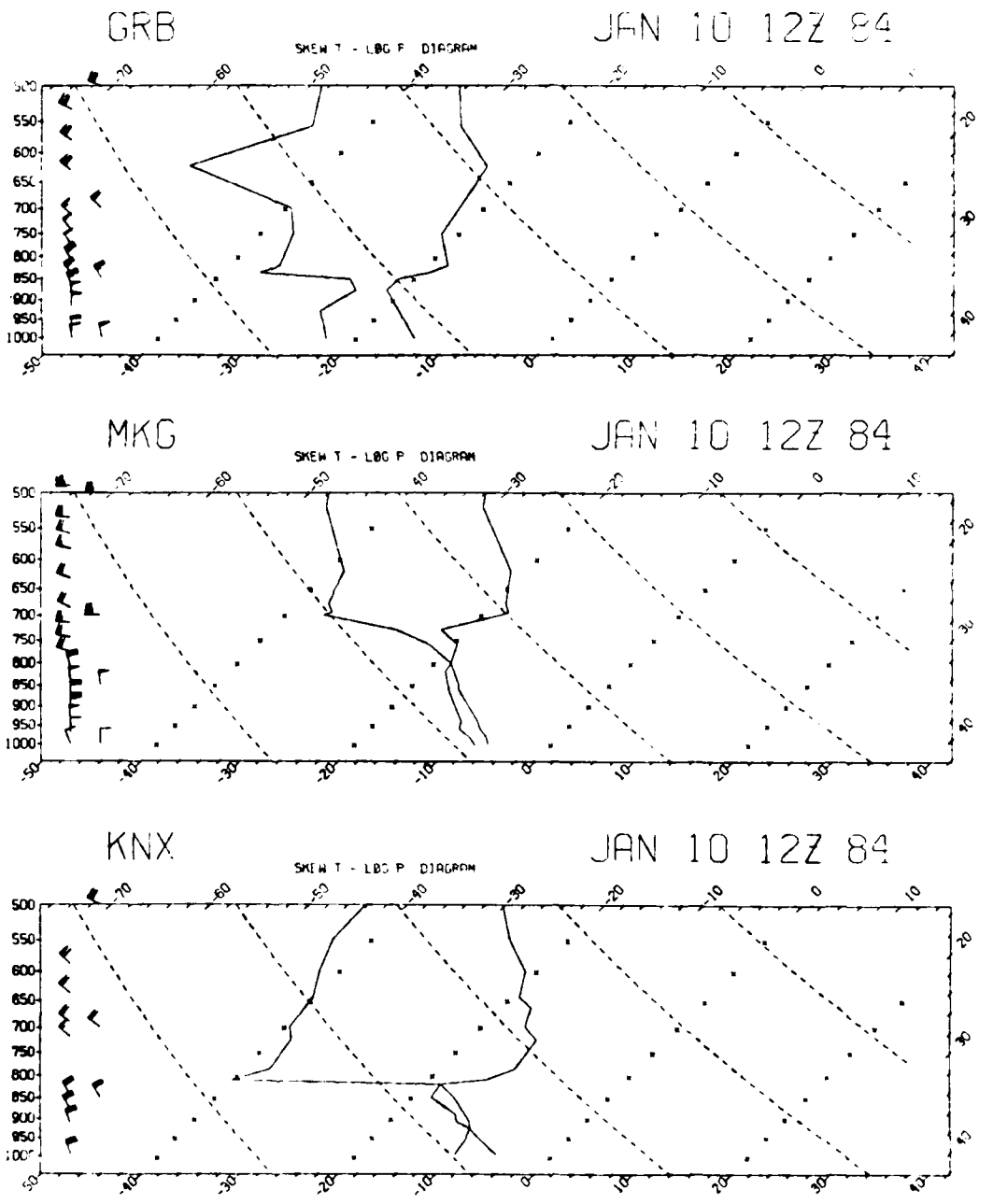


Figure 24. Temperature and dewpoint sounding for Green Bay, Wisconsin (GRB), Muskegon, Michigan (MKG), and the Knox aircraft sounding (KNX) at 1200 GMT 10 January 1984.

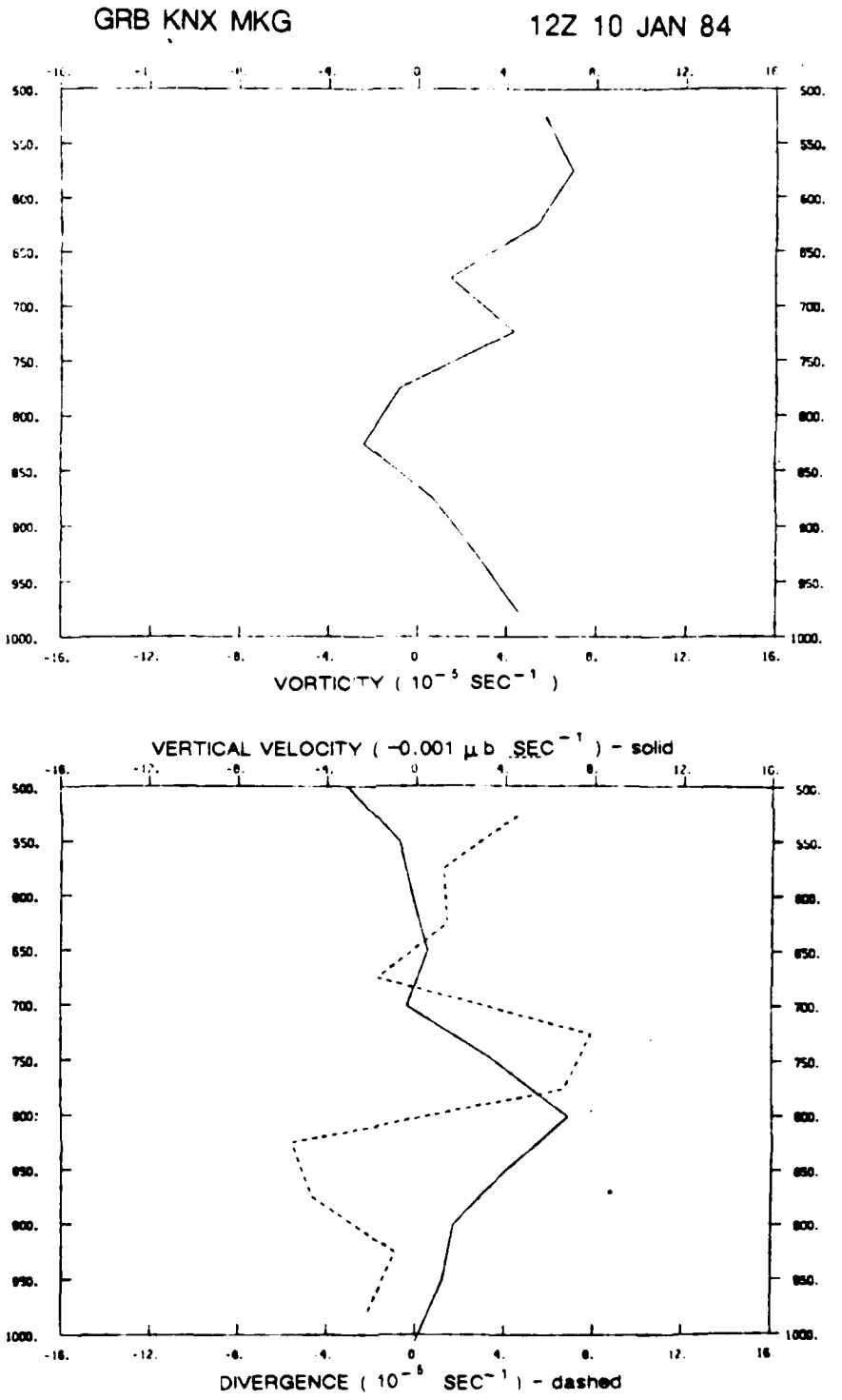


Figure 25. Top panel is the kinematic analysis of vorticity for GRB, KNX, and MKG at 1200 GMT 10 January 1984. Lower panel shows the divergence (dashed line) and vertical velocity (solid line) for the same region.

PUKAM vertical cross-sections of divergence, vorticity, and vertical velocity. Strong convergence is shown in the lower CTBL from the surface to ~825 mb. This is coupled with a maximum value for upward vertical velocities near 800 mb, with positive values continuing to 700 mb. Positive vorticity occurring in the CTBL from the surface to ~870 mb.

The vertical cross-section of virtual potential temperarture ($\theta_v$) demonstrates the effect the two lakes have on the modification of the air mass more clearly (see Fig. 26). There is a steep gradient of $\theta_v$ over STC which becomes weaker, indicating a decrease in the stability, as one approaches GRB. The point where the gradient begins to weaken and the isentrope intersects the surface was taken from the previously discussed streamline analysis which indicated the boundary of the unmodified air. Moving eastward, notice the slow increase in boundary layer depth between STC and GRB due to the limited amount of time the air spends over Lake Superior. This air is marked $cP_S$ to denote modification by Lake Superior alone. The gentle slope was found to be fortuitous during the examination of the aircraft data

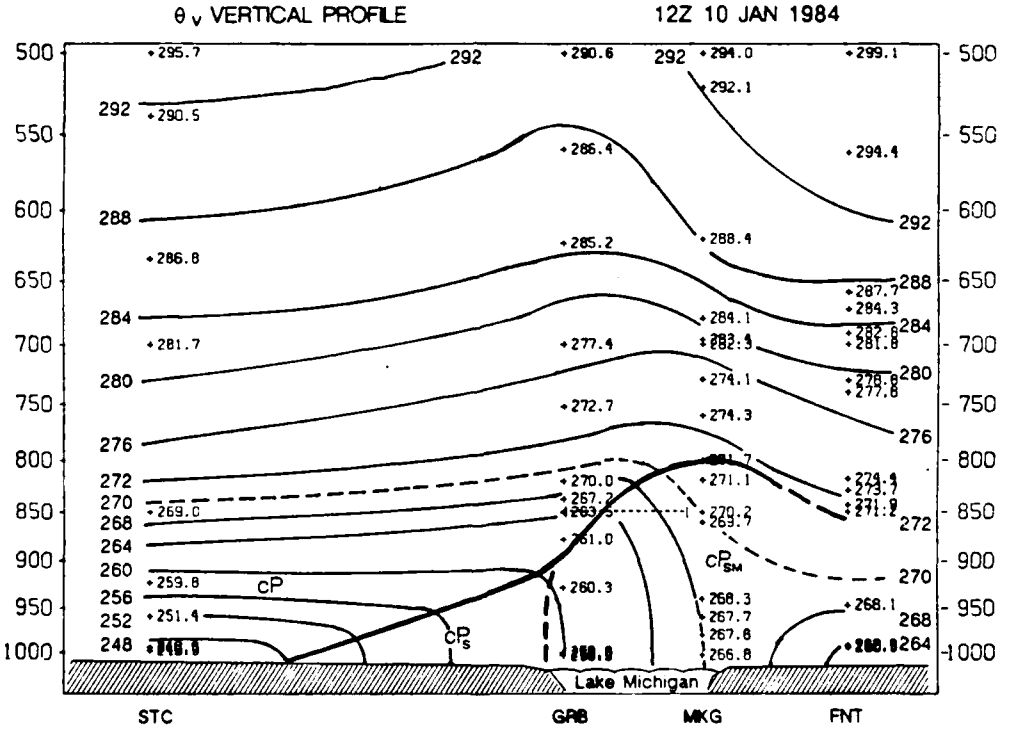


Figure 26. Vertical cross-section of virtual potential temperature for 1200 GMT 10 January 1984.

(to be discussed at length in a later chapter) as it allowed a longer flight time in each of the different types of air present over the lake. Over the lake, between GRB and MKG, the vertical gradient of $\theta_v$ decreases as the depth of the CTBL increases dramatically to near 800 mb. Again, this is due to the approximately 400 km fetch possible in the north–south direction over Lake Michigan. This air is marked in the figure as $cP_{SM}$ to note that the continental polar air has been modified by both Lake Superior and Lake Michigan. To the east of MKG the base of the inversion, and therefore, the top of the boundary layer, becomes difficult to find.

These same effects can be seen in planview using the analysis of inversion base heights for this time period as shown in Fig. 27. The base of the inversions were calculated from the soundings of upper–air stations in the area. One can easily see that the highest inversion base heights are to be found to the south and east of Lake Michigan. Since the flow is north–northwesterly the greatest boundary layer depth would be expected to be at the south end of the lake and slightly east of center. This coincides well with the highest reported inversion base at KNX of ~2440 m, which agrees with other measurements reported by Walters (1986). Figure 28 shows his results from the Marginal Ice Zone Experiment (MIZEX) conducted in the Bering Sea during February 1983 and the Mesoscale Air–Sea Exchange (MASEX) study conducted off the Atlantic coast in January 1983. This confirms that the 400 km fetch of Lake Michigan can create a boundary layer in excess of 2000 m provided the thermal forcing and moisture flux are sufficient. For details on these conditions, let us turn to higher resolution analyses, beginning with the meso–β scale.

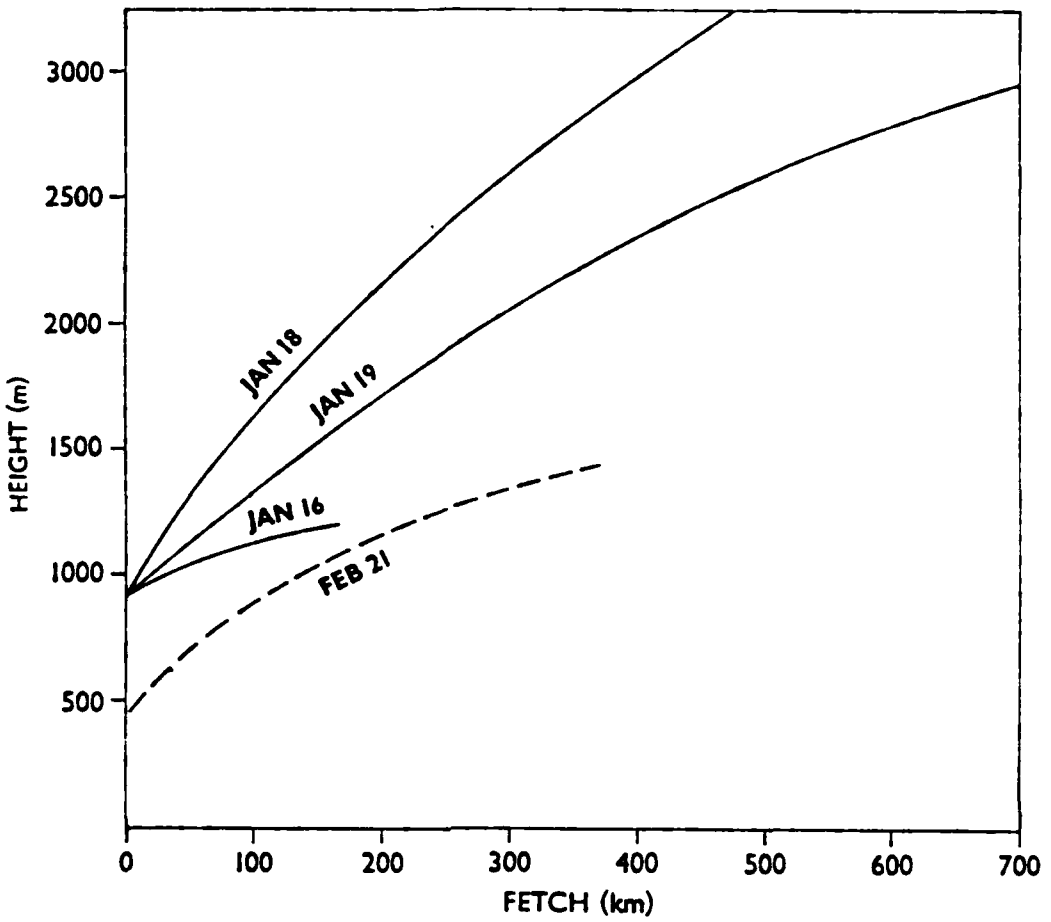


Figure 27. Height of the inversion base vs. fetch taken from aircraft observations during MIZEX and MASEX (from Walters, 1986).

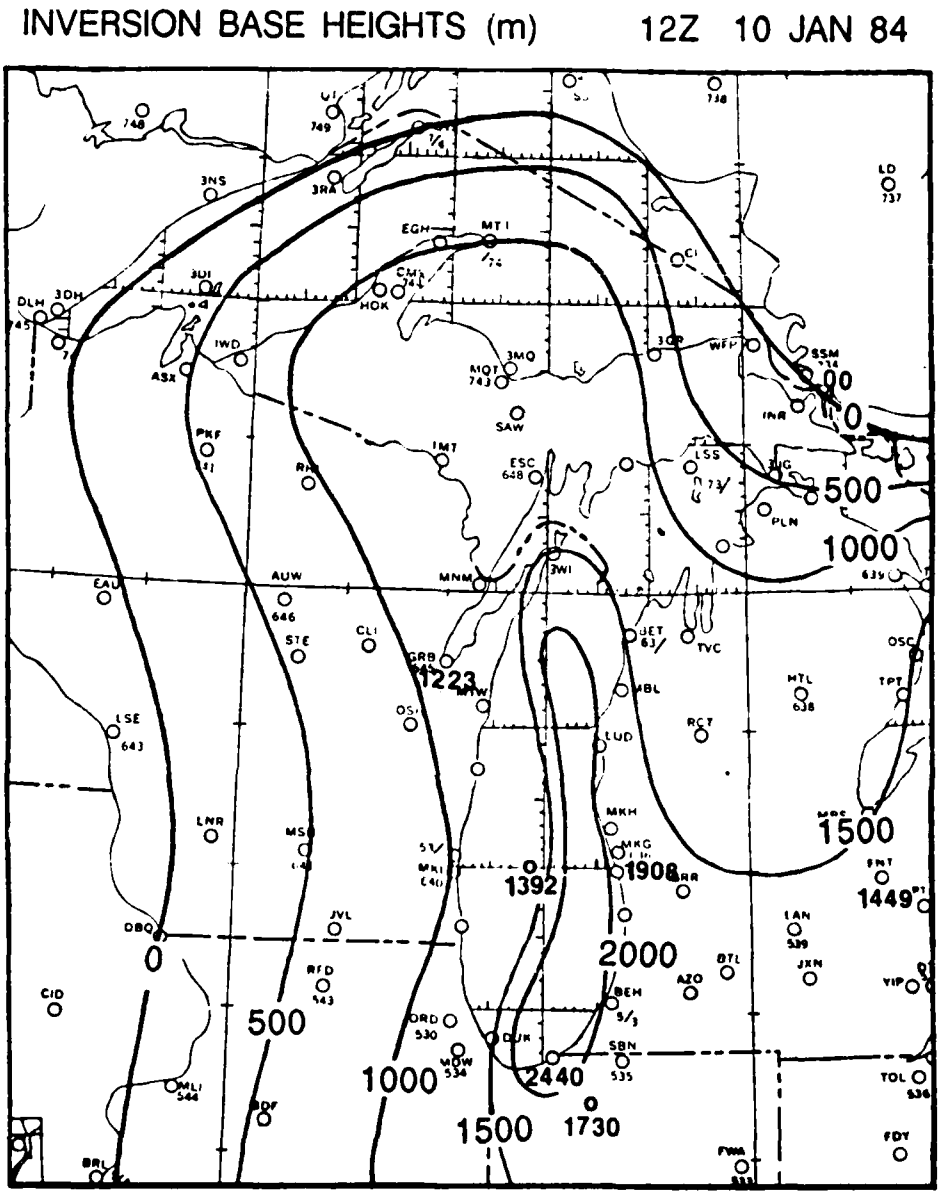


Figure 28. Analysis of inversion base heights calculated from 1200 GMT 10 January 1984 soundings in the vicinity of Lake Superior and Lake Michigan.

# 4. COLD AIR OUTBREAK: MESOSCALE β SETTING

This chapter describes the meso–β scale meteorological pheonmena (i.e. length scales on the order of 20–200 km) which occurred between 1200 GMT 10 January and 0000 GMT 11 January 1984. The method of analysis for this scale consisted of PROAM surface analyses at three hour intervals within the area delineated by the dashed lines shown in Fig. 29. The initial time for the start of the meso–β analyses was chosen as 1200 GMT 10 January 1984 since, and as pointed out by Agee (1987), the Type I CTBL generally takes 12–18 hours for full development. Analyses of the meso–α scale showed that frontal passage occurred over the northern half of Lake Michigan at 0000 GMT 10 January. Although 23 meteorological parameters are either analyzed or derived by the PROAM package (as mentioned in Chapter 2), the most pertinent 5 were chosen for discussion of this event: pressure (p), virtual potential temperature ($\theta_v$), specific humidity (q), isotachs, and convergence ($-\nabla \cdot V$). The reason for the choice of these parameters is to show the modification and resulting support for convection which occurred within the CTBL as the event progressed.

Beginning with the surface pressure field at 1200 GMT, Fig. 30 reveals a series of weak low pressure centers in Michigan and upper Wisconsin. High pressure centers are found over central Lake Superior, northern Minnesota, and westcentral Wisconsin. The most prominent feature to note in $\theta_v$ is the axis of warm air which is present to the east of the center line of the lake and which stretches nearly the entire length of the lake's north–south axis. This warm tongue is offset on both sides by pockets of cold air in Wisconsin to the west and Michigan to the east. The indications are that significant heat tranfer has occurred from the surface of Lake Michigan into the air traversing over the lake. In Wisconsin the virtual potential temperature reaches values as low as 250°K and in Michigan the low temperature is 257°K. This can be contrasted with a maximum value of 267°K slightly to the north of MKG, showing that Lake Michigan has added at least 10°K of heating to the air as it moves over the

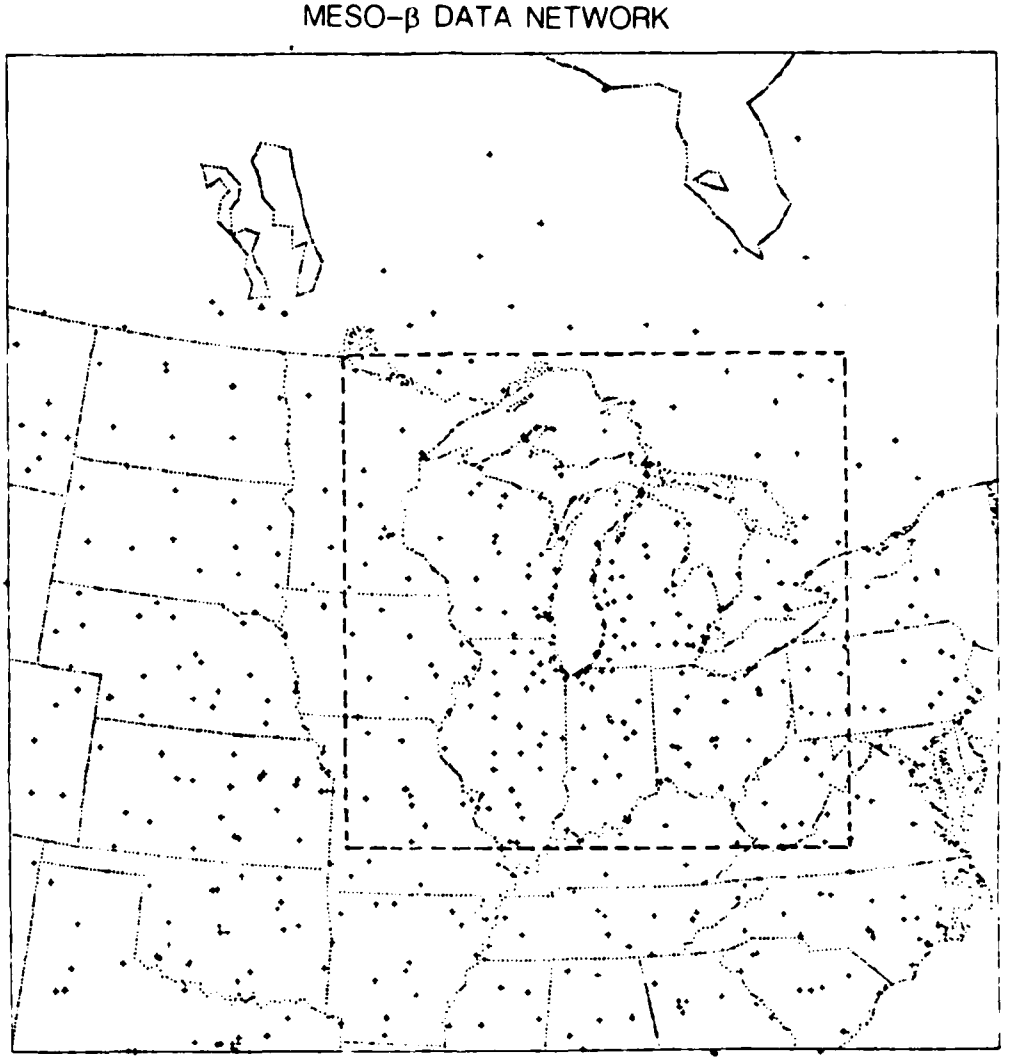


Figure 29. Data domain for the meso-β analyses. Stations used by PROAM are shown within the dashed lines.

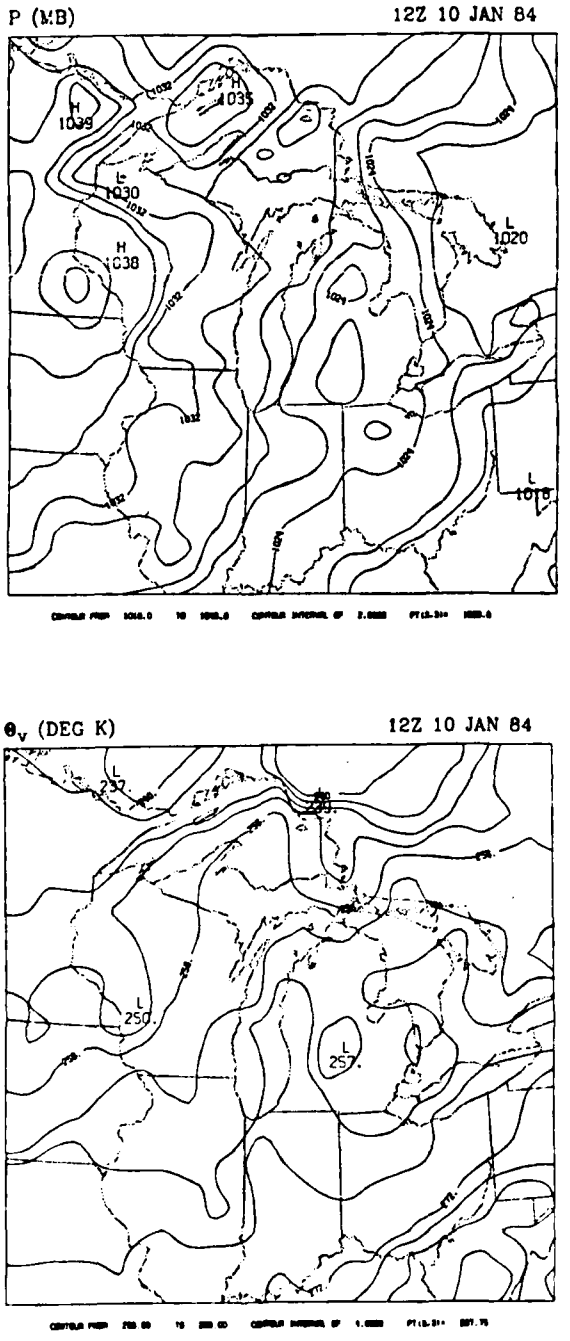


Figure 30. Surface pressure and virtual potential temperature analyses for 1200 GMT 10 January 1984.

water. The specific humidity analysis (moisture is recognized as a better tracer of convection than temperature, as reported by Lenschow and Stevens, 1980) shown in Fig. 31 supports the addition of moisture as well as heat to the the continental polar air mass. An axis of high moisture content is found to the east of center over the lake with minimum values representing dry air to either side, similar to the temperature analysis pattern. Isotach analysis reveals wind speed at the surface greater than 6 m/s over most of the lake with values as high as ~8 m/s at mid-lake. Further support for the development of convection can be seen in the convergence field (see Fig. 32). High values of convergence are found over the southern half of the Lake and in the southern half of Michigan near the lake shore.

The pressure pattern at 1500 GMT (Fig. 33) contains weak lows in southern Michigan and over Lake Huron. The $\theta_v$ analysis still shows the axis of warm air extending north-south along the east side of the lake, but the northern tip of the warm air has slid south and the maximum value is now found downstream over northcentral Indiana. Low $\theta_v$ values are still found to the east and west of Lake Michigan. The specific humidity analysis, as demonstrated in Fig. 34, shows the same pattern with the maximum value occurring over northcentral Indiana. Isotachs show that the wind speeds over the lake are still in excess of 6 m/s for most of the area, with the maximum occurring along the east shore at 8.2 m/s. The convergence (Fig. 35) is the only field that maintains support for convective activity over the center of the lake, without translation.

By 1800 GMT high pressure is nudging in from the southwest and has worked its way into the northern half of Lake Michigan (see Fig. 36). The virtual potential temperature again shows a flattening of the amplitude of the axis of warm air as well as continued movement to the south. The pocket of cold air is still present over southern Michigan, also migrating south, but the cold air to the west is no longer as discernable. The axis of maximum wind shown in Fig. 37 has moved to the east of Lake Michigan, over central Michigan state, with winds over the lake between 4 and 6 m/s. Relatively high values for specific humdity are still present over the southeast quadrant of the lake. The convergence pattern (Fig. 38) is becoming more complex with many extrema being noted by the PROAM analysis. However, it still maintains support for convective activity with convergence at the surface over the southern 1/2 to 2/3 of Lake Michigan.

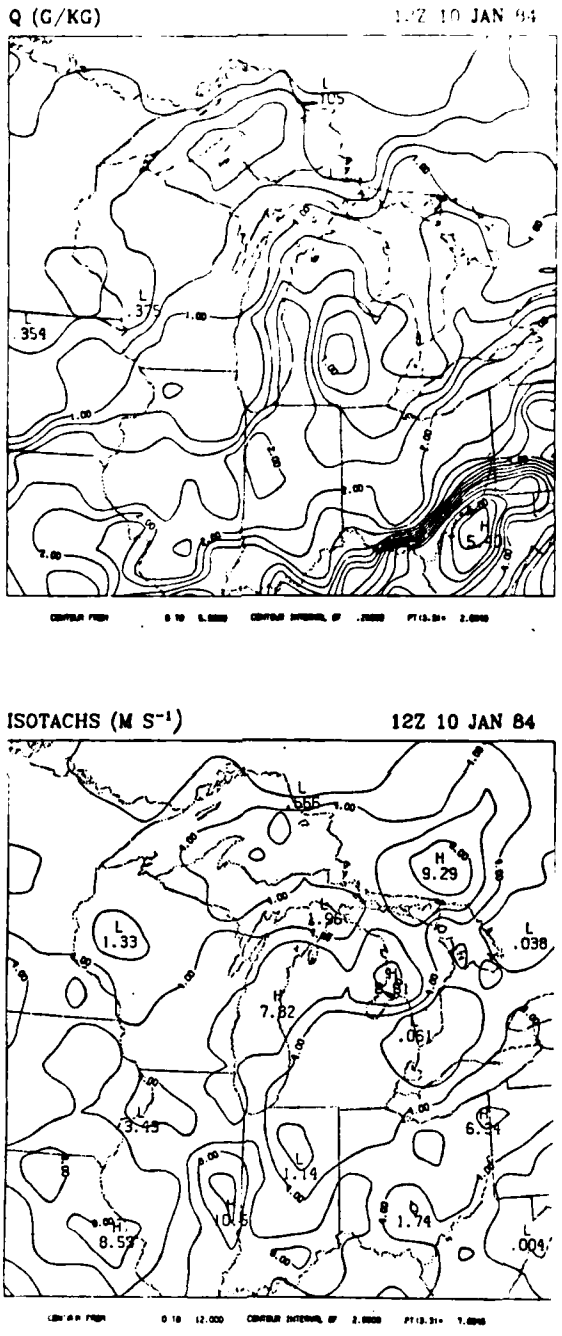


Figure 31. Surface specific humidity and isotach analyses for 1200 GMT 10 January 1984.

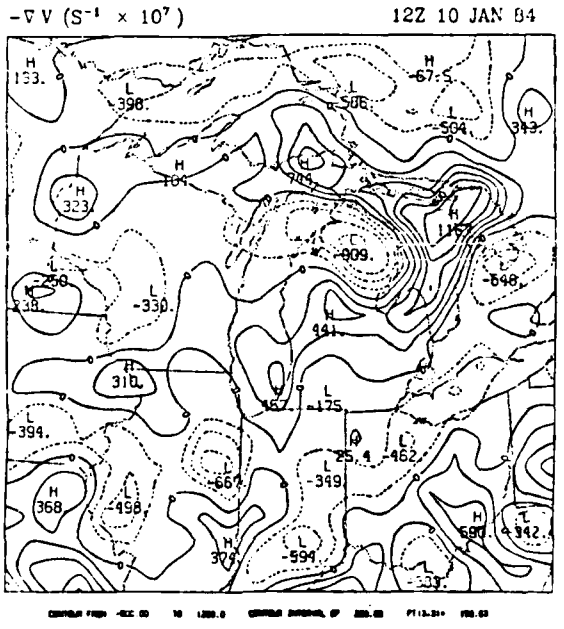


Figure 32. Surface convergence analysis for 1200 GMT 10 January 1984.

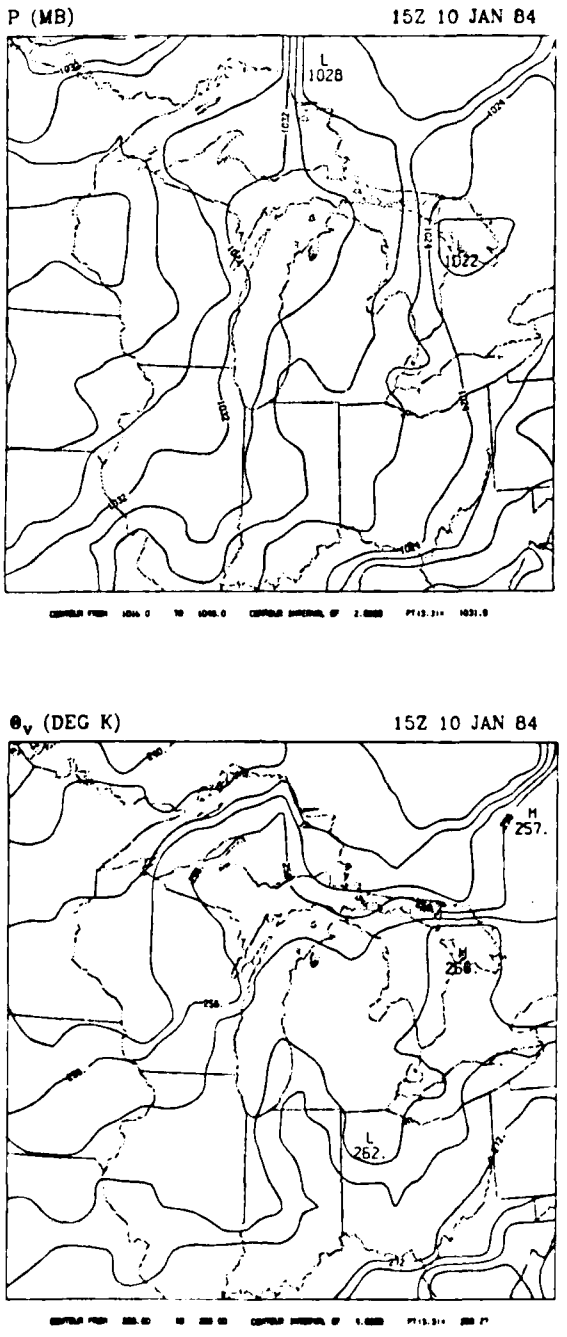


Figure 33. Surface pressure and virtual potential temperature analyses for 1500 GMT 10 January 1984.

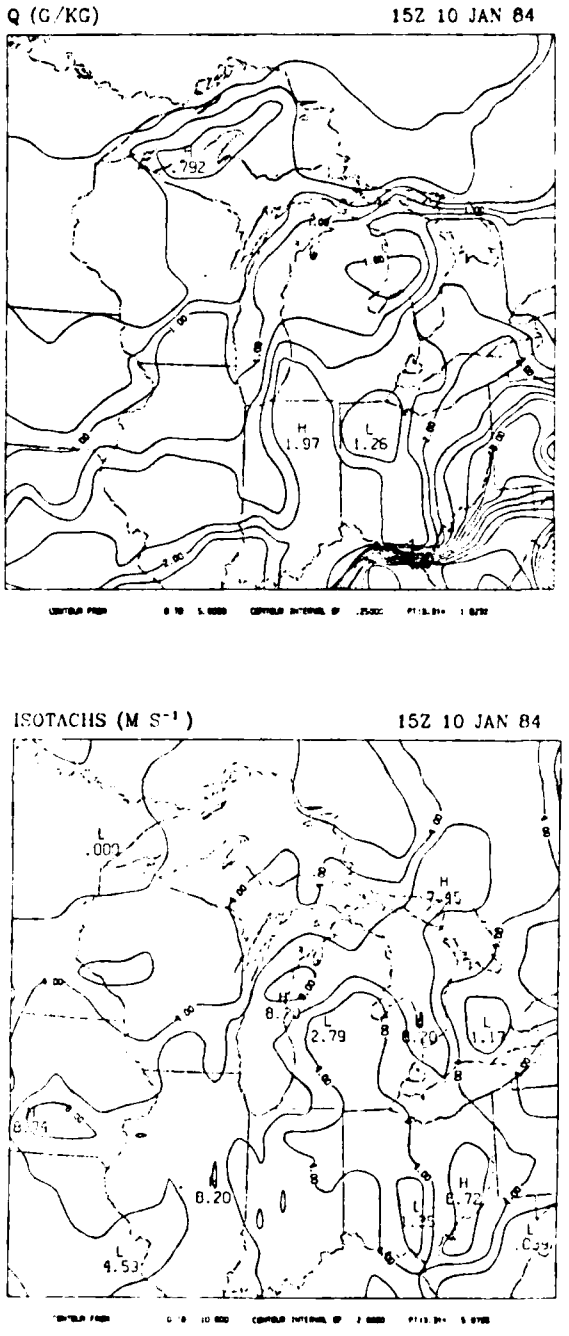


Figure 34. Surface specific humidity and isotach analyses for 1500 GMT 10 January 1984.

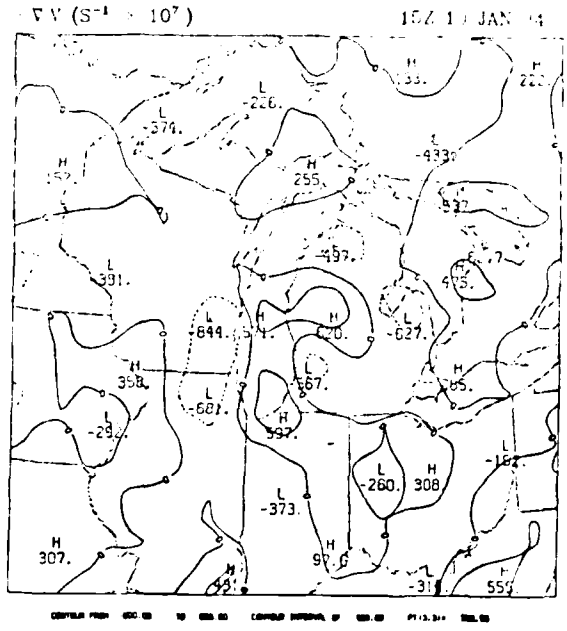


Figure 35. Surface convergence analysis for 1500 GMT 10 January 1984.

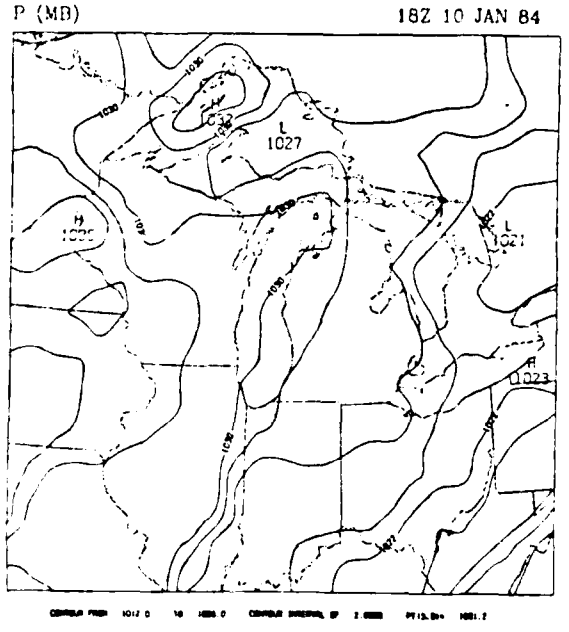


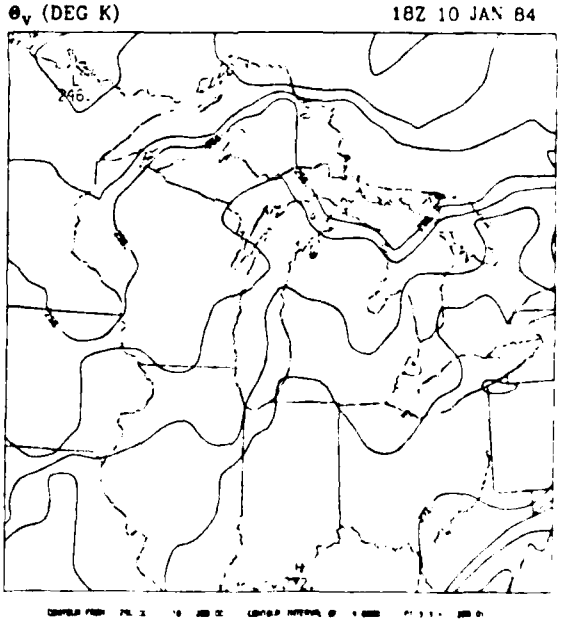


Figure 36. Surface pressure and virtual potential temperature analyses for 1800 GMT 10 January 1984.

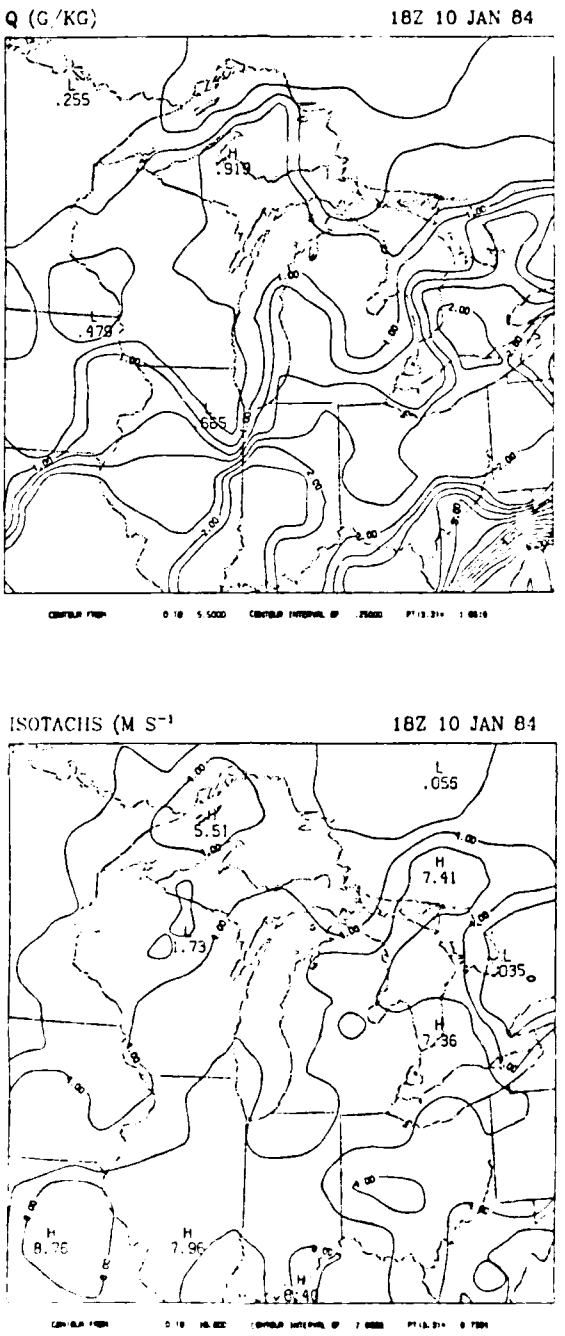


Figure 37. Surface specific humidity and isotach analyses for 1800 GMT 10 January 1984.

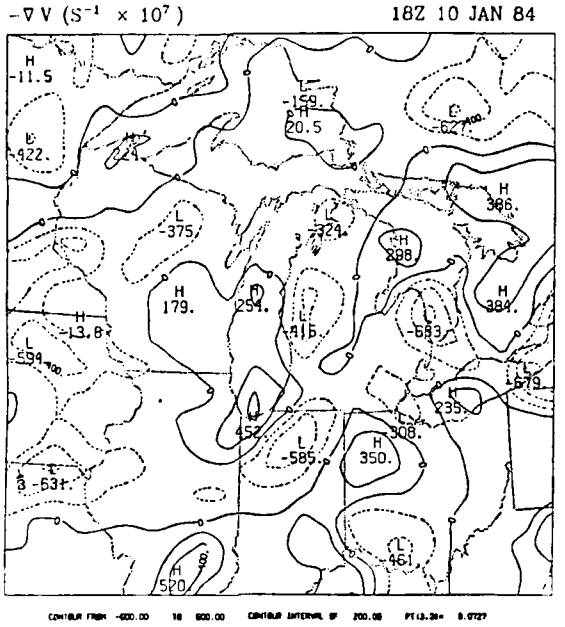


Figure 38. Surface convergence analysis for 1800 GMT 10 January 1984.

The PROAM surface pressure analysis (see Fig. 39) for 2100 GMT 10 January yields a weak low bulging into the high pressure ridge building over the entire Great Lakes region. High pressure centers increasing in intensity can now be found in central Michigan, western Wisconsin, and over Lake Superior. The gradient of $\theta_v$ continues to show the trend established earlier with the amplitude of the warm air axis decreasing and the difference between the cold and warm air also decreasing as the isotherms align more west to east. Even the maximum value for specific humdity, as shown in Fig. 40, has moved south into central Indiana with a weak moisture ridge in southern Michigan, along the east shore of the lake. Wind speeds, as shown by the isotach analysis, have also decreased even further, with speeds over Lake Michigan now ranging from 2 to 4 m/s. Nevertheless, the convegence band over the area (Fig. 41) has narrowed into a band ~150 km wide and intensified. This is more a result of shifting wind direction as the velocity vectors (not pictured) show a strong band of generally northwest flow over the southern half of Lake Michigan and weak north-northeast flow over the east shore of the lake.

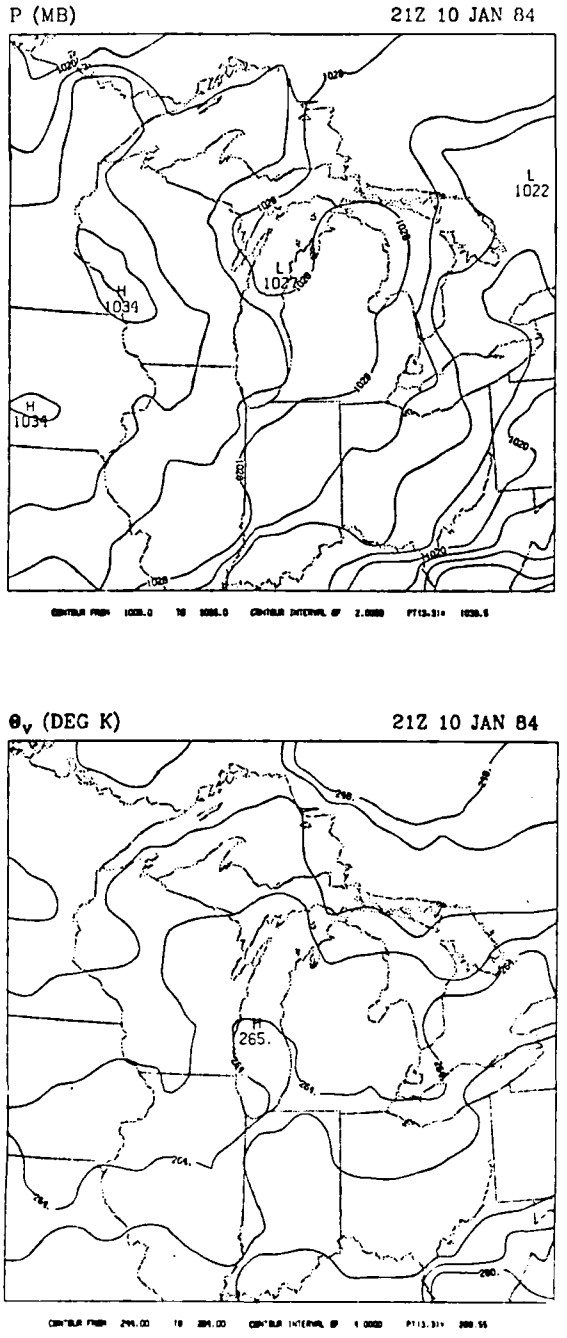


Figure 39. Surface pressure and virtual potential temperature analyses for 2100 GMT 10 January 1984.

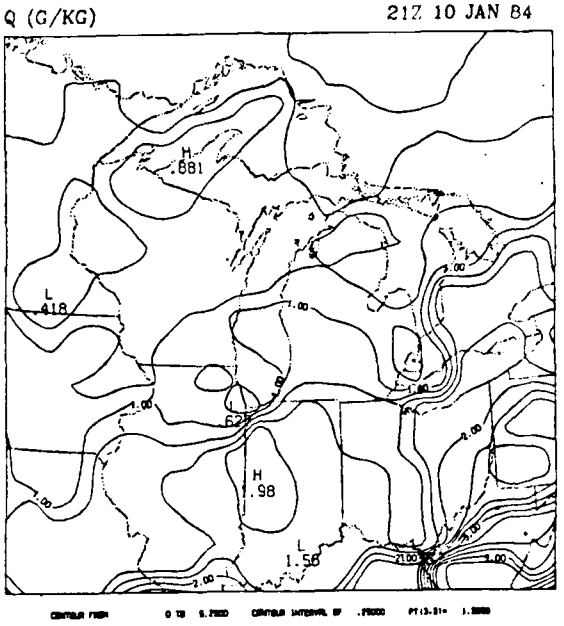


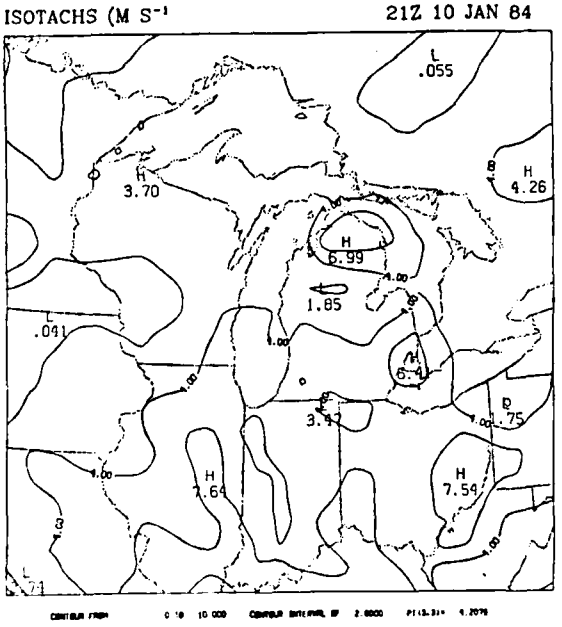


Figure 40. Surface specific humidity and isotach analyses for 2100 GMT 10 January 1984.

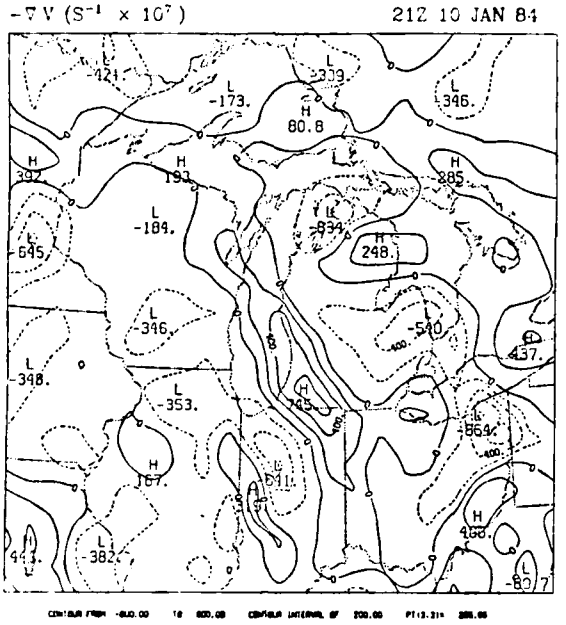


Figure 41. Surface convergence analysis for 2100 GMT 10 January 1984.

The weak low pressure centers evident three hours earlier have completely given way to high pressure by 0000 GMT 11 January (see Fig. 42). Distinct high pressure centers are present in northern and southern of Michigan and to the west in southeastern Iowa and southwestern Wisconsin. The virtual potential temperature pattern is reestablishing its initial warm air axis over the lake, flanked by cold air on both sides in response to the decrease in surface solar heating. The specific humidity (Fig. 43) also shows the same recovery, indicating a possible diurnal trend in the CTBL in which incoming solar radiation tends to warm the ground and decrease the contrast between the modified and unmodified continental polar air. The isotachs indicate that wind speeds over the lake have also increased slightly with a small maxiumum (4.3 m/s) developing on the west shore of Lake Michigan but a weakening of the band of strong winds along the east shore. As a consequence, the narrow band of strong convergence (Fig. 44) is no longer found to the southeast of the lake, but a weaker, broader area of convergence is present.

In summary, the meso-β analyses have shown that a Type I CTBL developed over Lake Michigan in response to the moisture and heat flux supplied by the relatively warmer

water surface. This sets the stage for a more detailed examination of the boundary layer by the NCAR research aircraft which flew on the afternoon of 10 January 1984.

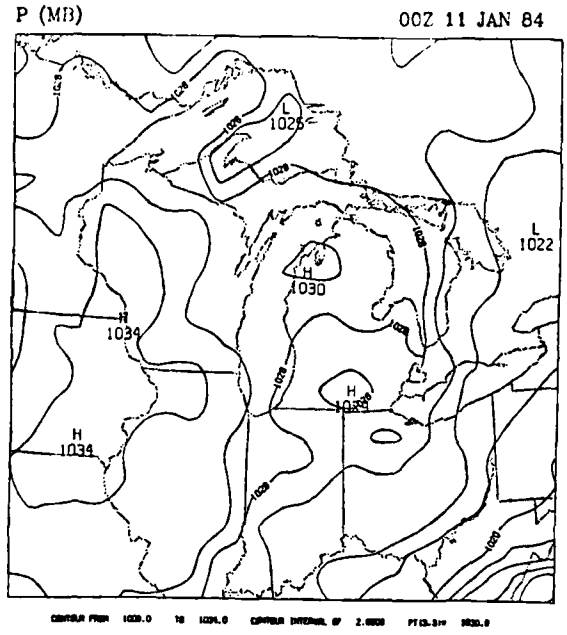


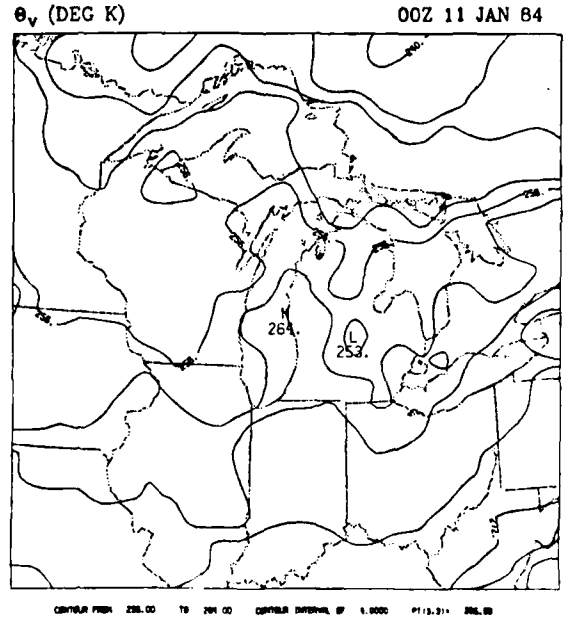


Figure 42. Surface pressure and virtual potential temperature analyses for 0000 GMT 11 January 1984.

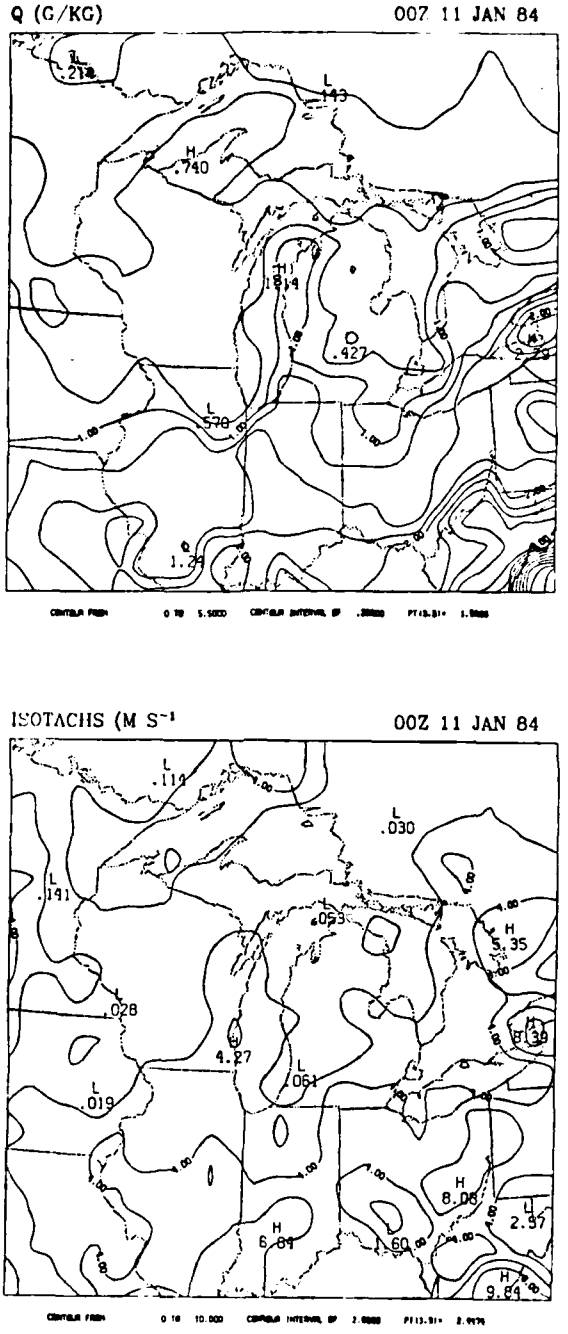


Figure 43. Surface specific humidity and isotach analyses for 0000 GMT 11 January 1984.

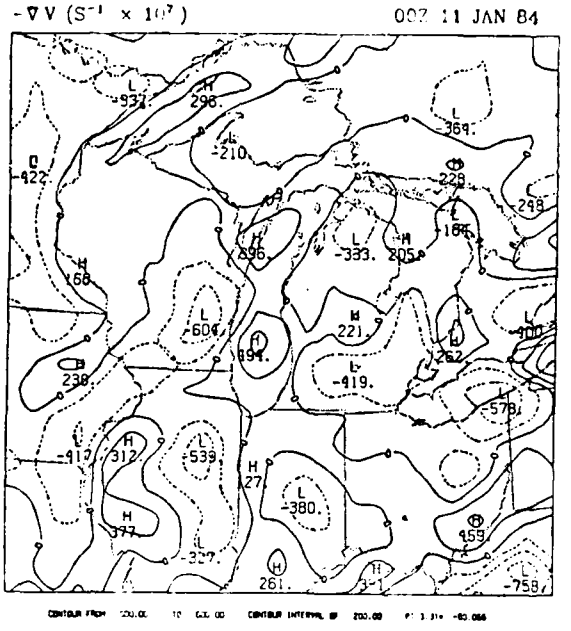


Figure 44. Surface convergence analysis for 0000 GMT 11 January 1984.

# 5. AIRCRAFT OBSERVATIONS: MESOSCALE $\gamma$ SETTING

This chapter contains the findings obtained from examination of the data collected by the NCAR King Air aircraft as it flew through the convective boundary layer which developed over Lake Michigan on 10 January 1984 in response to the CAO. The discussion is broken into three major areas. Firstly, a brief description of the aircraft flight path is given. This is followed by an examination and discussion of the raw data plots. Finally, a detailed discussion is provided which deals with the spectral representation of the raw data and the inferences that can be drawn from these spectra regarding the properties of the convectively-mixed layer, the capping inversion layer and their respective interactions.

## 5.1 Description of King Air Flight #85

As briefly mentioned in Chapter 2, the aircraft flew over and in the vicinity of Lake Michigan from 1558 to 2042 GMT 10 January 1984. Flight #85 was but one of fifteen research missions which were dispatched during Project LESS, but was the only one to be flown into a convective boundary layer during a northerly flow case. This was the particular event which the Purdue Mesoscale Convection Research Group was interested in because it resulted in the longest fetch and, therefore, the greatest possible amount of air mass modification in the Great Lakes region. Upon departing MKG, (see Fig. 7 for review) flight #85 turned south and flew into northwest Indiana. In the vicinity of Valparaiso, a vertical sounding (~one hour in duration) was taken during descent. After completion of the first sounding, the aircraft climbed to 2900 m and flew a general heading of 340° toward MKE (above the boundary layer and in accordance with the Aurora Flight Center). After diagonally crossing the southern tip of Lake Michigan and entering into Wisconsin, a second sounding was completed. The aircraft then flew southeast for a short distance in order to orient the aircraft so as to fly perpendicular to the cloud streets which had developed over the lake and, at the same time, assume a

heading which lined up with MKG in preparation for landing. After collecting nearly five hours of data, the research flight terminated at MKG at 2042 GMT.

Selecting a segment of the data for detailed examination (during a CAO event) involved using the criteria discussed in Section 2.3.4. Specifically, these were 1) the aircraft must maintain a constant heading, 2) the aircraft must remain at a constant height within the boundary layer, and 3) the flight leg must contain a maximum number of data points equivalent to a power of two. Using these contraints there were two choices for flight legs to examine. The first of these was the southeast to northwest leg which diagonally crossed the southern extreme of the lake. Although at first glance this segment represented the longest flight leg which met all three criteria, the altitude was well above the CTBL. The second segement, as represented in Fig. 45, is the one chosen for this study. The average altitude was 1392 m with an average ground speed and heading of 75.854 m/s at 090°. Not only does this leg meet all criteria, but the flight path also (ideally) crosses perpendicular to the cloud bands which can be seen just off the west shore of Lake Michigan (as shown in Fig. 46), thereby affording a maximum sampling rate of this feature in the Type I CTBL.

In total, the west–east flight leg contains 24.25 minutes or 29,100 bits of data when sampling at 20 Hz. Since the fast Fourier transform used in this study works most efficiently with powers of two, the data stream was truncated to the nearest power of two, which was $2^{14}$ or 16,384 data points. This is equal to a length scale of 110.4 km. Before detrending and spectral decomposition, the raw data were inspected to determine which set would provide the optimum amount of information on the CTBL.

## 5.2 Raw Data Plots

As stated above, the selected west–east flight segment contained 29,100 data points. The variables which were chosen for study included the specific humidity (q), liquid water content (lwc), ambient air temperature (T), virtual potential temperature ($\theta_v$), and the three wind components (u, v, and w). The plots of these variables are shown in Figs. 47–53. Since moisture has been reported as the best tracer of convection, as mentioned previously in Chapter 4, the specific humidity plot will be examined first.

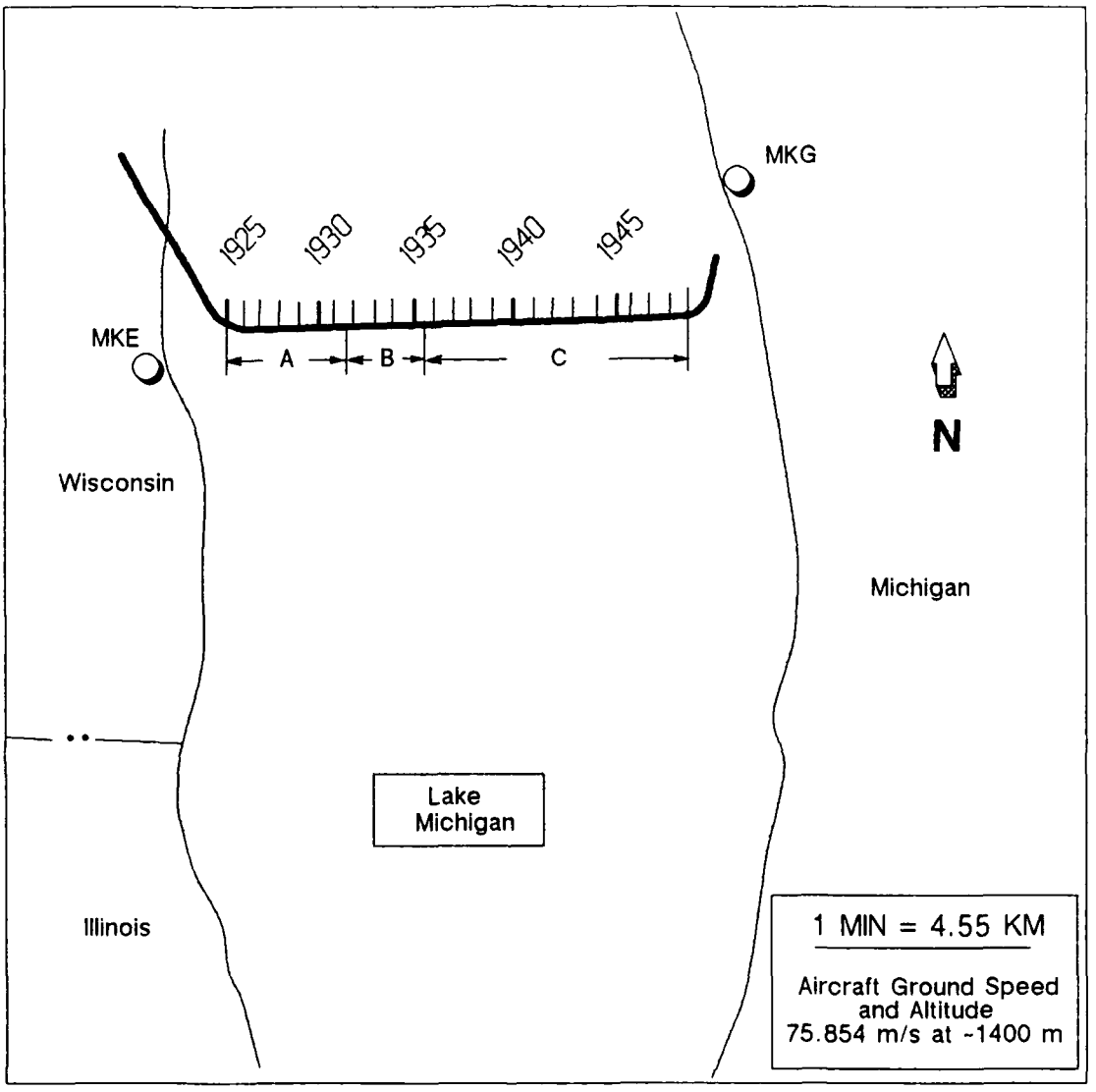


Figure 45. Heavy line displays segment of flight #85 across Lake Michigan. Section of flight leg, from 1925–1949 GMT 10 January 1984, was used for spectral decomposition in this case study. The segments denoted by A, B, and C represent the aircraft's flight through the warm inversion layer, transition layer, and well-mixed convective layer, respectively (discussed in a subsequent section of this chapter). Lengths of these segments are A = 30.9 km, B = 17.4 km, and C = 62.1 km for a total of 110.4 km.

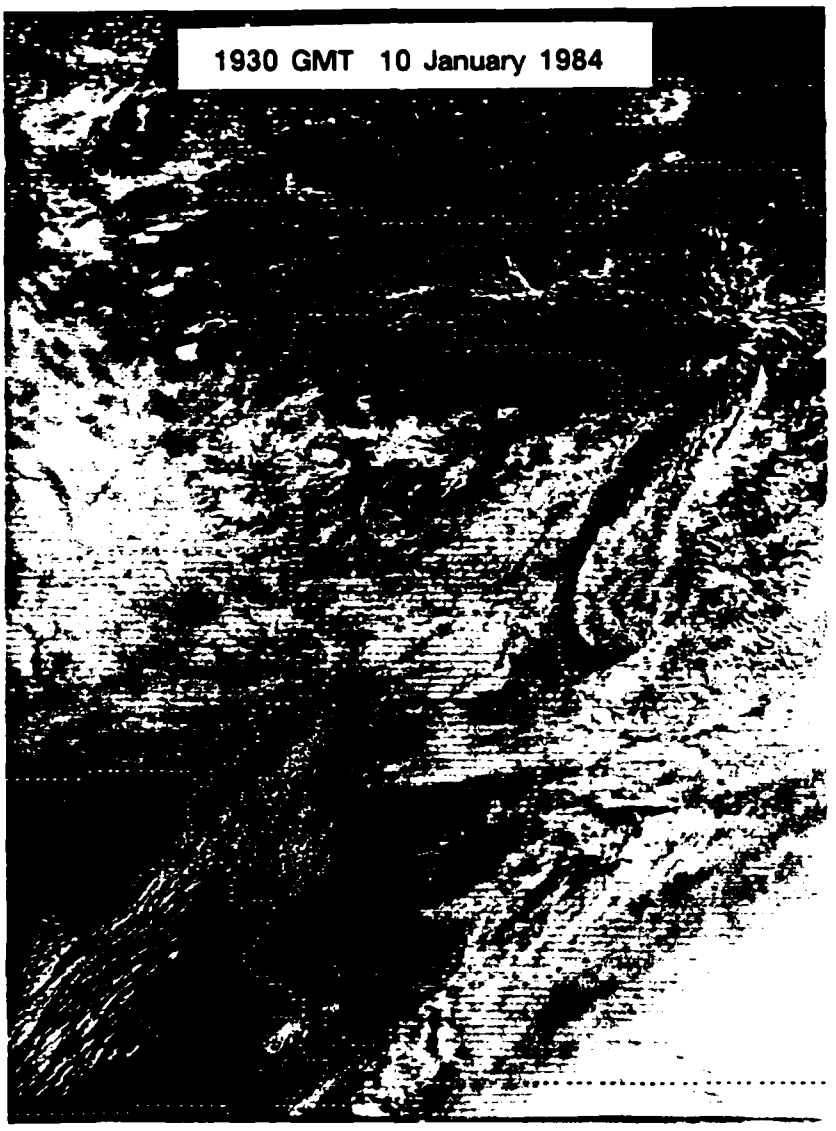


Figure 46. GOES visual satellite imagery for 1930 GMT 10 January 1984. Note the 2-D cloud bands present off the west shore of Lake Michigan which are aligned with the north-south flow in the Type I CTBL. Unrelated to this study is the CTBL (under northeasterly flow) from central Illinois into southwest Missouri, where 3-D BCM cells form and give way downstream to 2-D bands or cloud streets. Wind shear over the Ozarks forced the 2-D pattern.

The plot of specific humidity (Fig. 47) taken from the flight segment reveals three distinct regions. Initially the trace is flat at 0.14 g/kg with minimal response. There is a sudden rise in the moisture content which peaks at ~.68 and then rapidly decreases to near the initial value. This is followed by another sharp increase to almost 1.05 g/kg, a slight decrease, and then fairly steady undulations, vascillating around 1.05 g/kg. Two significant drops in the specific humidity are noted in this region, the first occurring at approximately 1938 GMT and the second near 1944 GMT.

The plot of the liquid water content begins in the same fashion as the specific humidity trace with small fluctuations centered about 0.045 g/m$^3$. After 1932 GMT these fluctuations become considerably more pronounced, peaking at maximum values of 0.16 g/m$^3$. A dome-like pattern with a length scale of ~ 14 km is also evident after 1932 GMT with a total of five repetitions found in the data. It is important to note that the liquid water content measurments do contain a systematic error. The sensor should measure zero liquid water content in the inversion layer where no clouds are present. The 0.045 g/m$^3$ value indicated that the Johnson-Williams sensor has drifted off baseline. Values less than 0.045 g/m$^3$, which occur after 1934 GMT, indicate that removal of the inital response will not entirely eliminate the systematic error. However, for this study the flight leg is broken into three segements, each with its own mimimum value. Since the focus is on the fluctuations in each of these segments and not the exact measured values, acceptable results can be obtained.

The ambient air temperature, plotted in Fig. 49, contains a pattern similar to that of the moisture parameters. The temperature shows little fluctuations at the beginning of the trace until ~1932 GMT. This is followed by several rapidly changing peaks with maximum values near −15°C and minima at −19°C. The trace then levels out at a temperature of −18°C with the exception of two peaks of warmer temperatures occurring in the vicinity of 1938 and 1944 GMT. The virtual potential temperature (Fig. 50) also contains this identical pattern of a flat response, followed by a series of rapid and pronounced fluctuations, and finally another flattening in the response, but at a colder value than the initial response and with two prominent warm peaks interrupting the signal at ~ 1938 and 1944 GMT.

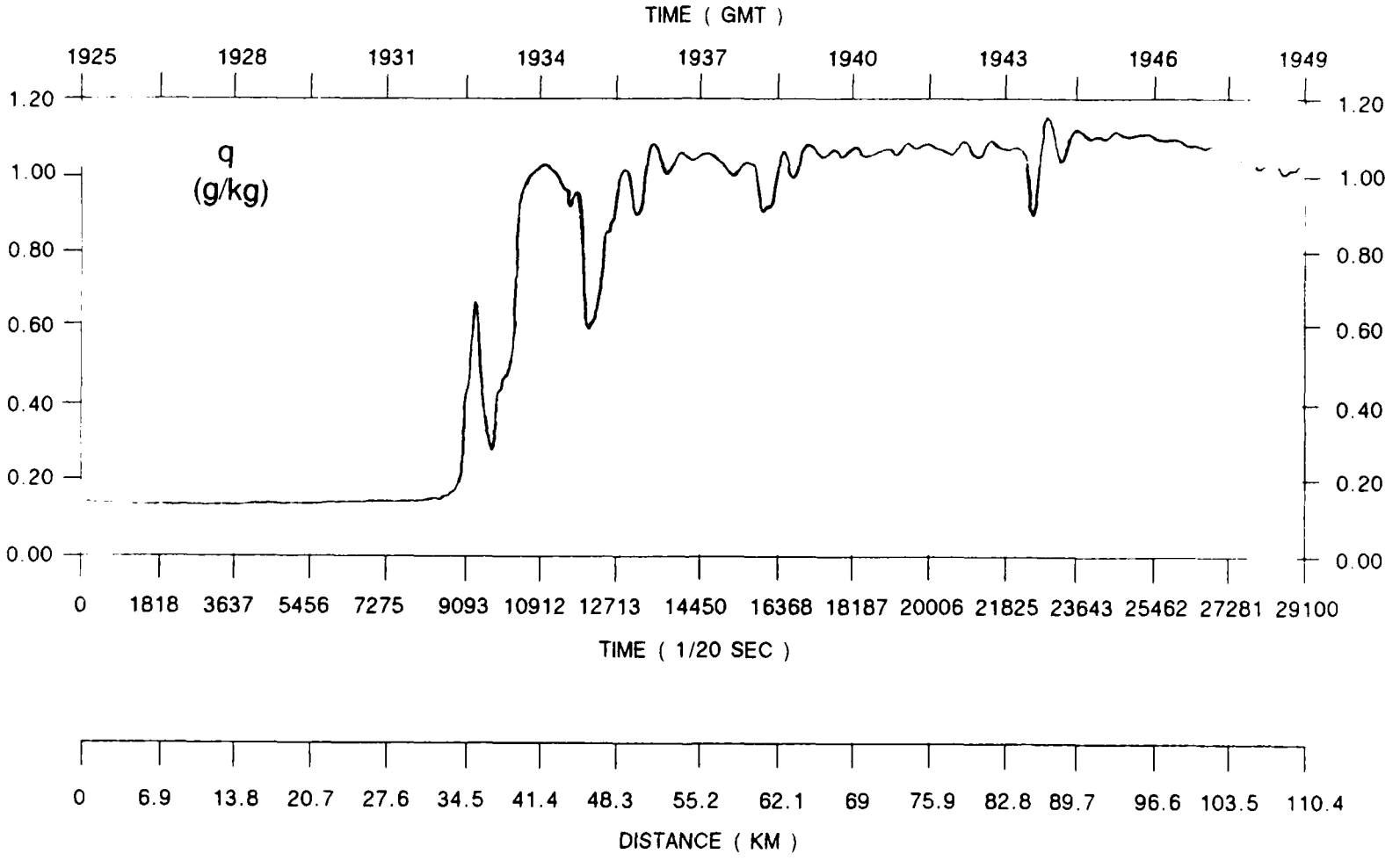


Figure 47. Plot of raw aircraft specific humidity measurements (g/kg) taken from 1925 to 1949 GMT 10 January 1984.

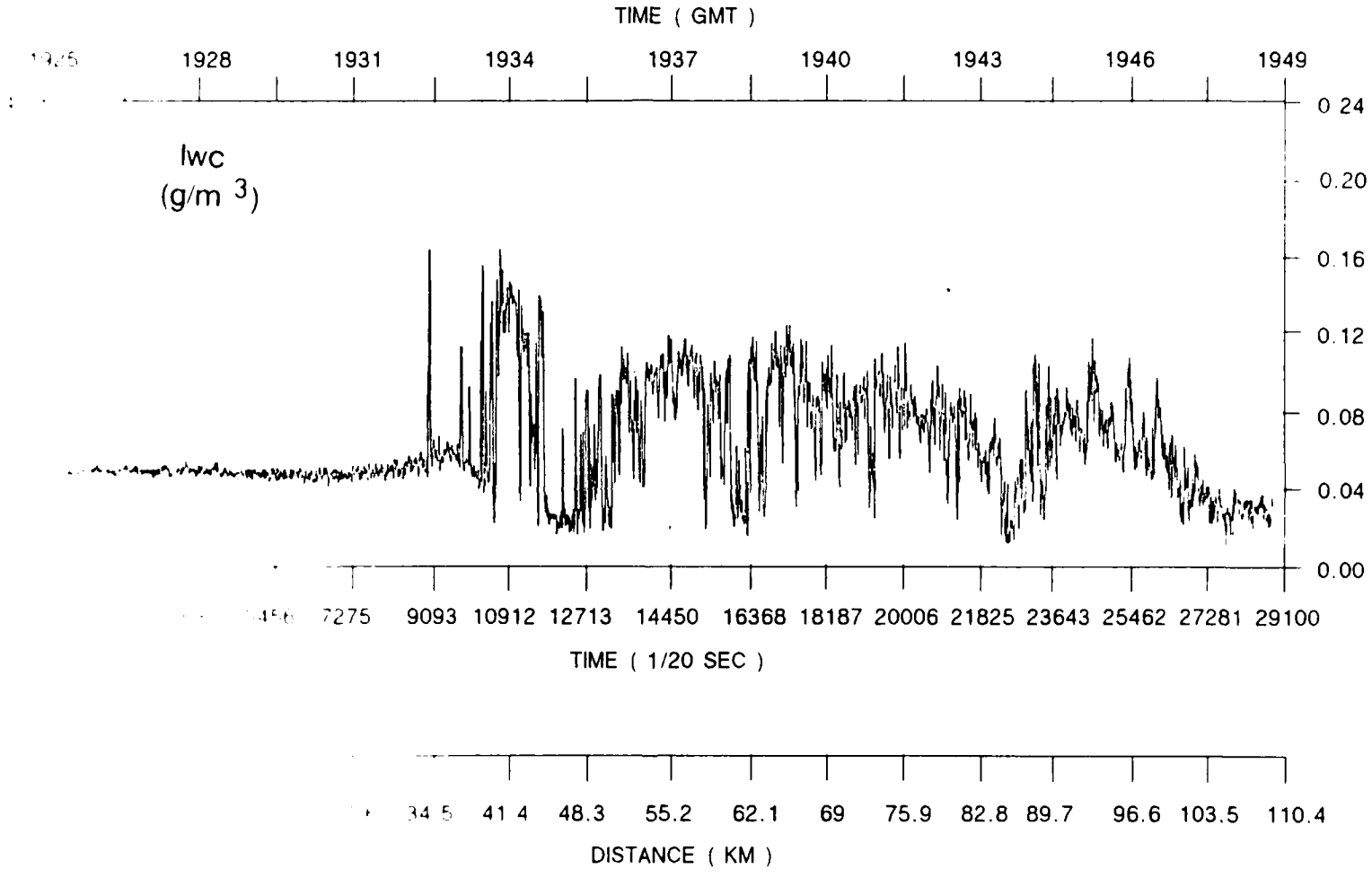


measurements (g/m³) taken from 1925 to 1949 GMT 10 January 1984.

AD-A185 671 AN OBSERVATIONAL CASE STUDY OF MESOSCALE CONVECTION 2/2
OVER LAKE MICHIGAN ON 10 JANUARY 1984(U) AIR FORCE INST
OF TECH WRIGHT-PATTERSON AFB OH S R GILBERT 1987
UNCLASSIFIED AFIT/CI/NR-87-74T F/G 4/2 NL

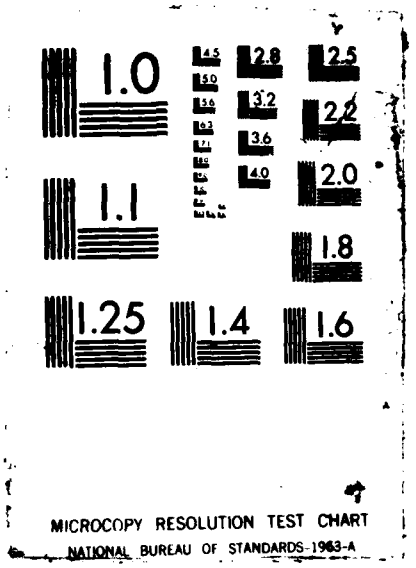
1.0
1.1
1.25
1.4
1.6
2.0
1.8
2.2
2.5
2.8
3.2
3.6
4.0
4.5
5.0
5.6
MICROCOPY RESOLUTION TEST CHART
NATIONAL BUREAU OF STANDARDS-1963-A

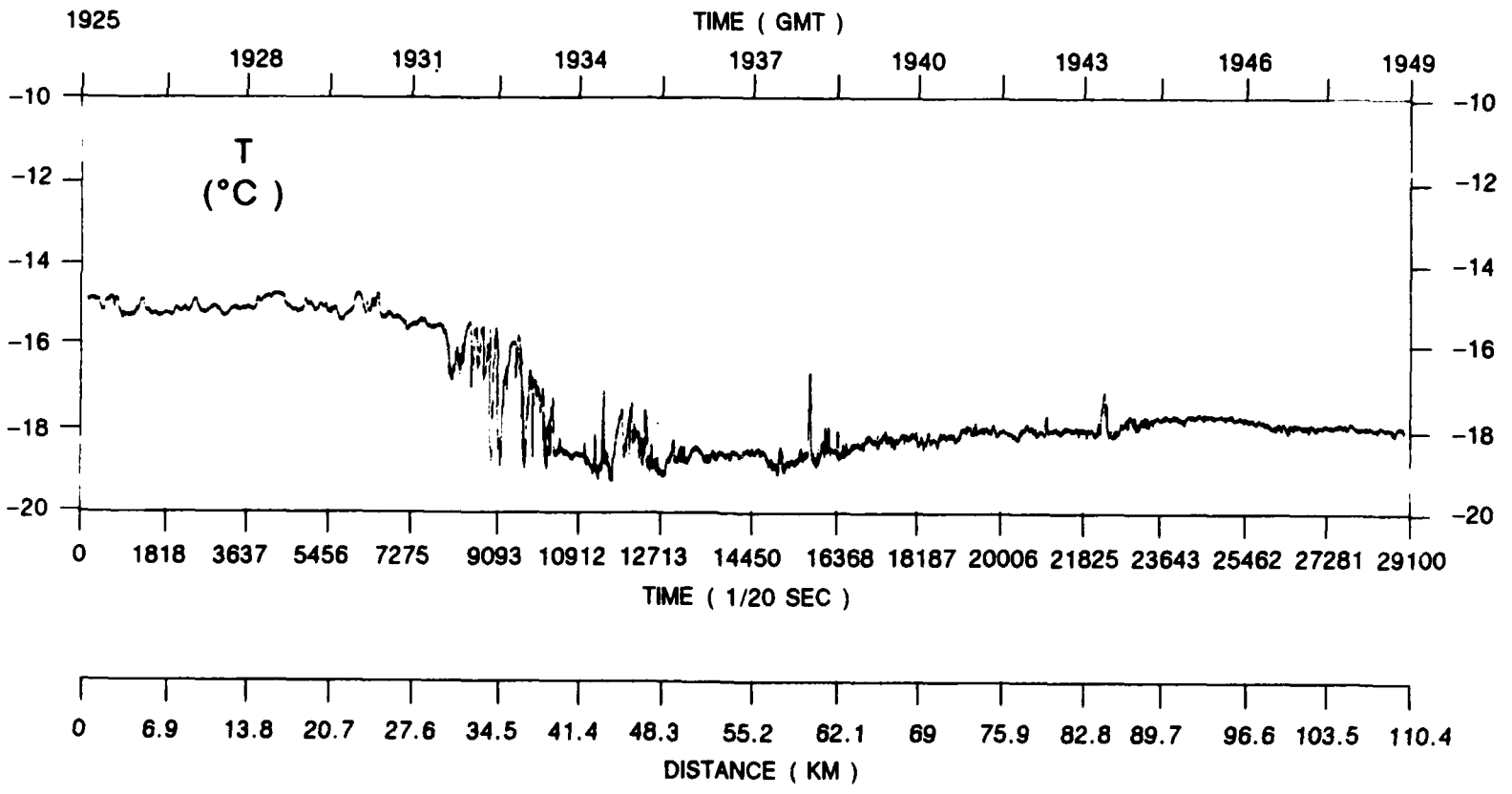


Figure 49. Plot of raw aircraft ambient air temperature measurements (°C) taken from 1925 to 1949 GMT 10 January 1984.

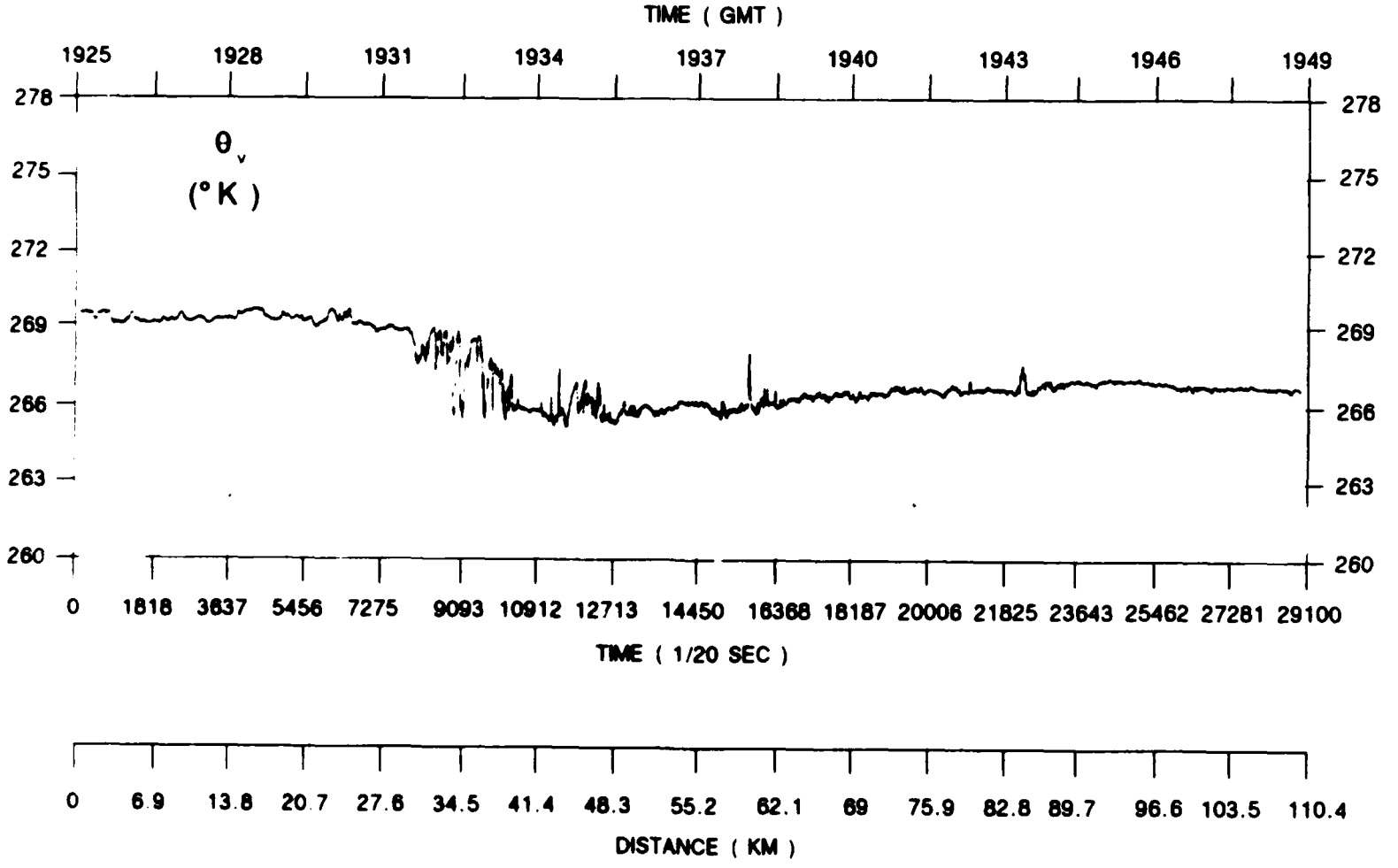


Figure 50 Plot of raw aircraft virtual potential temperature measurements (° K) taken from 1925 to 1949 GMT 10 January 1984.

The wind components, however, do not share quite this same pattern of changes. The u wind component (Fig. 51), for example, starts out in the same fashion (*i.e.* low amplitude, nearly flat response) with light westerly winds. The winds swing to light easterly near 1930 GMT, but the amplitude of the fluctuations remains small. This amplitude fluctuation changes and becomes much more pronounced at approximately 1932 GMT. This timing coincides well with the onset of increased amplitude seen in the moisture and temperature plots. Moving further eastward, only two significant features can be seen, the first being the peaks where the component wind speed approaches zero, and the second a regular pattern of spikes on the order of every 2 to 3 km which peak toward zero.

The v wind component (Fig. 52) displays a field of northerly flow along the entire flight path. As with previous plots, it begins with minor fluctuations which suddenly increase in amplitude near 1932 GMT. There is some organization present to the east, but in a different form than that possessed by the u component. In this plot, a dome shape of v component wind speeds can be seen occurring approximately 6 times at ~14 km intervals. The first of these can be seen beginning at ~10,500 (on the 1/20 sec time scale) through ~13,400, with a second from ~13,400 to ~16,700. Each of these and the subsequent "domes" initially show wind speeds near 12 m/s, decreasing at a steady rate to near 5 m/s, then increasing, again at a steady rate, to near the initial value of 12 m/s. The last two such features (~23,700–27,000 and ~27,000–29,100) are much less pronounced than the first four.

The w wind component, again, shows the same intial condition as all previous plots, with very small oscillations about zero which rapidly increase in amplitude at about 1932 GMT (see Fig. 53). This parameter deviates from the others in that no other pattern is readily discernable. The amplitude has increased, but a subjective estimate still yields a time average of zero for the vertical motion.

When integrating the raw plots together for a "big picture", it becomes apparent that the aircraft flew through three different regions. The first of these is toward the top of the warm inversion where the very minor fluctuations are seen in the raw data plots (represented in Fig. 45 by "A"). The second is the region where major changes were displayed in the raw data (almost a step function in the $q$, $T$ and $\theta_v$ plots) at the base of the inversion and will be called the transition layer (section "B" in Fig. 45). The last region is the well-mixed layer where convection was occurring (see "C" in Fig. 45). It is interesting to note that in the

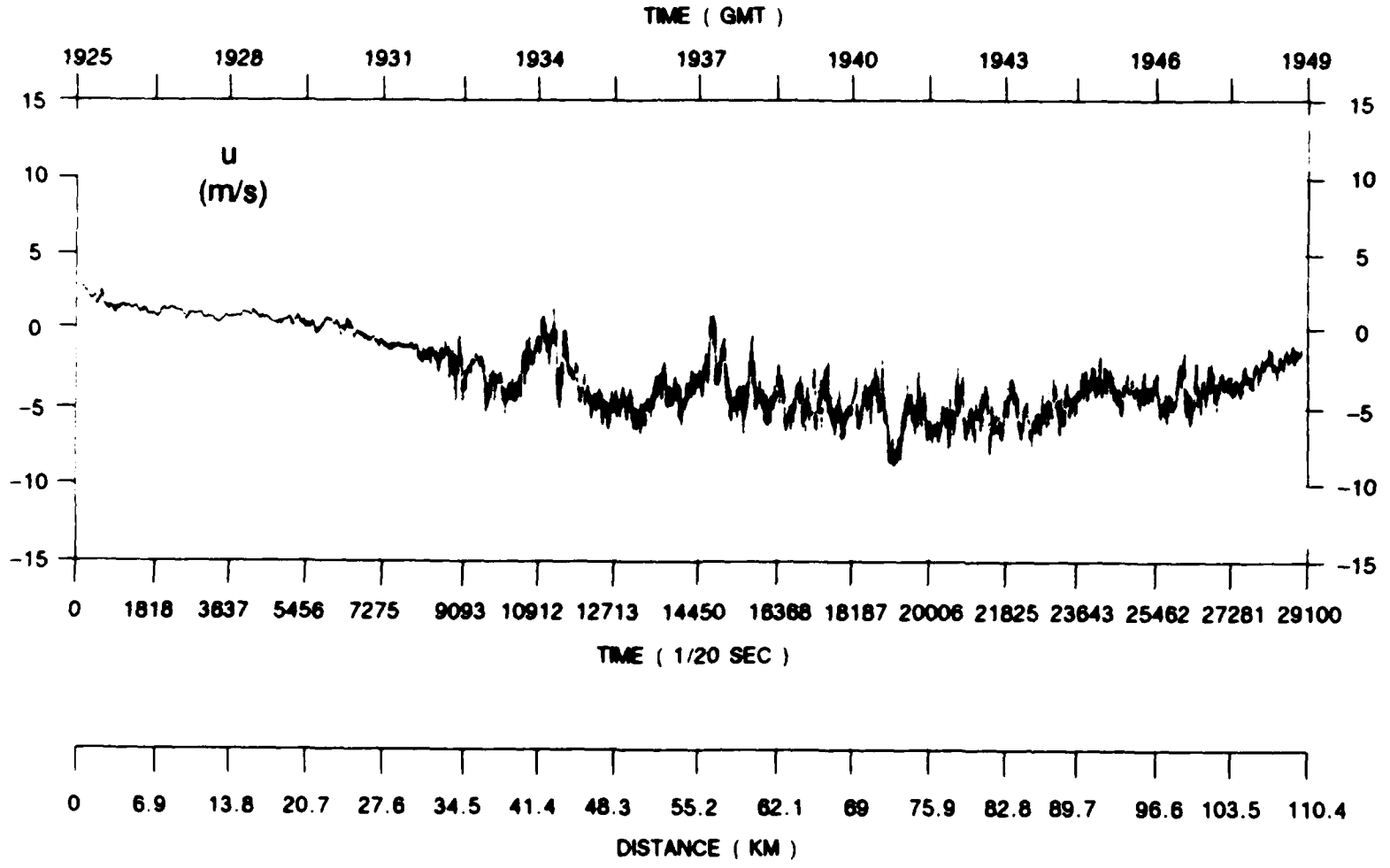


Figure 51. Plot of raw aircraft u wind component measurements (m/s) taken from 1925 to 1949 GMT 10 January 1984.

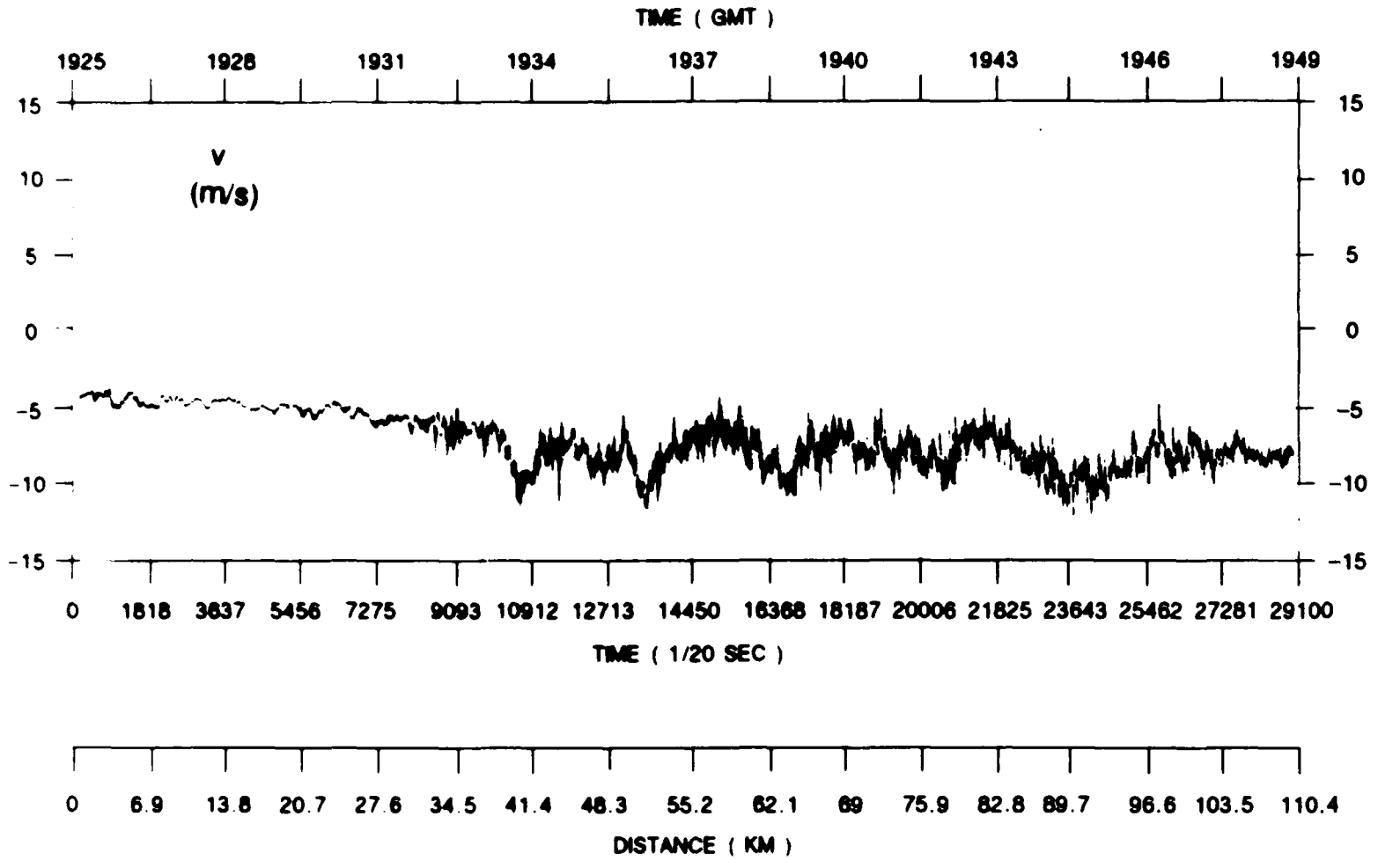


Figure 52. Plot of raw aircraft v wind component measurements (m/s) taken from 1925 to 1949 GMT 10 January 1984.

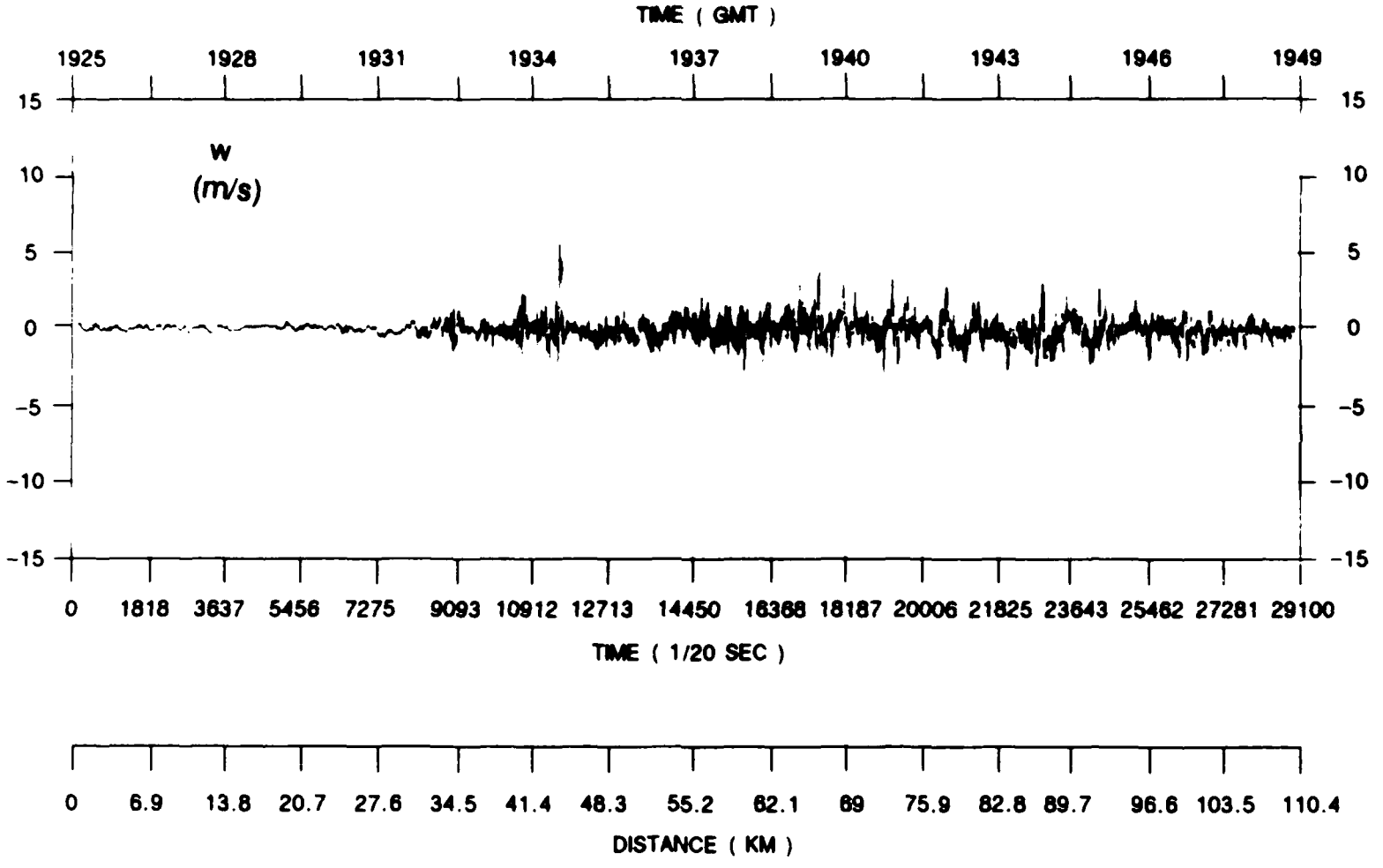


Figure 53. Plot of raw aircraft w wind component measurements (m/s) taken from 1925 to 1949 GMT 10 January 1984.

transition region, as the specific humidity increases (decreases), the temperature (both ambient and $\theta_v$) decreases (increases). This coupling holds true even for the two spikes present in the well-mixed convective layer. As such, two types of air can be identified; warm, dry air from the inversion layer, and cool, moist air from the well-mixed layer. This coupling is the result of the properties of the air in the two distinct regions, the inversion and well-mixed layers. Penetrative convection from the well-mixed layer into the inversion is responsible for the creation of the transition layer. For the purposes of this research, penetrative convection is defined as convection which penetrates out of the convective well-mixed layer and into, but not through, the transition layer. Even in the well-mixed layer, a response to penetrative convection (or entrainment) can be found in the two spikes where a sudden decrease in the specific humidity is coupled with warmer temperatures.

## 5.3 Detrending and Spectral Decomposition

The first choice of a segment for spectral decomposition was the tail end of the flight (section "C" in Fig. 45), in the well-mixed layer. This area contains only well-mixed air and thus represents a near homogeneous sample. As such, data points between 12,716 and 29,100 (on the 1/20 sec time scale in Figs. 47-52) were used in the primary data set. The minimum resolvable wavelength from the 20 Hz data is ~7.5 m. This is calculated as

$$2 \cdot \frac{\text{Aircraft speed}}{\text{Sampling rate}} \tag{5.1}$$

where the aircraft speed is 75.854 m/s and the sampling rate is 20 $s^{-1}$. It was also evident that spectral decompostion of the transition region may yield some interesting results even though the homogeneity of the sample is violated. Thus, the segment of the flight between data points 8,150 and 24,534 was chosen as a second data set for spectral representation.

Before the data sets are spectrally decomposed using the fast Fourier transform, the data must be detrended. This is done by fitting a straight line to the data and then removing the slope and y-intercept. The IMSL routine RLONE, a linear regression for one variable, was used for the detrending. The data are then sent through the IMSL fast Fourier transform FFTRC to determine the spectral energy present at each frequency. The normalized spectral energy is then multiplied by its respective frequency and plotted against the log of the frequency so

that equal areas under the curve represent equal energy. This is the same technique employed by Rothermel and Agee (1980) and Ross and Agee (1985) for AMTEX aircraft data.

The use of spectral decomposition does impose several limitations upon the data analysis. The first of these is the representation of length scales. The total path of the aircraft flight segment, represented by the 16,384 data points, is 62.14 km long. This represents a wavenumber of one in the spectra of the aircraft data. A wave number of two represents the total distance divided by two or 31.07 km. Any energy present in phenomena with a wavelength between 62.14 km and 31.07 km can only be represented at either the first or second wave numbers. Table 3 includes the first 30 wave numbers as well as the respective frequencies and wavelengths. As the Table indicates, this problem occurs primarily at low wave numbers (generally less than 10).

A second problem exists in using a straight line fit to detrend the data. This can introduce false signals if the correlation coefficient (*i.e.* the degree of fitness) is not close to one. Finally, the statistical siginificance of peaks present at the low frequency/wave number end of the spectrum must be considered. Statistical theory would dictate that any results obtained from wave numbers less than 12 or 13 should be considered questionable due to insufficient sampling. In this study, however, the problem is largely bypassed due to the high degree of detail acquired concerning the data and their environ. In other words, using "blind" statistics with little or nothing known about the data or the context from which they were obtained, any energy present in a wave number of two (which means the pheonomena is sampled only twice) must be considered questionable at best. However, by knowing the data and the condition under which they're taken, the likelihood exists that low wave number phenomena can be described, with a high degree of accuracy. This negates to some degree the requirement for a larger sample in the raw data.

Before looking at the results of the detrending and spectral decomposition, several predictions can be made about the final results. Firstly, since moisture is the best tracer of the convection, the cloud bands present on the GOES satellite imagery in Fig. 46 should be better represented by the specific humidity, rather than the temperature. Secondly, the basic convective mode or BCM defined by Ross and Agee (1985) should be present on the order of a 3- 5 km length scale or at approximately 1.5 $z_i$ ($z_i$ - 2000 m along flight path of

Table 3. The first 30 wave numbers represented in the spectra of the aircraft data and their associated frequencies and wavelengths.

| WAVE NUMBER | FREQUENCY (Hz) | WAVELENGTH (km) |
|---|---|---|
| 1 | 1.2207 E-03 | 62.18 |
| 2 | 2.4414 E-03 | 31.06 |
| 3 | 3.6621 E-03 | 20.71 |
| 4 | 4.8828 E-03 | 15.53 |
| 5 | 6.1035 E-03 | 12.42 |
| 6 | 7.3242 E-03 | 10.35 |
| 7 | 8.5449 E-03 | 8.87 |
| 8 | 9.7656 E-03 | 7.76 |
| 9 | 1.0986 E-02 | 6.90 |
| 10 | 1.2207 E-02 | 6.21 |
| 11 | 1.3428 E-02 | 5.64 |
| 12 | 1.4648 E-02 | 5.17 |
| 13 | 1.5869 E-02 | 4.78 |
| 14 | 1.7090 E-02 | 4.43 |
| 15 | 1.8311 E-02 | 4.14 |
| 16 | 1.9531 E-02 | 3.88 |
| 17 | 2.0752 E-02 | 3.65 |
| 18 | 2.1973 E-02 | 3.45 |
| 19 | 2.3193 E-02 | 3.27 |
| 20 | 2.4414 E-02 | 3.11 |
| 21 | 2.5635 E-02 | 2.95 |
| 22 | 2.6855 E-02 | 2.82 |
| 23 | 2.8076 E-02 | 2.70 |
| 24 | 2.9297 E-02 | 2.59 |
| 25 | 3.0518 E-02 | 2.48 |
| 26 | 3.1738 E-02 | 2.39 |
| 27 | 3.2959 E-02 | 2.30 |
| 28 | 3.4180 E-02 | 2.22 |
| 29 | 3.5400 E-02 | 2.14 |
| 30 | 3.6621 E-02 | 2.07 |

aircraft) as defined by Kaimal *et al.* (1976). Thirdly, the north–south convective bands should provide a sharp spectral peak in the v component of wind for a transverse (west–to–east) flight.

Figure 54 displays the spectral representation of the specific humidity distribution found within the convective layer. The most prominent peak is found at a wavelength of ~3 km and represents the initial mode at which convection occurs. This is the BCM defined by Ross and Agee (1985) in the AMTEX data and occurs at 1.5 $z_i$ as reported by Kaimal *et al.* (1976). In addition, two significant peaks occur at ~ 10 km and ~ 15 km. These are

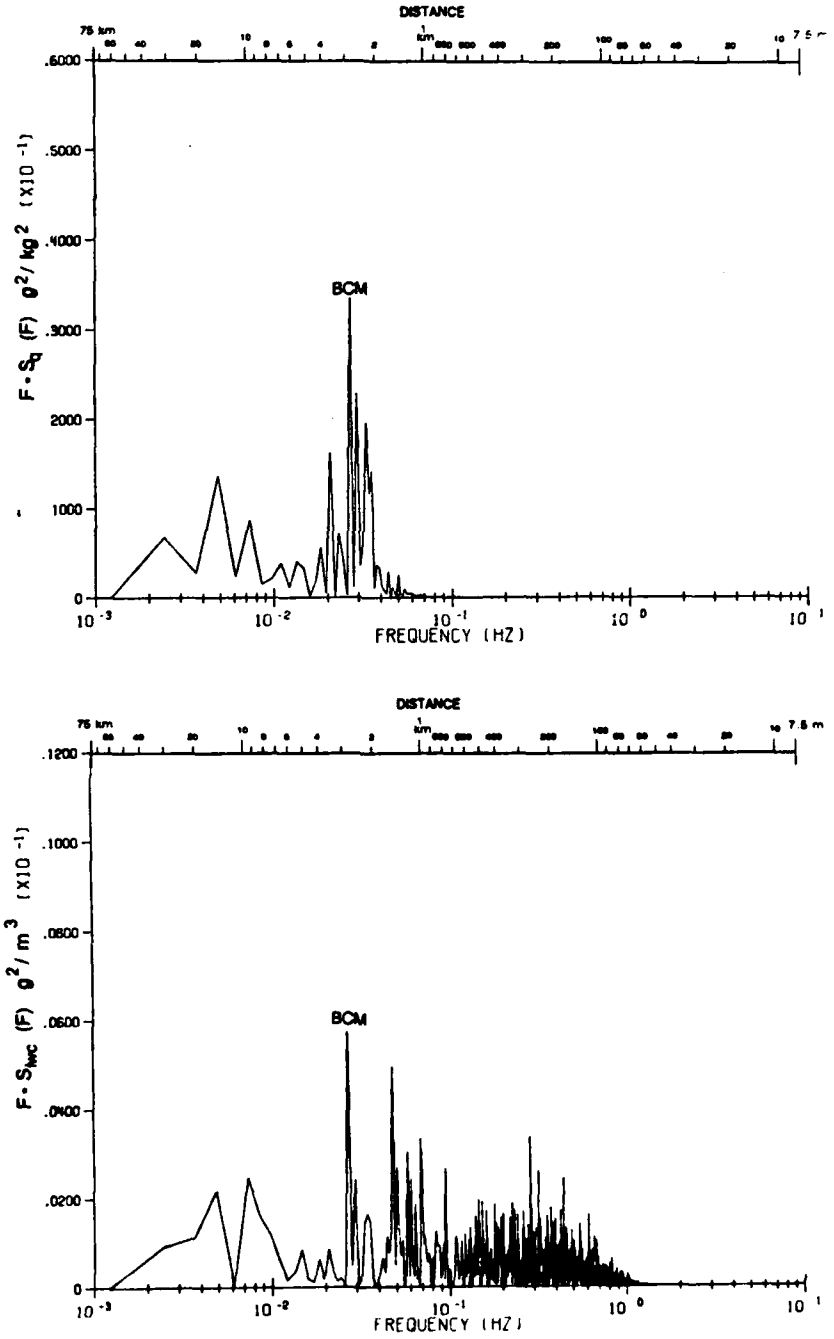


Figure 54. Spectral representation of the specific humidity (top) and liquid water content (bottom) in the well-mixed convective boundary layer. BCM denotes the Basic Convective Mode occurring near the 3 km length scale.

representative of the wavelength of the two–dimensional cloud bands seen in the satellite imagery. Other peaks are present in this plot but at less energy. The BCM peak is again found in the liquid water content (bottom half of Fig. 54) at a wavelength of 3 km. Secondary peaks of much lesser energy are, likewise, present at the low end of the frequency scale.

The spectral plots of ambient and virtual potential temperature (top of Fig. 55) are almost identical, as were the raw data plots, with the most prominent peak in each at 30 km. There are two possible explanations for this energy. The first is that the energy present is due to the two major fluctuations seen in the raw data separated by a distance of ~ 25 km. These spikes represent the entrainment of warm, dry air from the inversion into the convective boundary layer. This may even be the beginning of mesoscale entrainment instability (MEI) discussed by Fiedler (1984). A second possibility is that this energy may represent MCC since this is the same length scale, but the MCC is suppressed and not realized due to the fact that the air runs out of water (*i.e.* no further modification can occur). The time scales of the phenomena involved (MEI ~40 hours and MCC ~15 hours) would support MCC in favor of MEI.

Turning to the wind components, the spectral energy density distribution of the u wind component (top half of Fig. 56) shows the most energy present at a wavelength of 31 km. This represents the entrainment of u momentum air, as seen in the raw u wind plot, centered about 10,900 and 14,600 on the 1/20 sec time scale. However, there is only a minor peak near 10 km to represent the 2–D cloud bands. Figure 56 also shows that the v wind component contains the most energy for the 2–D bands. This would be expected, since this is a northerly flow case. A spacing of approximately 10 km means the cloud bands, lined up in a north–south direction, are sampled six or seven times during the flight segement. Using the 10 km wavelength and a depth of 2 km, an aspect ratio of 5:1 is obtained. Finally, Fig. 57 shows that the w wind component, as might be expected, is composed primarily of turbulence and noise. Here, noise is referred to as any signal which does not possess enough energy to be statistically significant from the strength of the turbulence signal. The turbulence signal begins at the start of the inertial subrange or wavelengths less than 0.1 $z_i$ (200 m for this case) as reported by Kaimal *et al.* (1976). Note the –2/3 slope present in the intertial subrance of the log–log plot of the w wind component (bottom half of Fig. 57). This is identical to the slope for the vertical wind component found by Caughey *et al.* (1982) in a nocturnal Type II CTBL.

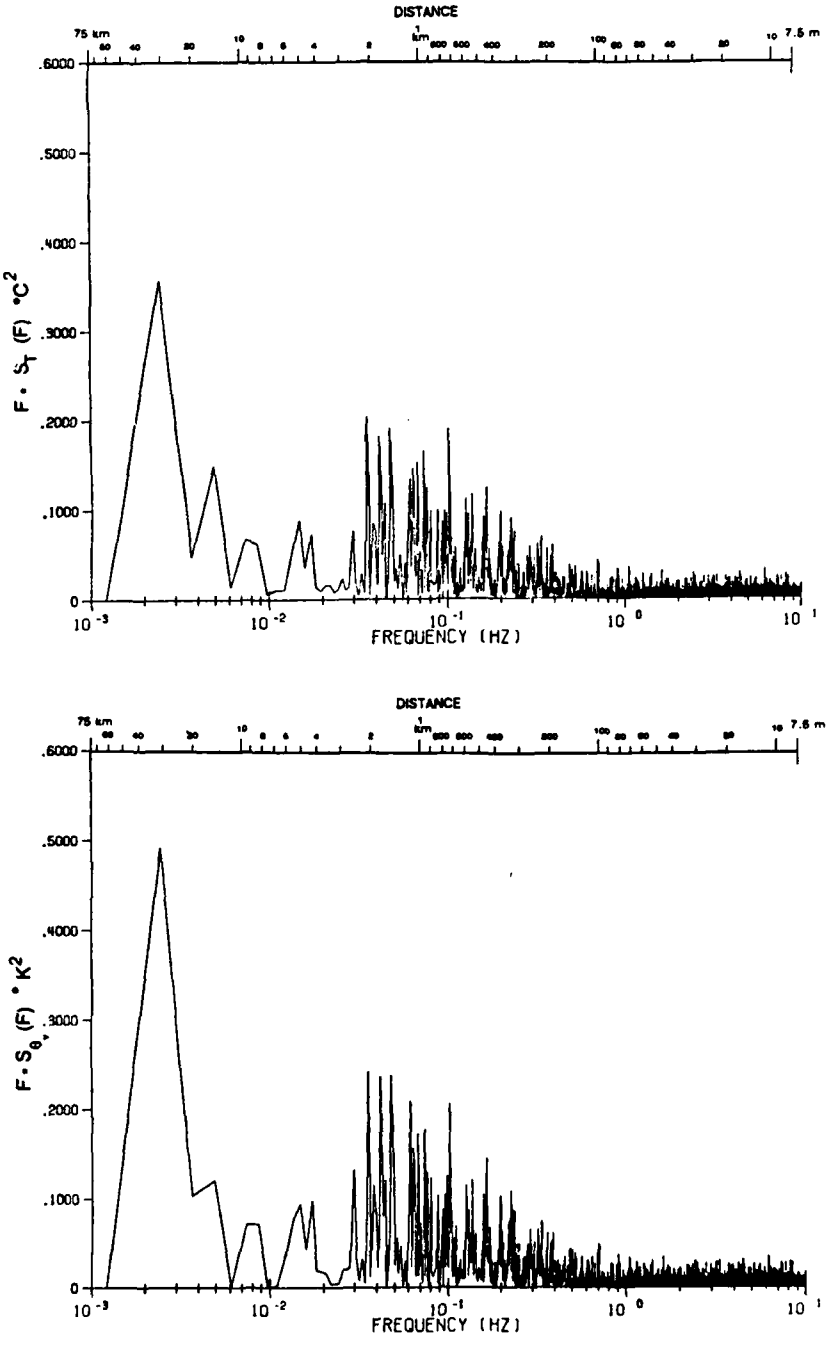


Figure 55. Spectral representation of the ambient air temperature (top) and virtual potential temperature (bottom) in the well-mixed convective boundary layer.

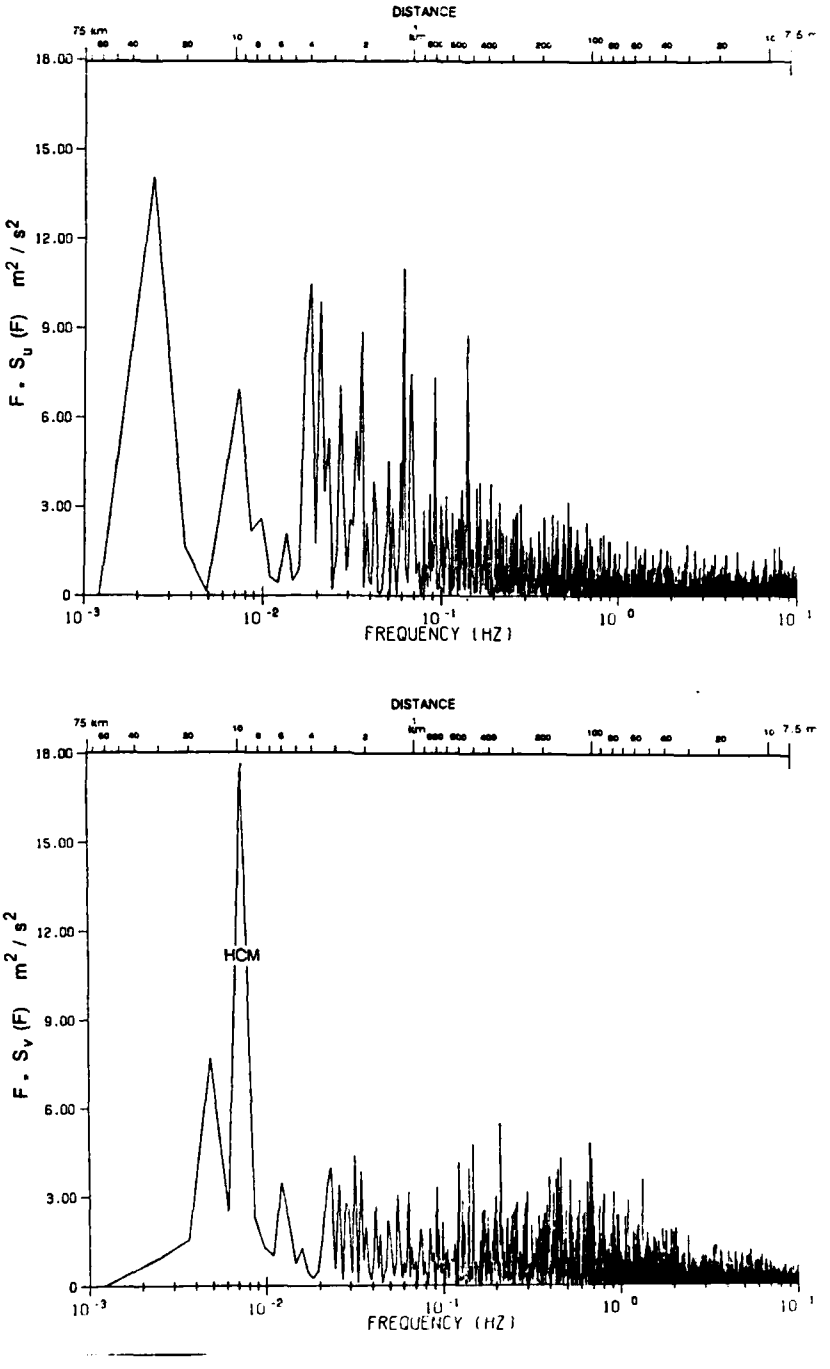


Figure 56. Spectral representation of the u (top) and v (bottom) wind components in the well-mixed convective boundary layer. HCM denotes the cloud streets, oriented north-south down the major axis of Lake Michigan.

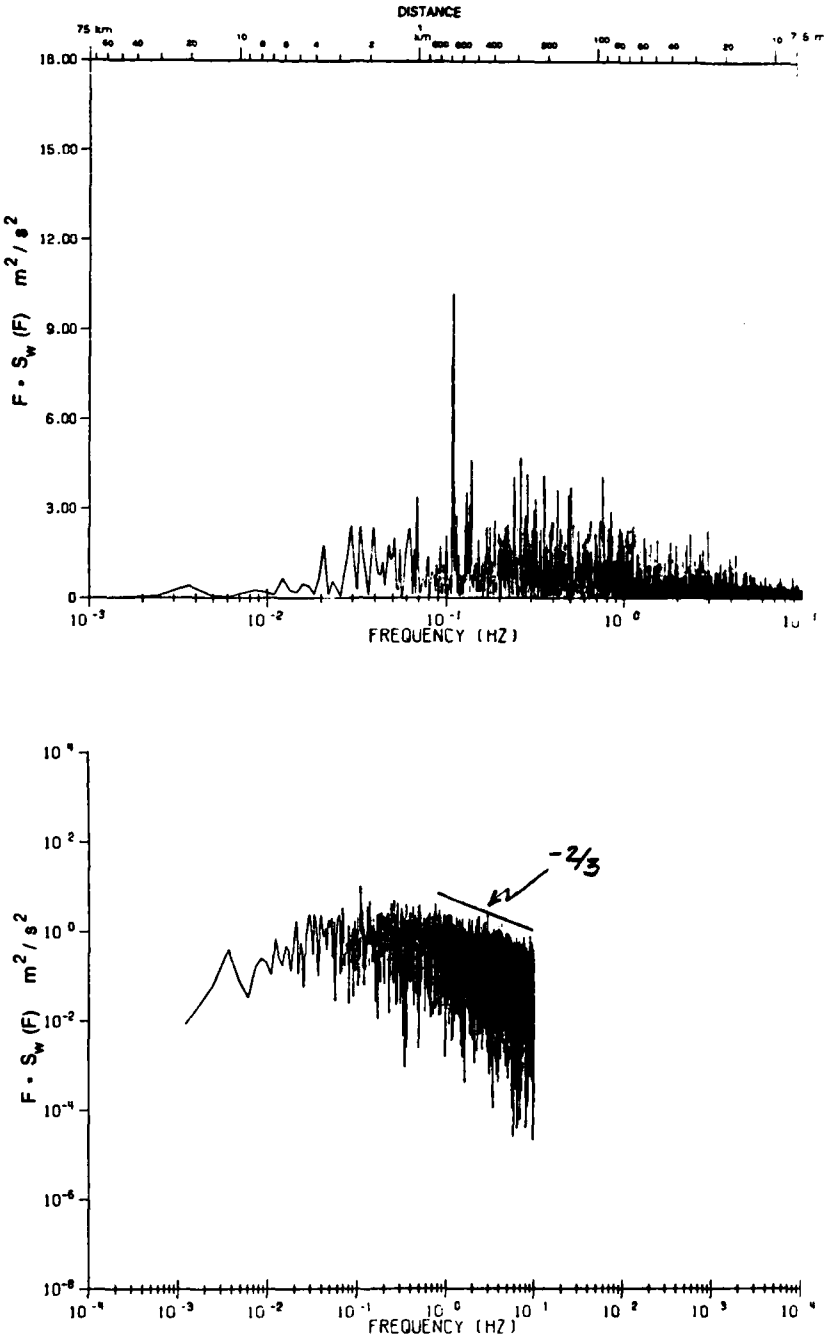


Figure 57. Spectral representation of the w wind component in the well-mixed convective boundary layer. Bottom log-log plot shows -2/3 slope in the inertial subrange.

## 5.4 Covariance Calculations

To determine if the transition layer more closely resembled the well-mixed convective layer or the inversion layer (or was a separate entity) covariance calculations were performed in each of the three regions (inversion layer, transition layer, and well-mixed convective layer). The covariances are calculated by first subtracting the instantaneous measurement from the average value for the region to determine the magnitude of the perturbation. The perturbations of two selected quantities are then multiplied to form the covariance of the parameters within the layer. Those covariances in which the perturbation of the w component of wind occur can also be referred to as vertical fluxes. The average value of each variable in the different layers, as well as the covariance values, are given in Table 4 and represented graphically in Fig. 58. The use of the eddy correlation technique, when applied to the aircraft data, results in the following degree of accuracy when using the raw air temperature, specific humidity and velocity data:

1) The temperature is accurate to within $\pm$ 0.2 °K with a fluctuation error on the order of 0.03 °K as reported by LeMone (1976).

2) The dewpoint temperature, for temperatures greater than 0 °K, is accurate to within $\pm$ 0.5 °K, and within $\pm$ 1 °K for temperatures less than 0 °K (Kelley and Zrubek, 1973).

3) The mean free air velocity is measured to within $\pm$ 1 m/s with the error in the three velocity fluctuations on the order of 0.1 m/s (Lenschow, 1973b).

As Fig. 58 demonstrates, the area identified as the warm inversion behaves exactly as expected. The environment is warm, dry and very stable with no identifiable parcels intruding into the area from below. The flux calculations are small, some nearly zero. These facts all support this layer as being the warm inversion where turbulent transfer is minimal.

At the far right hand side of Fig. 58 are the scaled arrows depicting the flux and covariance calculations at the top of the well-mixed convective layer. At the top of this layer the enviornment is cool and moist (extracted from the raw data) and in general the parcels are ceasing to rise as the top of the CTBL is encounted. Using the flux and covariance results, the characteristics of the parcels can be determined. The vertical flux of temperature is positive, indicating that upward moving parcels are warm and downward moving parcels are cold. The covariance of q and T are also positive, thus parcels with high specific humidity will be warm as would be expected in a rising convective plume. The

Table 4. The average value of each parameter in the warm inversion, transition, and convective layers and their covariance values.

| COVARIANCE CALCULATIONS | | | | | |
|---|---|---|---|---|---|
| Calculation | Quantity | Units | Warm Inversion Layer | Transition Layer | Well-mixed Convective Layer |
| Average of parameter | $\overline{u}$ | ( m/s ) | 0.585 | -2.793 | -8.086 |
| | $\overline{v}$ | ( m/s ) | -4.724 | -7.343 | -8.087 |
| | $\overline{w}$ | ( m/s ) | -0 125 | -0.098 | -0.016 |
| | $\overline{T}$ | ( °C ) | -15.169 | -17.692 | -18.159 |
| | $\overline{q}$ | ( g/kg ) | 0.143 | 0.635 | 1.055 |
| | $\overline{\theta_v}$ | ( °K ) | 269.501 | 266.942 | 266.683 |
| | $\overline{\theta_e}$ | ( °K ) | 269.929 | 268.648 | 269.443 |
| Covariance | $\overline{w'T'}$ | ( m/s °K ) | 4.319 E-03 | -4.327 E-02 | 1.896 E-02 |
| | $\overline{q'T'}$ | ( g/kg °K ) | -1.363 E-03 | -7.389 E-01 | 4.369 E-02 |
| | $\overline{w'q'}$ | ( m/s g/kg ) | 3.607 E-05 | 2.317 E-01 | 3.134 E-02 |
| | $\overline{u'w'}$ | ( $m^2$ / $s^2$ ) | 2.272 E-02 | 1.934 E-01 | -1.638 E-02 |
| | $\overline{v'w'}$ | ( $m^2$ / $s^2$ ) | -2.957 E-03 | -6.531 E-02 | -1.901 E-03 |
| | $\overline{w'\theta_v'}$ | ( m/s °K ) | 5.277 E-03 | -4.009 E-02 | 2.755 E-02 |
| | $\overline{w'\theta_e'}$ | ( m/s °K ) | 5.265 E-03 | 1.803 E-02 | 3.563 E-02 |

Figure 58. Graphical representation of the covariance calculations for the inversion layer, transition layer, and well-mixed convective layer. Bold line represents the flight path of the aircraft through the different regions. The inversion is represented by the thin, positively sloped lines, with the dashed line marking the boundary between the warm inversion and the transition layers.

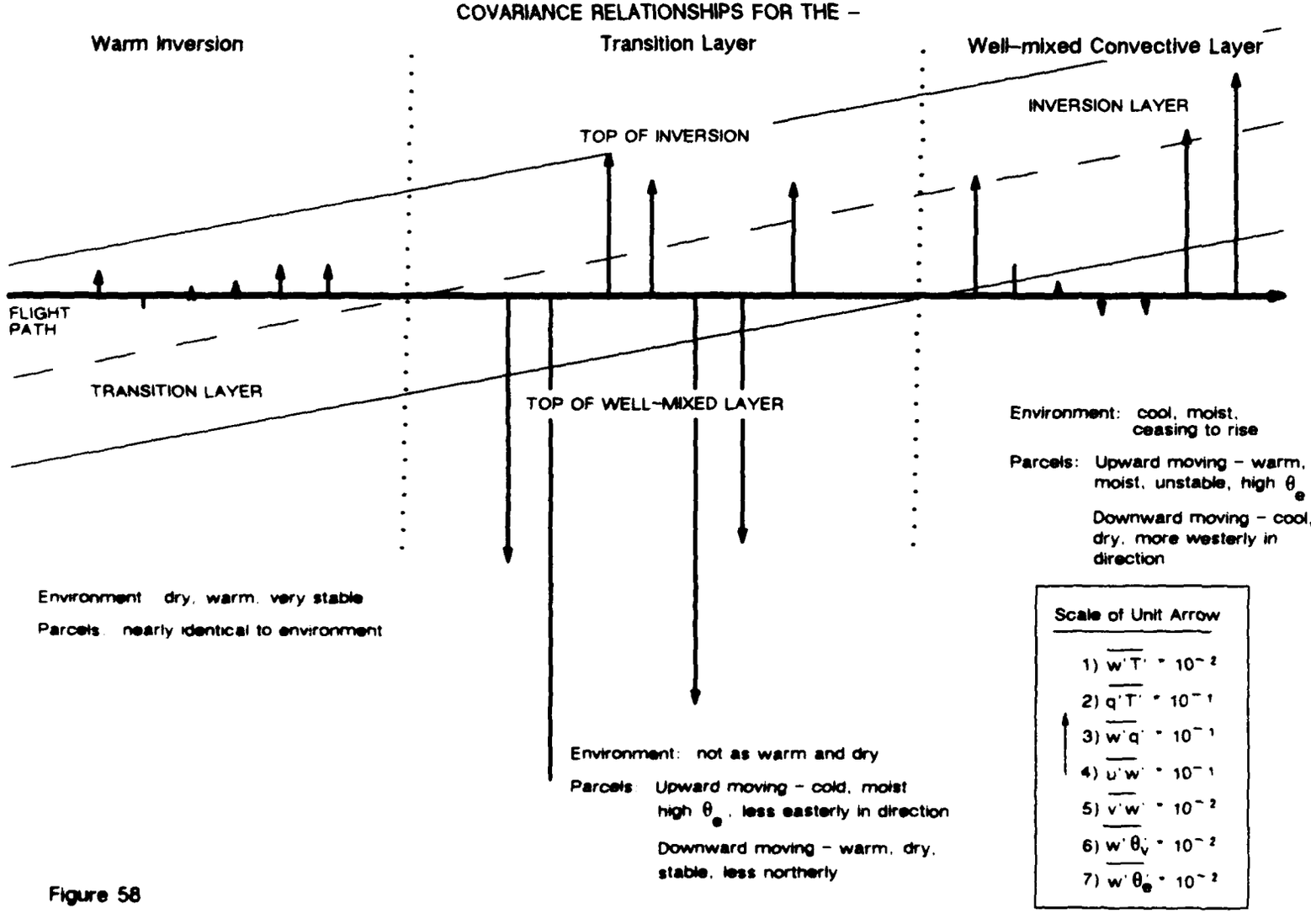
COVARIANCE RELATIONSHIPS FOR THE –
Warm Inversion
Transition Layer
Well-mixed Convective Layer
INVERSION LAYER
TOP OF INVERSION
FLIGHT PATH
TRANSITION LAYER
TOP OF WELL-MIXED LAYER
Environment: cool, moist, ceasing to rise
Parcels: Upward moving – warm, moist, unstable, high $\theta_e$
Downward moving – cool, dry, more westerly in direction
Environment: dry, warm, very stable
Parcels: nearly identical to environment
Environment: not as warm and dry
Parcels: Upward moving – cold, moist high $\theta_e$, less easterly in direction
Downward moving – warm, dry, stable, less northerly
Scale of Unit Arrow
1) $\overline{w'T'} = 10^{-2}$
2) $\overline{q'T'} = 10^{-1}$
3) $\overline{w'q'} = 10^{-1}$
4) $\overline{u'w'} = 10^{-1}$
5) $\overline{v'w'} = 10^{-2}$
6) $\overline{w'\theta_v'} = 10^{-2}$
7) $\overline{w'\theta_e'} = 10^{-2}$

Figure 58

positive value for the vertical flux of specific humidity also fits well with convective parcels in that upward moving parcels will be moist. As with all the flux calculations, the opposite is true when reversing the direction of the parcel, such that downward moving parcels are drier. The u and v momentum fluxes are both negative indicating that upward moving parcels possess: 1) less easterly direction and 2) less northerly direction. This is in excellent agreement with the streamline analysis (shown earlier) which indicated the flow at the surface was north–northeast over the eastern half of Lake Michigan, backing to northwesterly over the Great Lakes at 850 mb. Thus, as the air is warmed from below and rises, the parcels in the convective thermals will become more westerly and lose some of their northerly momentum (assuming wind speeds remain nearly constant within the layer). The last fluxes to be discussed in this area are the equivalent potential and virtual potential temperatures. Both possess large vertical flux values indicating that upward moving parcels have high $\theta_e$ and $\theta_v$. Therefore, in the region identified as the well–mixed layer, upward moving parcels are warm, moist, and unstable as would be expected in the convective boundary layer.

To this point, ample support has been demonstrated for the correct identification of the warm inversion and the well–mixed convective layers. What remains is to identify the nature of the transition layer, and how it can be perceived as separate from the inversion layer and fully–mixed layer. From the raw aircraft data, the environment of the transition region can be described as either cooler and more moist than the inversion, or warmer and drier than the well–mixed layer. The flux and covariance calculations show some suprising results for this region. First, by looking at the center of Fig. 58, it is obvious that this region contains the strongest fluxes due to the length of the arrows. The upward moving parcels in this area are shown to be cold, moist, and possess a high $\theta_e$. This is contrasted to upward moving parcels in the convective layer which were warm and moist. The downward moving parcels are warm, dry and stable (as if from the inversion layer) and can, again, be contrasted to the convective layer parcels which were cool and dry when moving downward. Because of their properties, entrainment of these parcels into the well–mixed layer below would result in the dissipation of turbulent kinetic energy. As such, the identified transition layer possesses the characteristics of the inversion layer but penetrative convection is protruding into the layer, creating vast amounts of turbulent exchange which is contradictory

to the nature of the inversion layer. Therefore, necessary and sufficient conditions exist for rethinking the classic structure of the Type I CTBL.

In this context, the classic inversion should be restructured to include two layers. The top layer consists of the typical inversion layer where little turbulent exchange occurs. The bottom layer should be considered a region where penetration by convective plumes allows for a large amount of energy transfer due to the turbulent motion. It is proposed that this area be singled out as a new and distinct layer, since it is in fact the transition between the well-mixed convective layer, below, and the inversion layer, above. A vertical profile of potential temperature for the revised conceptual model is shown below in Fig. 59.

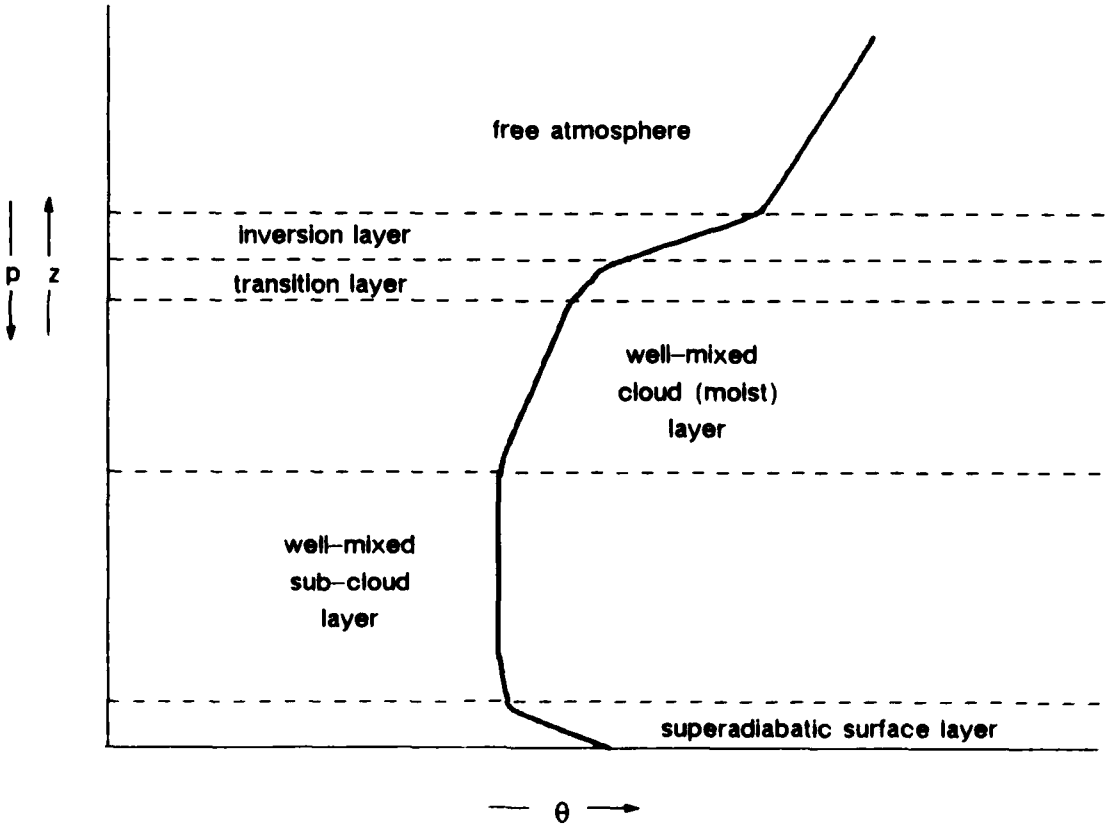


Figure 59. Vertical profile of potential temperature for a Type I CTBL which includes the transition layer where penetrative convection occurs.

# 6. SUMMARY AND CONCLUSIONS

Data from three different sources (conventional surface and upper-air, special surface and upper-air, and aircraft) have all been combined to study the modification which took place over Lake Michigan on 10 January 1984 as the result of a cold air outbreak. While this observational case study has been rather narrow in its temporal and spatial examination of the event, it has been quite broad in the depth of length scales examined.

The PROAM and PROAMU analysis packages were used to show the frontal passage through the Great Lakes region and to give some idea of the extent of the modification which occurred on the meso-$\alpha$ scale. Surface analyses showed the temperature decreasing from 4°C at 0000 GMT 10 January to -9°C by the same time on 11 January 1984. Even on this scale, the flux of sensible heat from the relatively warmer water surface to the air mass was apparent as the isotherms bulged northward, over the lake, at both 1200 GMT 10 January and 0000 GMT 11 January 1984. The 850, 700 and 500 mb upper-air analyses indicated the presence of intense cold air advection through most of the period. This was coupled with the strong northerly flow over Lake Michigan as displayed in the velocity vectors. Due to this northerly flow, the air which passed over Lake Michigan was first modified by Lake Superior. Stream line analyses of the surface and 850 mb were used to show the trajectory of the air parcels and thus the horizontal extent of Lake Superior's effects at both the surface and aloft.

Further demonstration of the presence of unmodified and modified polar air was provided by the PUKAM analyses. The skew T- log p thermodynamic diagrams plotted by this package displayed a typical cold and dry continental polar air mass over INL and STC at 1200 GMT 10 January 1984. The sounding for SSM and GRB contained added moisture and heat as a result of the flux of these quantities from the surface of Lake Superior. On the other hand, the soundings for MKG and KNX showed significant additonal heat and moisture due to the added fetch of Lake Michigan. In particular, the vertical distribution of temperature and dewpoint for KNX contained the classic profile of a well-mixed convective layer, a

superadiabatic surface layer topped by a well-mixed cloud layer and then capped by a warm inversion with a rapid decrease in moisture content. The vertical cross-sections of vorticity, divergence and vertical velocity, also provided by the PUKAM analyses, expressed the same results. The unmodified air displayed negative vorticity, divergence and downward vertical motion in the boundary layer. The modified air, however, possessed upward vertical motion, convergence, and positive vorticity throughout the boundary layer in support of convection within the planetary boundary layer.

Analysis of the meso-β scale through use of PROAM analyses provided further insight into the extent of the modification. This smaller scale, which focused on the Great Lakes region, displayed an omega-like appearance in the analysis of the convective tracers, namely, specific humidity and virtual potential temperature. Unmodified or slightly modified air occupied most of Wisconsin and Michigan which created cold, dry conditions to the east and west of Lake Michigan. Along the axis of the lake, the northerly flow dramatically changed the characteristics of the air by the addition of heat and moisture. This created an axis of high values along the southeast shore of Lake Michigan. Also, the wind speeds were greater than the 5 m/s necessary for the formation of a well-mixed convective boundary layer capable of supporting cellular convection.

The warming by Lake Superior caused the temperature contrast between the polar air and Lake Michigan's surface to decrease slightly. Due to this fact, the build up of the convective boundary layer was more gradual across the lake in the west-east direction as shown in the cross section of virtual potential temperature and the analysis of the inversion base heights. This allowed the NCAR research aircraft a more optimal amount of flight time in the thin zone between the warm inversion and the well-mixed convective layer. The participation of the NCAR aircraft during the Project LESS field experiment provided a unique opportunity for the study of the air mass modification which occurred over Lake Michigan.

A track across Lake Michigan, from 1925-1949 GMT, was chosen for spectral decomposition to study the smaller scale phenomenon. The plots acquired during this time indicated three different regimes in the raw data. The first of these was a region of little instrument response. The sensors indicated that this region was stable, warm and dry, all properties of the capping inversion in the Type I CTBL. The second region was characterized by were abrupt oscillations which gradually dampened out. Past this transition region, the air

took on different properties from the inversion, but the observed fluctuations were much less than in the transition region. The air became cool and moist, as would be expected near the top of a well-mixed convective layer. Similar results were found in the raw plots of the u, v, and w wind components.

After the raw data were examined, spectral decomposition was performed on data from the well-mixed layer. This segment represented a large sample from a homogeneous population which was necessary for valid results. In all, three length scales were present in the spectra. At a spectral peak of ~3 km there was significant energy present, representing the basic convective mode (BCM) as defined by Ross and Agee (1985). This was also in agreement with the findings of Kaimal *et al.* (1976), which suggest the presence of a peak near 1.5 $z_i$, where $z_i$ is the inversion base height (2000 m in this study). The second length scale found in the spectra of the well-mixed layer data was found at 10 km. Since the satellite imagery corresponding to the time the data were collected shows the presence of two-dimensional, north-south oriented cloud streets over Lake Michigan, it was concluded that this peak represented the 2-D cloud bands. This yielded an aspect ratio of 5:1 for this case study. The third prominent peak occured at 31 km. This peak was thought to represent an imposed weaker mode due to MCC or MEI. The time scale for MEI requires approximately 40 hours, and thus was eliminated as a possibility. MCC remained a plausible explanation for this length scale, however, the raw data contained evidence of entrainment on a 50 km length scale (somewhat larger than expected). Due to the problems of representing length scales in spectral decomposition, it was concluded that the entrainment spikes were also a likely candidate.

Finally, calculations were presented which showed the magnitude of the sensible heat, moisture, and momentum fluxes in the warm inversion, transition layer, and well-mixed convective layer. The calculations indicated that the transition layer, which has been considered the base of the inversion, contained the region of greatest exchange. It was concluded that this is the region where the warm, dry air from the inversion was mixed with the cool, moist air from the convective region by either entrainment or pentrative convection. Atlas *et al.* (1986) found similar results when examining airborne lidar and conventional 40 Hz aircraft data. They found small scale undulations in the inversion which they concluded were representing the "transition zone between the clear warm air above and the well-mixed

cooler air below", but attached no signifigance to the finding. On the other hand, Caughey *et al.* (1982) and Caughey and Kitchen (1984), describe in detail the entrainment interfacial layer (EIL) found in nocturnal stratocumulus cloud decks occurring in Type II CTBLs. A comparison of the raw temperature plot from the Type II CTBL (shown in Fig. 60) with the results of this study, shows the two are nearly identical, indicating similar processing may be occurring. Additionally, the spectra of vertical velocity reveal a -2/3 slope in the inertial subrange of both types of CTBLs. Finally, it was pointed out that by definition, turbulent exchange does not occur in the inversion layer. Therefore, it was proposed that, based upon the evidence found in the aircraft data, the zone between the well-mixed convective layer and the inversion in the Type I CTBL be referred to as the transition layer.

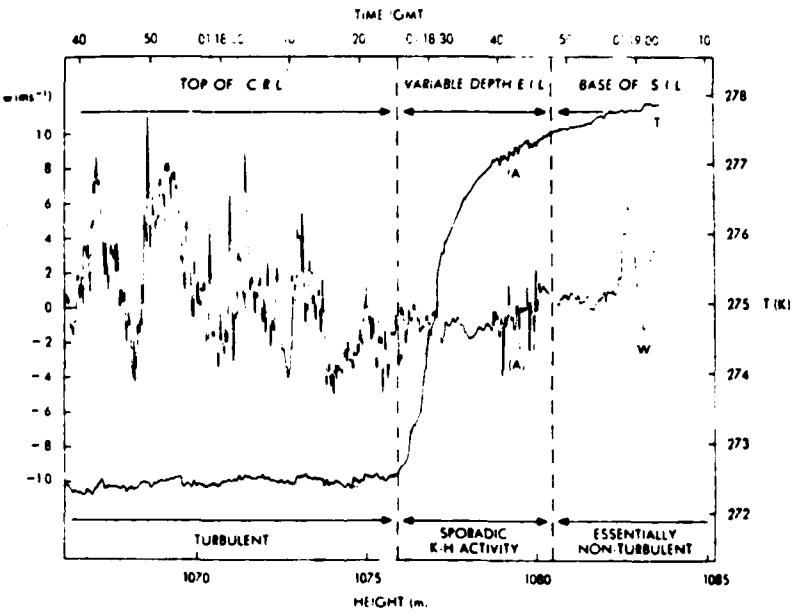


Figure 60. Details of the vertical velocity and temperature measurements taken during a traverse of a relatively non-turbulent EIL. CRL denotes the cloud radiative layer; SIL the subsidence inversion layer (from Caughey *et al.*, 1982).

# LIST OF REFERENCES

## LIST OF REFERENCES


Agee, E.M. and T.S. Chen, 1973: A model for investigaing eddy viscosity effects on mesoscale cellular convection. *J. Atmos. Sci.*, **30**, 180–199.

Agee, E.M., T.S. Chen and K.E. Dowell, 1973: A review of mesoscale cellular convection. *Bull. Amer. Meteor. Soc.*, **54**, 1004–1012.

Agee, E.M. and R.P. Howley, 1977: Latent and sensible heat flux calculations at the air–sea interface during AMTEX 74. *J. Appl. Meteor.*, **16**, 443–447.

Agee, E.M. and F.E. Lomax, 1978: Structure of the mixed layer and inversion layer associated with patterns of mesoscale cellular convection during AMTEX 75. *J. Atmos. Sci.*, **35**, 2281–2301.

Agee, E.M., 1987: Mesoscale cellular convection over the oceans. *Dyn. Atmos. Oceans*, **10**, 317–341.

Atlas, D., B. Walter, S. Chou and P.J. Sheu, 1986: The structure of the unstable marine boundary layer viewed by lidar and aircraft observations. *J. Atmos. Sci.*, **43**, 1301–1318.

Barnes, S.L., 1964: A technique for maximizing detail in numerical weather map analysis. *J. Appl. Meteor.*, **3**, 396–409.

Barnes, S.L., 1973: Mesoscale objective map analysis using weighted time–series observations. NOAA Tech. Memo. ERL–NSSL–62, 60 pp.

Benard, H., 1901: Les tourbillons cellulaires dans une nappe liquids transportant de la chaleur par convection en regime permanent. *Ann. Chim. Phys.*, **23**, 62–144.

Bunker, A.F., 1960: Heat and water vapor fluxes in air flowing southward over the western North Atlantic Ocean. *J. Meteor.*, **17**, 52–63.

Caughey, S.J., B.A. Crease and W.T. Roach, 1982: A field study of nocturnal stratocumulus II turbulence structure and entrainment. *Quart. J. Roy. Met. Soc.*, **108**, 125–144.

Caughey, S.J. and M. Kitchen, 1984: Simultaneous measurements of the turbulent and microphysical structure of nocturnal stratosumulus cloud. *Quart. J. Roy. Met. Soc.*, **110**, 13–34.

Chandrasekhar, S., 1957: Thermal convection. *Daedalus*, **86**, No. 4, 325–339.

Christopherson, D.G., 1940: Note on the vibrations of membranes. *Quart. J. Math.*, **11**, 63–63.

Fiedler, B.H., 1984: The mesoscale stability of entrainment into cloud–topped mixed layers. *J. Atmos. Sci.*, **41**, 92–101.

Helfand, H.M. and E. Kalnay, 1983: A model to determine open or closed cellular convection. *J. Atmos. Sci.*, **40**, 631–650.

Hubert, L.F., 1966: Mesoscale cellular convection. *Rept. 37*, Meteorological Satellite Laboratory, Washington, D.C., 68 pp.

Kaimal, J., J. Wyngaard, O. Cote, V. Izumi, S. Coughey and C. Readings, 1976: Turbulence structure in the convective boundary layer. *J. Atmos. Sci.*, **33**, 2152–2169.

Kelley, N.D., and M.N. Zrubek, 1973: Instrumentation aboard the Electra. *Atmospheric Technology*, **1**, 18–20.

Koch, S.E., M. des Jardin and P.J. Kochin, 1983: An interactive Barnes objective map analysis scheme for use with satellite and conventional data. *J. Climate. Appl. Meteor*, **22**, 1487–1503.

Krishnamurti, R., 1975: On cellular cloud patterns. Part 3: Applicability of the mathematical and laboratory models. *J. Atmos. Sci.*, **32**, 1373–1383.

Krueger, A.F. and S. Fritz, 1961: Cellular cloud patterns revealed by TIROS I. *Tellus*, **13**, 1–7.

LeMone, M.A., 1973: The structure and dynamics of horizontal roll vortices in the planetary boundary layer. *J. Atmos. Sci.*, **33**, 1308–1320.

Lemone, M.A. 1976: Modulation of turbulence energy by longitudinal rolls in an unstable planetary boundary layer. *J. Atmos. Sci.*, **33**, 1308–1320.

Lenschow, D.H., 1965: Airborne measurements of atmospheric boundary layer structure. Studies of the Effects of Variations in Boundary Conditions on the Atmospheric Boundary Layer, Sec. 4, Final Rept., Contract DA–36–039–AMC–00878(E), Dept. of Meteor., University of Wisconsin, 147–208.

Lenschow, D.H., 1973a: Two examples of planetary boundary layer modification over the Great Lakes. *J. Atmos. Sci.*, **30**, 568–581.

Lenschow, D.H., 1973b: Air sensing probes on the Buffalo. *Atmospheric Technology*, **1**, 40–43.

Lenschow, D.H. and P.L. Stevens, 1980: The role of thermals in the convective boundary layer. *Bound.-Layer Meteor.* **19**, 509–532.

Lidrbauch, J.J., 1986: An observational study of polar low phenomena in the vicinity of Lake Michigan. M.S. thesis, Purdue University, 147 pp.

Lilly, D.K., 1968: Models of cloud–topped mixed layers under a strong inversion. *Quart. J. Roy. Met. Soc.*, **94**, 292–309.

O'Brien, J.J., 1970: Alternative solutions to the classical vertical velocity problem. *J. Appl. Meteor.*, **9**, 197–203.

Orlanski, I. 1975: A rational subdivision of scales for atmospheric processes. *Bull. Amer. Meteor. Soc.*, **56**, 527–530.

Palm, E., 1960: On the tendency toward hexagonal cells in steady convection. *J. Fluid Mech.*, **8**, 183–192.

Pellew, A. and R.V. Southwell, 1940: On maintained convection motion in a fluid heated from below. *Proc. Roy. Soc.*, A, **176**, 312–343.

Randall, D.A., 1980: Conditional instability of the first kind upside–down. *J. Atmos. Sci.*, **37**, 125–130.

Rayleigh, O.M., 1916: On convection currents in a horizontal layer of fluid, when the higher temperature is on the underside. *Phil. Mag.*, Ser. 6, **32**, 529–546.

Roberts, P.H., 1967: Convection in horizontal layers with internal heat generation. Theory. *J. Fluid Mech.*, **30**, 33–50.

Rokosz, S. D., 1985: Modification of polar air mases over Lake Michigan. M.S. thesis, Purdue University, 216 pp.

Ross, B. and E.M. Agee, 1985: Aircraft investigation of wintertime convective and non–convective boundary layers over the East China Sea. *J. Meteor. Soc. Japan*, **63**, 405–416.

Rothermel, J. and E.M. Agee, 1980: Aircraft investigation of mesoscale cellular convection during AMTEX 75. *J. Atmos. Sci.*, **37**, 1027–1040.

Rothermel, J. and E.M. Agee, 1986: A numerical study of atmospheric convective scaling. *J. Atmos. Sci.*, **43**, 1185–1197.

Sheu, P. J. and E. M. Agee, 1977: Kinematic analysis and air–sea heat flux associated with mesoscale cellular convection duriing AMTEX 75. *J. Atmos. Sci.*, **34**, 793–801.

Sheu, P.J., E.M. Agee, and J.J. Tribbia, 1980: A numerical study of physical processes affecting convective cellular geometry. *J. Meteor. Soc. Japan*, **58**, 489–499.

Smith, D. R., and F. W. Leslie, 1982: Evaluation of a Barnes–type objective analysis scheme for surface meteorological data. NASA Tech. Memo., 82509, 25 pp.

Smith, D. R., M. E. Pumphry and J. T. Snow, 1986: A comparison of errors in objectively analyzed fields for uniform and nonuniform station distributions. *J. Atmos. Oceanic Technol.*, **3**, 123–132.

Van Delden, A., 1985: On the preferred mode of cumulus convection. *Beitr. Phys. Atmosph.*, **58**, 202–219.

Walters, B. A., Jr., 1986: The mesoscale organization, dynamics, and evolution of the marine planetary boundary layer during cold air outbreaks. Ph.D. dissertation, University of Washington, 200 pp.

END

12-87

DTIC